Rib length variation with age and sex - Measurements from high-resolution low-radiation X-ray images of volunteer subjects

Damien, Subit
Arts et Métiers ParisTech, LBM/Institut de Biomécanique Humaine Georges Charpak, 151 bd de l'Hôpital 75013 Paris
France

University of Virginia, Center for Applied Biomechanics, 4040 Lewis and Clark dr, Charlotesville VA 22902
USA

Baptiste, Sandoz
Julie, Choisne
Célia, Amabile
Claudio, Vergari
Wafa, Skalli
Sébastien, Laporte
Arts et Métiers ParisTech, LBM/Institut de Biomécanique Humaine Georges Charpak, 151 bd de l'Hôpital 75013 Paris
France

Paper Number 15-0313

ABSTRACT

Research Question: Human surrogates such as anthropomorphic test devices and computational models are common tools used by the automotive industry to characterize injury mechanisms and design countermeasures. The surrogates currently available were designed to be representative of certain sex and percentile of the population, such as the 5th- and 50th-percentile females, and the 50th- and 95th-percentile males. Great improvements were achieved in crash protection thanks to these models, but there is a need for more refined models that take into account a greater variation of the human diversity, such as the geometric variation due to aging. Therefore, the objective of this study was to determine how the length of ribs varies with age and sex.
Methods and Data Sources: A total of 103 asymptomatic volunteer subjects aged 0 to 84 years old were included in the study. First, each volunteer was imaged either with a standard clinical CT-scan, or in a standing position with the EOS imaging system, a low-radiation X-ray system that acquired one frontal and one sagittal high resolution images of the ribcage. Second, a custom-made software toolbox was used to create a subject-specific geometrical 3D model of each subject bony ribcage by registration of a statistical parametric ribcage model. Third, the rib length and mean thoracic index were extracted from the 3D ribcage models.
Results: The two main results were that the thoracic index (depth to width ratio of the thorax) was found to be fairly age-independent, and that the ribs length increased linearly with age between 0 and 20 years old before reaching a plateau. The growth rate of the ribs increased between each rib level from rib 1 (4 mm/year) to rib 10 (10.5 mm/year). This indicates a change in the size and shape of the ribcage during growth.
Conclusion and relevance: The study provides a quantitative characterization of age and sex-induced variation in the ribcage geometry, based on asymptomatic adult volunteer data. This study addresses the need for the geometric data required to build a set of computational models that represent male and female subjects of various age.

INTRODUCTION

A significant research effort has been undertaken in the last four decades to document motor vehicle crashes (MVC) such as vehicle speed, types of occupants, and injury outcomes, and develop typical scenarios for frontal, lateral and oblique impacts. In parallel, models of the human body were developed to estimate the severity of an impact, by determining the mechanical response and strength of the human body during a crash to describe the mechanisms of injury as well as the injury thresholds. Physical and computational human body models, or human surrogates, are used to achieve this goal. The surrogates currently available were designed to be representative of certain sex and percentile of the population, such as the 5th- and 50th-percentile females, and the 50th- and 95th-percentile males. Great improvements were achieved in crash protection thanks to these models, but there is a need for more refined models that take into account a greater variation of the human diversity, such as the geometric variation due to

aging, to create human surrogates that represent a larger spectrum of the population. In that effort, the ribcage is of particular interest: older drivers are more likely to die of a chest injury and less likely to die from a head injury compared to the youngest group (Morris et al., 2003). This is a direct consequence of the high rate of seat belt used in this population: in frontal crash, seat belts are designed to load the thorax to limit the forward excursion of the body and, in combination with airbags, prevent the impact of the head and thorax with the vehicle interior structures. However, determining the maximum load that can be safely applied to the thorax without fracturing ribs and how it varies with age has yet to be done. There is a need for geometric and morphologic data to develop a ribcage model that include age-dependent features. Several dataset are available in the published literature and provide valuable information about the age-related changes in the adult (Gayzik et al; 2008) and pediatric ribcage (Holcombe et al, 2013), however they all rely on computed tomography images obtained during routine trauma medical exams. Although, these studies included only subjects that were free of skeletal pathology, CT analysis obtained from hospital databases suffer two important limitations: the subjects are lying on the CT bed, and the resolution of the X-ray images is limited to minimize exposure for the subject for health concerns. Therefore, the goal of the present study was to measure the variations in the length of the ribs as a function of age and sex, based on high-resolution low-dose X-ray images obtained with the EOS system. The EOS system has been developed and used for several years now (Dubousset et al, 2010) to perform follow-up for spine deformity treatments for patients with scoliosis through the creation of subject-specific models of the spine (Humbert et al, 2009). The present study is the first step towards the description of age- and sex-induced variations in the ribcage geometry, and focused on the variation in the rib lengths for a wide range of age.

MATERIALS AND METHDODS

This study uses pediatric data from the literature (Sandoz et al, 2013), and new data for the adult population obtained with the EOS system.

The EOS imaging system

The EOS system is a system approved worldwide for clinical exam. Its main feature is to be a low-dose X-ray imaging system that allows the acquisition of the geometry of the musculoskeletal structure of volunteer subjects in a weight-bearing posture from two 'head-to-toe' X-ray images (Dubousset et al, 2010)(Figure 1). Furthermore, these images are high resolution (0.2 mm/pixel) compared to standard CT images of living patients (typically 2 to 5 mm/pixels). Several statistical models were developed to create subject geometry from the biplanar images obtained with EOS, in particular the spine (Humbert et al, 2009), and the ribcage (Aubert et al, 2014). The subject-specific geometry are created by registering a statistical parametric model of the spine and of the ribcage on the frontal and sagittal images obtained with EOS.

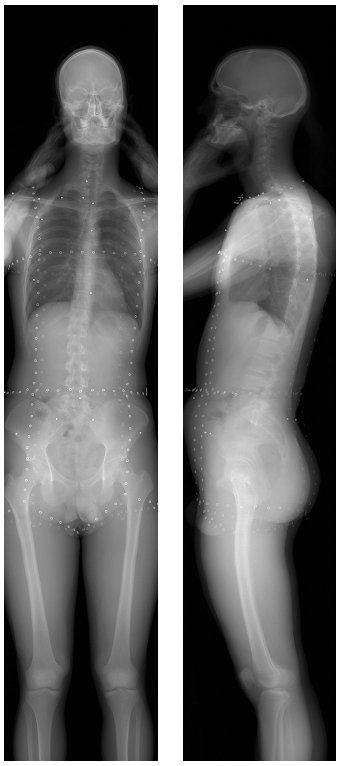

Figure 1.Frontal and sagittal views obtained with EOS and used to create subject-specific spine and ribcage.

Adult morphological data

Fifty five asymptomatic adult volunteers were included in this study (36 men, 19 women), aged 20 to 84 years (mean 38), with a body mass index ranging from 15.4 to 29.5 kg/m² (average: 22.9). Participants were confirmed to be free of spine pathologies or instrumentation anywhere in the upper body. Each participant completed and signed an informed consent form approved by the ethical committee at Hôpital Pitié Salpêtrière (Paris, France) (CPP 6001 and CPP 6036 Ile-de-France VI). The acquisition of the X-ray images took about 20 seconds. No specific instructions about breathing were given to the volunteers.

For each volunteer, a subject-specific geometric model was created: this model included the spine and the ribs 1 to 10. The length of each rib was calculated based on the method described in Aubert et al (2014): the rib length was defined as the length of the centroidal line from the costo-vertebral joint to the costo-chondral junction.

The rib cage morphometry was also described by the mean thorax index that is defined as the mean value of the thorax lateral width to thorax anteroposterior depth ratio calculated for eight horizontal slices equally distributed between the 2nd and the 12th thoracic vertebrae.

Pediatric morphological data

The pediatric data consisted of 960 ribs reconstructed from CT images from 48 children aged 4 months to 15 years (22 girls, 26 boys) (Sandoz et al., 2013). The pediatric data were organized in 16 age groups (less than 1 year-old, 1 year old, 2 years old, …, and 15 years old), and male and female data were combined in a single data set. Similar to the procedure used with the EOS images, the rib length was defined for ribs 1 to 10 as the length of the centroidal line from the costo-vertebral joint to the costo-chondral junction.

RESULTS

Rib lengths

The rib lengths were plotted for each rib level from 1 to 10. The data for the age 0 to 15 years old combine both sex, while the new data generated in this study separates male and female (figures 2 and 3).

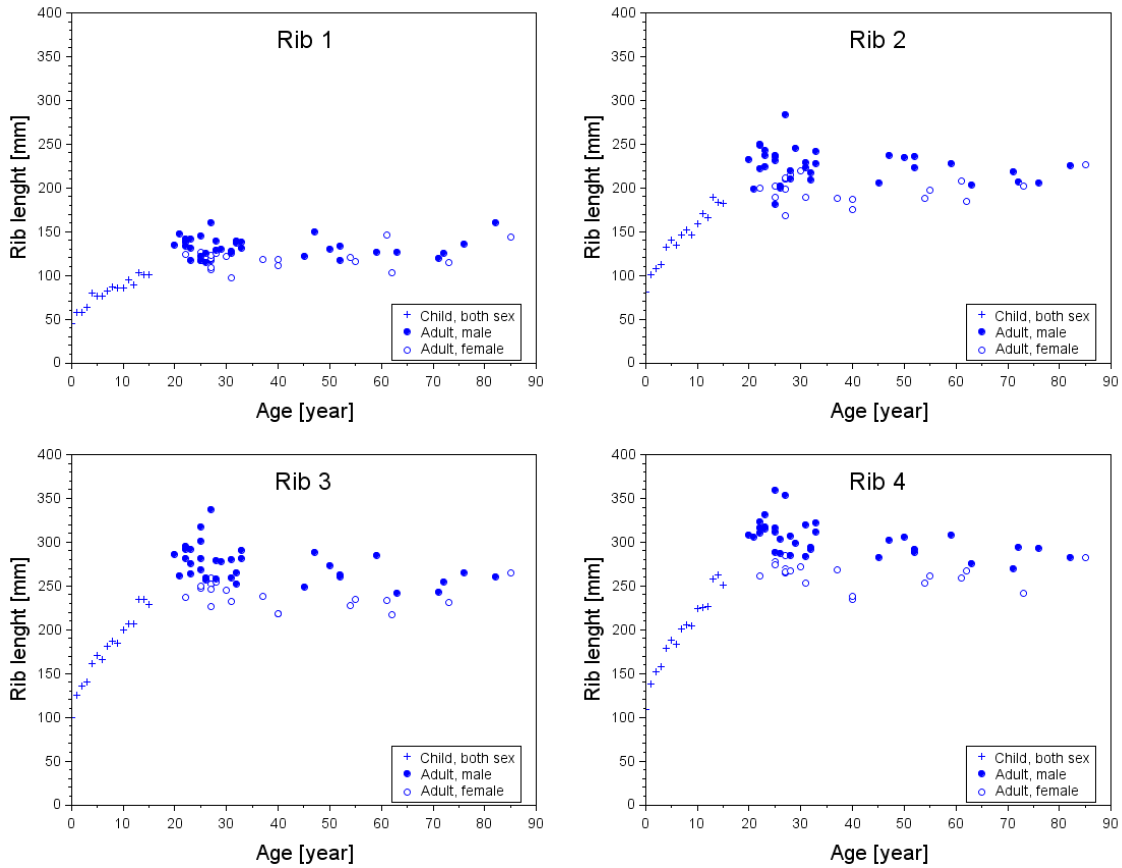

Figure 2. Rib lengths from 0 to 84 years old (ribs 1 to 4).

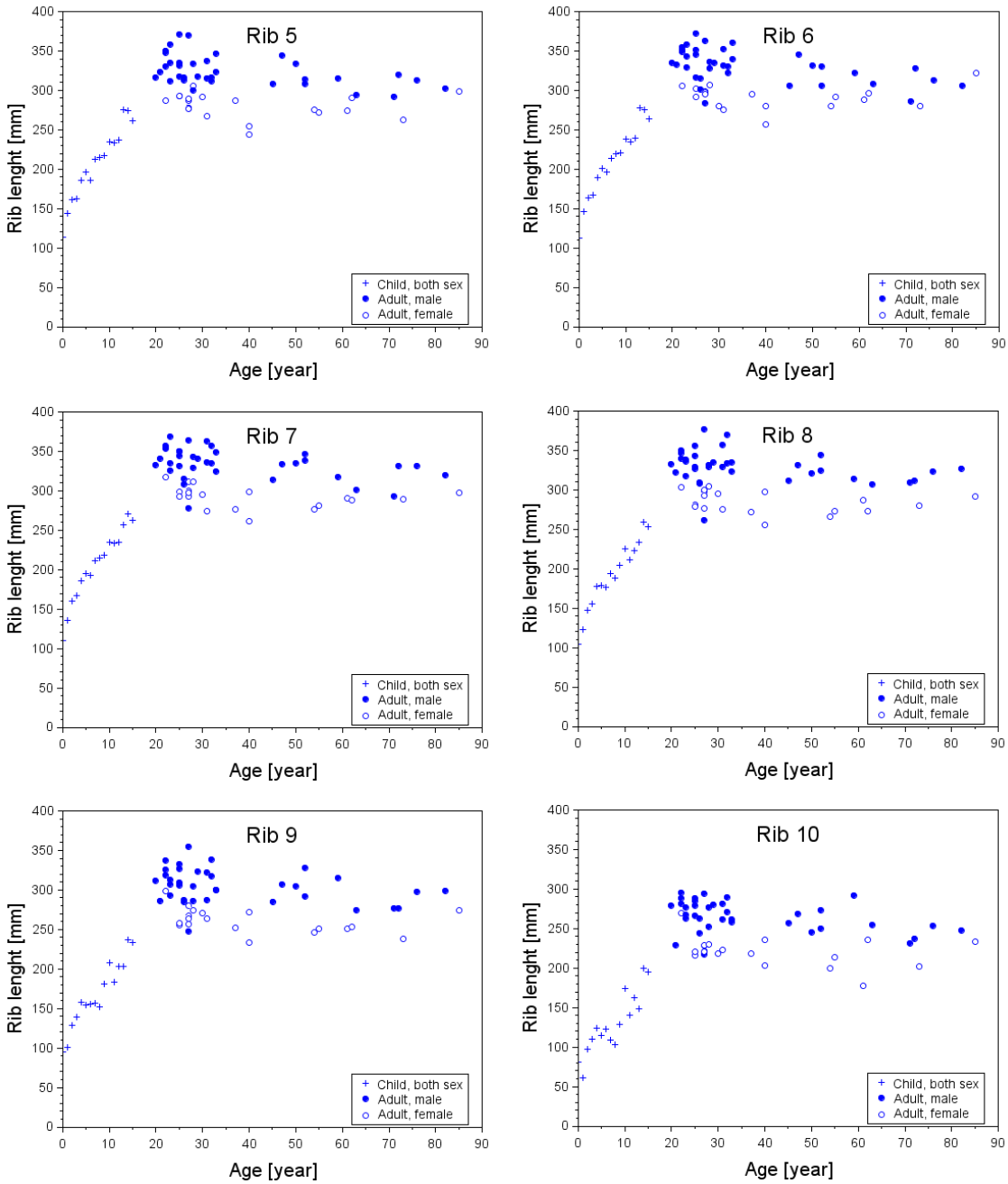

Figure 3. Rib lengths from 0 to 84 years old (ribs 5 to 10).

Mean thoracic index

The mean thoracic index was calculated for the male and female adult subjects (figure 4).

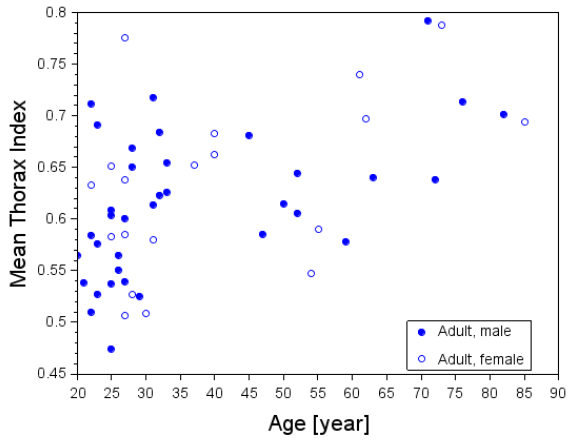

Figure 4. Mean thoracic index.

DISCUSSION

Effect of age

Both the rib length and mean thoracic index were found to vary with age. The rib length increased linearly with age between 0 and 20 years old before reaching a plateau; this trend was common to all rib levels. The growth rate of the ribs before age 20 increased between each rib level from rib 1 (4 mm/year) to rib 10 (10.5 mm/year). This indicates a change in the size and shape of the ribcage during growth. After 20 years of age, the rib length was nearly independent of age. One could have expected the rib to lengthen with age because of the calcification of the costal cartilage, but this trend was not obvious from the data presented in this study. As for the mean thoracic index, it was found to increase with age, indicating that the thorax widens to become 'rounder", which is consistent with the results from other study based on CT images (Kent et al, 2005; Weaver et al, 2014). The data provided in Sandoz et al (2013) for the range 0 to 15 years old are averaged (3 subjects in each 1-year age group), while the adult data was not.

Effect of sex

The female ribs were found to be on average per rib level 10 to 17 % shorter than the male's ribs (figure 5). Conversely, the mean thoracic index was found to be rather insensitive to sex, which suggests that the female ribcage is similar is shape to the male ribcage, but potentially smaller. However, the orientation of the ribs was not reported in this study, although it could be a factor in the overall size and shape of the ribcage.

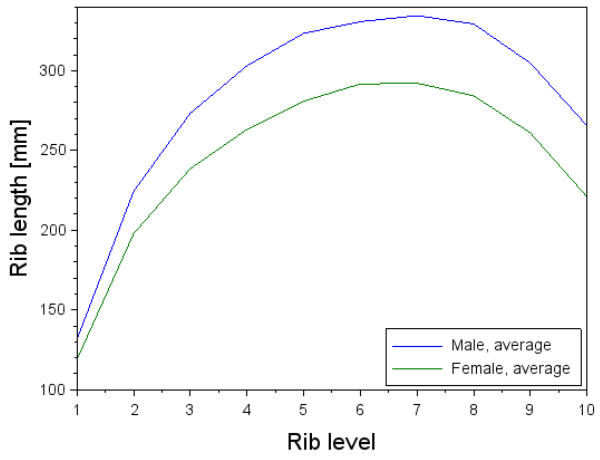

Figure 5. Mean rib length for male and female volunteers.

LIMITATIONS

The analysis presented in this paper is based upon a transversal study, and therefore the inter-individual differences may contribute to the differences that are attributed to age. Furthermore, the data set is biased towards the young adults age group (20 to 35 years of age), and the male subjects.

CONCLUSIONS

The study presented in this manuscript relies on a unique imaging system that can be used to image asymptomatic volunteer subjects with no pathology. In addition, subjects can be imaged in a standing or sitting position. The results presented in this paper focused on the variation of rib length with age and sex, for a relatively small data set. This manuscript provides a first set of results. The analysis is on-going to further established the morphological differences between male and female subjects, as a function of age, to elucidate the link between the geometry of the ribcage and the risk of injury during a motor vehicle crash.

ACKNOWLEDGEMENT

The authors thank the Banque Public d'Investissement for financial support through the French Fonds unique interministériel program (FUI14, project dexEOS), and the ParisTech BiomecAM chair program on subject-specific musculoskeletal modelling, and in particular COVEA and Société Générale. D. Subit thanks the European Union for financial support through the Marie Curie International Incoming Fellowship (FP7-PEOPLE-2013-IIF, project BioAge # 622905). The views expressed in this article are those of the authors and do not necessarily represent the views of the funding bodies.

REFERENCES

Aubert, B, Vergari, C, Ilharreborde, B, Courvoisier, A, Skalli, W. 2014. "3D reconstruction of rib cage geometry from biplanar radiographs using a statistical parametric model approach", Computer Methods in Biomechanics and Biomedical Engineering: Imaging & Visualization, in press.

Dubousset, J, Charpak, G, Skalli, W, Deguise, J, Kalifa, G. 2010. "EOS: a new imaging system with low dose radiation in standing position for spine and bone & joint disorders", Journal of Musculoskeletal Research, 13(1):1-12.

Gayzik F, Yin M, Danelson K, Slice D, Stitzel J. 2008. "Quantification of age-related shape change of the human rib cage through geometric morphometrics", Journal of Biomechanics, 41:1545–1554.

Holcombe S, Kindig M, Zhang P, Parenteau C, Rabban P, Hully L, Wang S. 2013. "Age-based predictive model of the pediatric ribcage", International Journal of Automotive Engineering 5:15-22.

Humbert, L, De Guise, JA, Aubert, B, Godbout, B, Skalli, W. 2009. "3D reconstruction of the spine from biplanar X-rays using parametric models based on transversal and longitudinal inferences", Medical Engineering & Physics, 31(6):681-687.

Kent R, Lee S, Darvish K, Wang S, Poster C, Lange A, Brede C, Lange D, Matsuoka F. 2005. "Structural and material changes in the aging thorax and their role in crash protection for older occupants", Stapp Car Crash Journal 49: 231-249.

Morris A, Welsh R, Hassan A (2003). Requirements for the crash protection of older vehicle passengers. Annual Proceedings of Association for the Advancement of Automotive Medicine (AAAM), 47:165-80.

Sandoz, B, Badina, A, Laporte, S, Lambot, K, Mitton, D, Skalli, W. 2013. "Quantitative geometric analysis of rib, costal cartilage and sternum from childhood to teenagehood", Med Biol Eng Comput.,51(9):971-9.

Weaver, A, Schoell, S, Stitzel, J. 2014. Morphometric analysis of variation in the ribs with age and sex, J Anat;225(2):246-61.

UNVEILING THE STRUCTURAL RESPONSE OF THE RIBCAGE: CONTRIBUTION OF THE INTERCOSTAL MUSCLES TO THE THORACIC MECHANICAL RESPONSE

David Poulard
Center for Applied Biomechanics, University of Virginia
USA

Damien Subit
Institut de Biomécanique Humaine Georges Charpak, Arts et Métiers ParisTech
France

Paper Number 15-0387

ABSTRACT

Current finite element (FE) models of the human body do not properly include the contribution of the intercostal muscles (ICM), which is believed to limit their rib fracture prediction capabilities. In the present study, an existing full body model for a seated 50th-percentile male was evaluated under five cases of loading: point loading of the denuded ribcage, frontal pendulum impact tests, lateral and oblique pendulum impact tests and table top tests. The sensitivity of the model to changes in material model of the ICM was evaluated by using two material models: an isotropic linear elastic material model and a foam model defined by a single uniaxial load curve extracted from a recent literature. The performance of these models compared to the experiments was assessed quantitatively through a correlation analysis on the force and chest deflection time histories. The simulations found that that the material properties of the ICM have little effect on the externally measured impact force and chest deformation except in point loading.

INTRODUCTION

Thoracic injuries are the most common blunt trauma sustained by restrained occupants in motor vehicle crashes [1]. Amongst thoracic injuries, rib fractures are commonly used as an indicator of a crash severity as these fractures are relatively straight forward to detect and the increase of their number was shown to be associated to an increase of the risk of sustaining more severe injuries to the internal organs (aorta, lungs, heart). The structure of the thoracic segment structure is complex because of its geometry and the material heterogeneity: it consists of the ribcage, the viscera, the musculature and the skin, and its mechanical response results from the contribution of these tissues, soft and hard. Understanding how the thorax deforms under dynamic solicitations is an active area of research.

Finite element (FE) models of the human thorax or the entire body have been developed to investigate the structural response of the thorax and establish its injury tolerance [2-9]. These models rely on two types of data: the material and geometrical information to build them, and the experimental data required to evaluate their biofidelity, i.e. their ability to predict a mechanical response under dynamic loading similar to what would experience a real person. In both cases, post-mortem human (PMHS) data are used, and the capabilities of the models depend on the availability of the experimental data.

Material constitutive models and the required data to validate the models created for the isolated thoracic components are available for nearly all the tissues: clavicle [10, 11], ribs [12-14] and costal cartilage [15, 16]. However, there is little information in the literature for the intercostal muscles (ICM), and therefore the FE models currently available use material properties reported on in by [17]. This study lists properties of some thoracic muscles, such as the pectoralis major and the trapezius but not specifically identify intercostal material properties. Therefore, as thoracic muscle structure differs along the thorax, modeling the ICM using properties of other thoracic muscles may be not appropriate. It was found from animal experiments that the intercostal muscles could generate substantially less tensile force than other muscles like the diaphragm [18, 19]. Recently, Kindig et al. [20] found that decreasing the elastic modulus of the intercostal muscles of a FE ribcage model alter significantly the ribcage

deformation under quasi-static point loading and dynamic sternal loading. Moreover, while an isotropic linear elastic material model is commonly used for modeling the ICM, it was found from cadaver tests that ICM exhibit a hyperelastic behavior in tension [21]. Thus, it appears that the FE models currently available do not properly include the contribution of the intercostal muscles, which is believed to limit the rib fracture prediction capabilities of the thorax model.

Therefore, the goal if this present study is to examine the sensitivity of a thorax FE to the changes in intercostal muscle material constitutive model based on recent literature. To do, a parametric analysis was performed to evaluate the sensitivity of the thorax to the constitutive models used for the ICM using a human body model (HBM). The different versions of the HBM were exercised under several loading conditions with various constitutive models for the ICM and their performance was assessed quantitatively to experiments through a correlation analysis.

METHODOLOGY

Finite Element Body Model Overview

The HBM used in this study was the version 4.1 of the seated 50th-percentile male, developed in LS-DYNA for the Global Human Body Models Consortium (GHBMC). This full model has been described in a previous study [9, 14, 22] and evaluated under various loading environments (antero-posterior rib bending, point loading of the denuded ribcage, omnidirectional pendulum impact and table top) through a correlation metric tool (CORA) based on linearly independent signals [9].

The intercostal muscles were defined as a single layer of triangular planar shell elements of 1.5 mm thickness which were attached between adjacent ribs. The membrane element formulation was used since it was assumed that the intercostal could not support a through-thickness bending load. By default, an isotropic linear elastic material model with E=0.5 MPa, was used for these elements. This material model was changed in the present study.

Defining new material properties for the intercostal muscles

Material Type 181 (*MAT_SIMPLIFIED_RUBBER/FOAM) was used for a new model of the behavior of the ICM. This material model provides a rubber and foam model defined by a single uniaxial load curve defining the force versus actual change in a gauge length. The single uniaxial load curve was defined to cover the complete range of expected loading.

In tension, the load curve was defined from the hyperelastic behavior of the ICM found in [21]. In this study, tensile tests were performed on three ICM samples harvested from one cadaver at different locations: one sample (#A) located between ribs 8 and 9 from the anterior aspect of the rib cage, and two samples (#B and #C) located between ribs 9 and 10 in the lateral and posterior aspects of the rib cage. For the three samples, a toe region was observed, followed by quasi-linear response after about 30 % of stretch and failure at 60%. An average stress-strain response from the three samples was extracted and converted to a load-displacement curve by assuming a specimen gauge length, width and thickness of 1 mm.

Figure 1 shows the stress-strain curve used in the rubber/foam model, the experimental curves used for its definition and the stress-strain curve based on the default material for comparison. In compression, the load curve was defined to eliminate the compressive action since the ICM exhibit similar behavior [21]. Nevertheless, stiffen up the material stress-strain curve at large compression ($\varepsilon<0.8$) was found essential for avoiding negative volume.

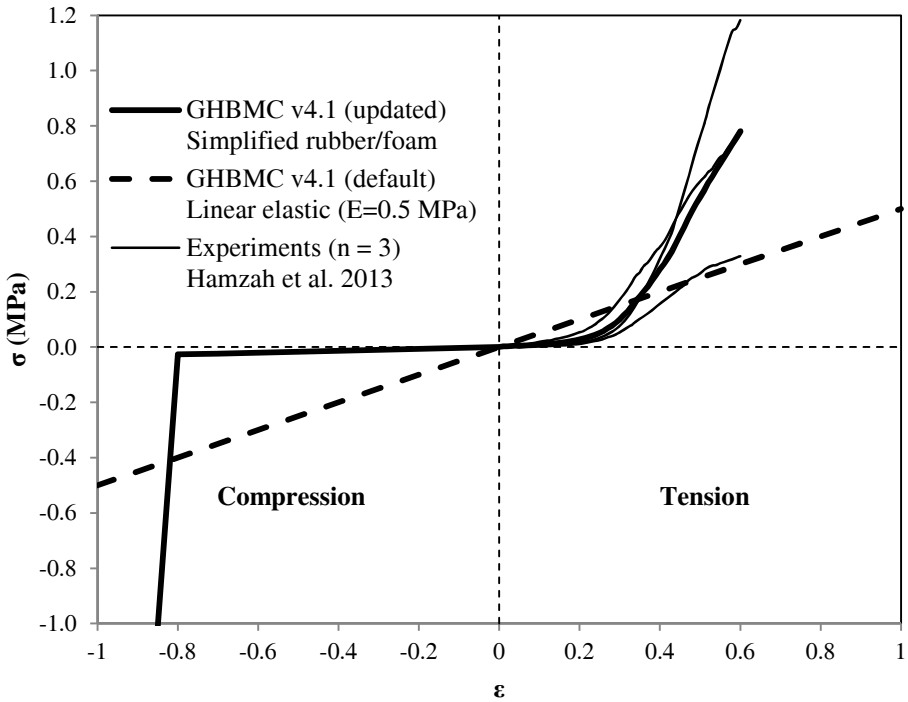

Figure1. Stress-strain curves used in the ICM for the updated version the GHBMC model, the experimental curves used for its definition and the stress-strain curve based on the default material for comparison.

Evaluation cases

The influence of the ICM material on thoracic mechanical response was evaluated from the denuded ribcage to the full body model using four sets of experiments. These experimental cases were selected based on their previous use for the validation of the HBM [9]. The experimental tests and model validation process are described below.

Point loading of the eviscerated ribcage Quasi-static point loading of the ribcage was simulated, using the method outlined in Kindig et al. [23]. The FE model of the ribcage was positioned oriented in an upright position similar to the experiment and the six degrees of freedom of the thoracic vertebrae were constrained. The spherical segment was positioned and oriented such that the contact surfaces on the sphere did not initially penetrate the ribcage mesh (Figure 2a). The loading plate was positioned initially in contact with the contact surface of the sphere and aligned such that the vector normal to the plate was directed along the average vector direction used in the experiments at this particular loading location. The plate was constrained to translate along this vector only, with no rotation allowed, consistent with the experimental boundary conditions. The plate was displaced at a constant 200 mm/sec up to the prescribed displacement used in the experiment (varied with the loading location). The loading rate to 200 mm/sec provided a reasonable simulation time while maintaining stable contact forces. To avoid strain-rate effects, the Cowper-Symonds yield-stress scaling in the bone material models was disabled. The reaction force onto the plate nodes was outputted for comparison with experiment.

Simulations were performed at the lower and upper sternum levels and the costochondral junction (CCJ) of rib levels 1, 3, 4, 6, and 9 (Figure 2b). The average value of the maximum normalized displacement obtained in experiments for each location was used to define the maximum displacement reached in simulation and

consequently the termination time. No modifications were made on the force and displacement obtained from simulations.

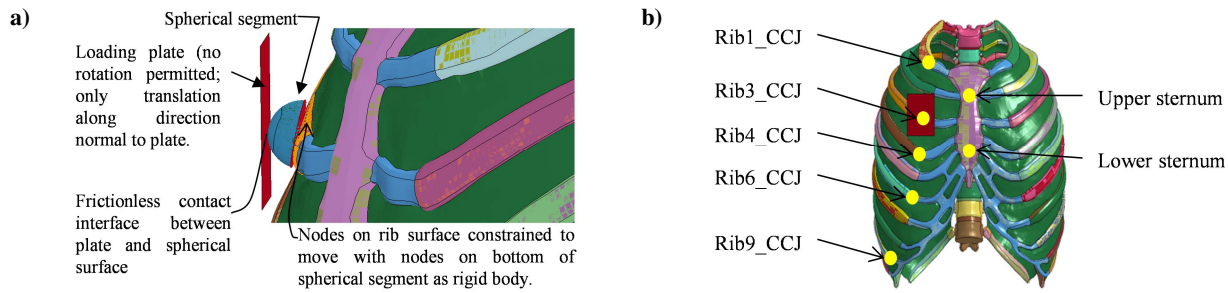

Figure2. Setup for point loading simulation [9]. (a) Close-up at loading site (b) anterior view.

<u>Frontal pendulum impact</u> The FBM was exercised under frontal pendulum impact [24]. In the simulation, the FBM was seated on a rigid plate and the impactor positioned at the midsternum level (Figure 3a). An initial velocity of 4.3 m/s was imposed on the impactor. The impact force was measured as the contact force between the impact and model. Chest deflection was defined as the variation of length between the middle of two nodes taken on the pectoral muscles and a node taken on the skin at T8 level [9]. The impact force chest deflection curve from the FE model simulations was compared to the experimental corridors normalized to the 50th percentile male developed by Lebarbé and Petit [25] to evaluate the response of the thorax model.

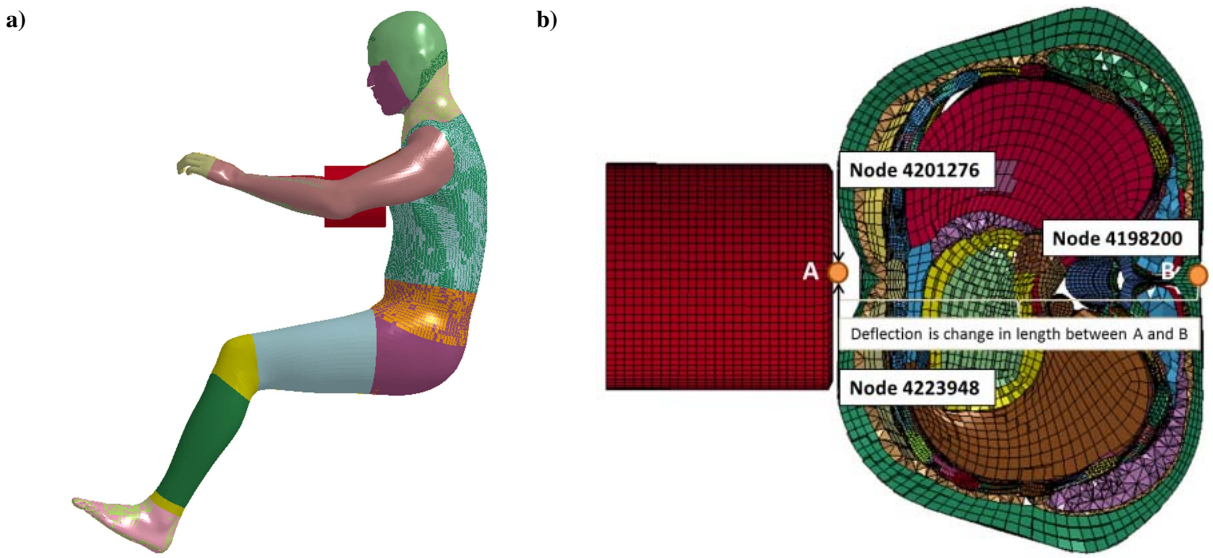

Figure3. Setup for frontal pendulum impact [9]. (a) Lateral view, (b) Superior view of the cross-section of the thorax at the mid-sternum showing the points used to measure the chest deflection.

<u>Pure lateral impact</u> The FBM was further run according to a pure lateral impact configuration available in the literature [26]. In the simulation, the FBM was seated on a rigid plate and the impactor positioned under the axiliary level, similar to the experiments (Figure 4a). The cylindrical impactor with a diameter of 152 mm, a mass of 23.4 kg and an initial impact velocity of 2.5 m/s was centered with the transverse plane through the fourth interspace of the ribcage. The impact force was measured as the contact force between the impactor and model. The chest deflection was defined as the change in length between two bilateral nodes aligned with the center of the impactor (Figure 4b).

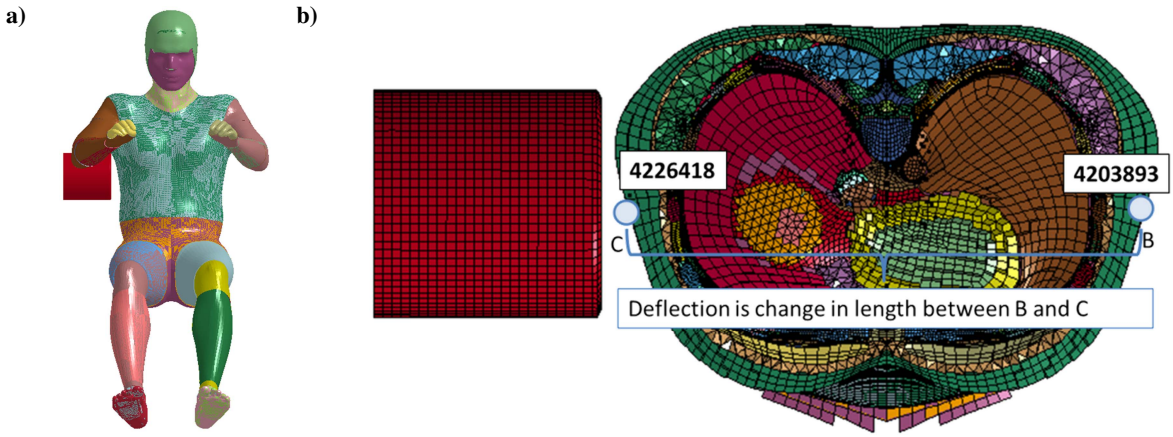

Figure4. Setup for lateral pendulum impact [9]. (a) Frontal view, (b) Superior view of the cross-section of the thorax at the level of sternum the fourth interspace showing the points used to measure the chest deflection.

In a qualitative evaluation, the force-deflection curve from the FE model was compared to the experimental corridors normalized to the 50th percentile male developed by Shaw et al. [26]. For the quantitative evaluation, the force/time and deflection/time histories were used.

Table top tests The FBM was set-up to simulate four tabletop restrained configurations [27]:

- hub loading, where the hub was simulated as a cylindrical rigid body with a diameter of 152 mm,
- belt loading, where single and double diagonal belts were modeled by a layer of 2-mm thick shell elements,
- distributed loading, where an extra-wide belt was modeled by a layer of 2-mm-thick shell elements and was 203-mm wide.

The pulley system used in the experiments was simulated by slip ring elements and several 1-D belt elements so that the loading angles of the 1D-belt elements were maintained and consistent with experimental configurations (Figure 6a). These tabletop models were loaded using the displacement-time history reported on in Kent et al. [27] up to 20% of chest compression (non-injurious level) for all the four loading conditions (Figure 6b). The displacement was applied symmetrically to the extremities of the single, double and distributed loading, and to the hub. Prior to applying the loading, the models were allowed to settle on the table for 100 ms under its own weight. The settling process was applied in a pre-simulation and the initial stress was imported in the FBM for the table top simulations. The limbs were cut to reduce the computation time.

The reaction force was defined as the contact force between the support table and the model. The compression was defined as the ratio of the Z-displacement of a node taken on midsternum (A, Figure 6a) divided by the initial distance between A and the support table.

The reaction force versus compression curves were then compared to the thoracic response corridors developed from the fifteen PMHS tested by Kent et al. [27].

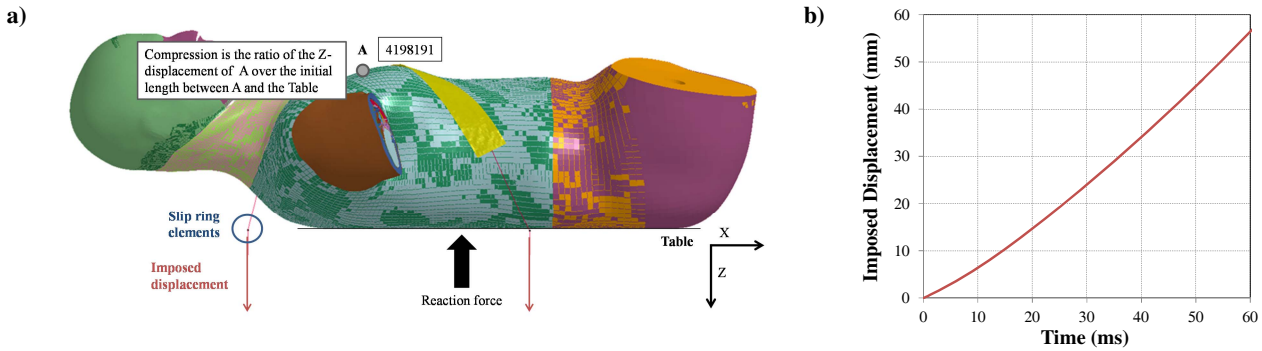

Figure5. Setup for single belt table top test [9]. (a) Lateral view, (b) Displacement imposed to the loading structure.

Quantitative assessment of the response of the model

A quantitative assessment of the response of the models compared to the five sets of experiments was performed through metrics obtained with the CORA software (CORelation and Analysis, Parternship for Dummy Technology and Biomechanics). Each of these metrics is given a score and the weighed sum of these score is the CORA score ranging between 0 and 1. A CORA score above 0.8 is considered as a good fit between the model and the experimental response [28]. As CORA calculates the correlation of each signal separately, those single ratings were combined to a global model rating by calculating the mean value of all the ratings. Table 1 shows which data were used to establish the rating for each load cased. Ratings with a score of 0.8 or higher were assumed as good.

The experimental response was defined from the average response and inner/outer corridors derived from the experimental results [9].

Table1.
`Signals used in the correlation analysis [9].

Load case	Sub load case(s)	Signals
Point loading of the ribcage	Lower sternum, Rib1_CCJ, Rib3_CCJ, Rib4_CCJ, Rib6_CCJ, Rib9_CCJ, Upper sternum	1. Force vs. Displacement*
Frontal pendulum impact	Impact velocity 4.3 m/s	1. Force vs. Time 2. Deflection vs. Time
Lateral pendulum impact	Impact velocity 2.5 m/s	1. Force vs. Time 2. Deflection vs. Time
Table top	Hub, Single Belt, Double Belt, Distributed Loading	1. Force vs. Compression*

*: Equivalent to Force vs. Time in CORA, as displacement and chest compression were the independent variables.

RESULTS

Point loading of the eviscerated ribcage

The scaled force versus scaled deflection curves predicted by the HBM after ICM modification different from the baseline model (Figure 6). In all tested locations, the model after modification was found to be more compliant, up to be out of the corridors. Quantitatively, the average CORA model score was 0.73 ± 0.12 after modification was lower than the baseline model (0.80 ± 0.12)(Table 2).

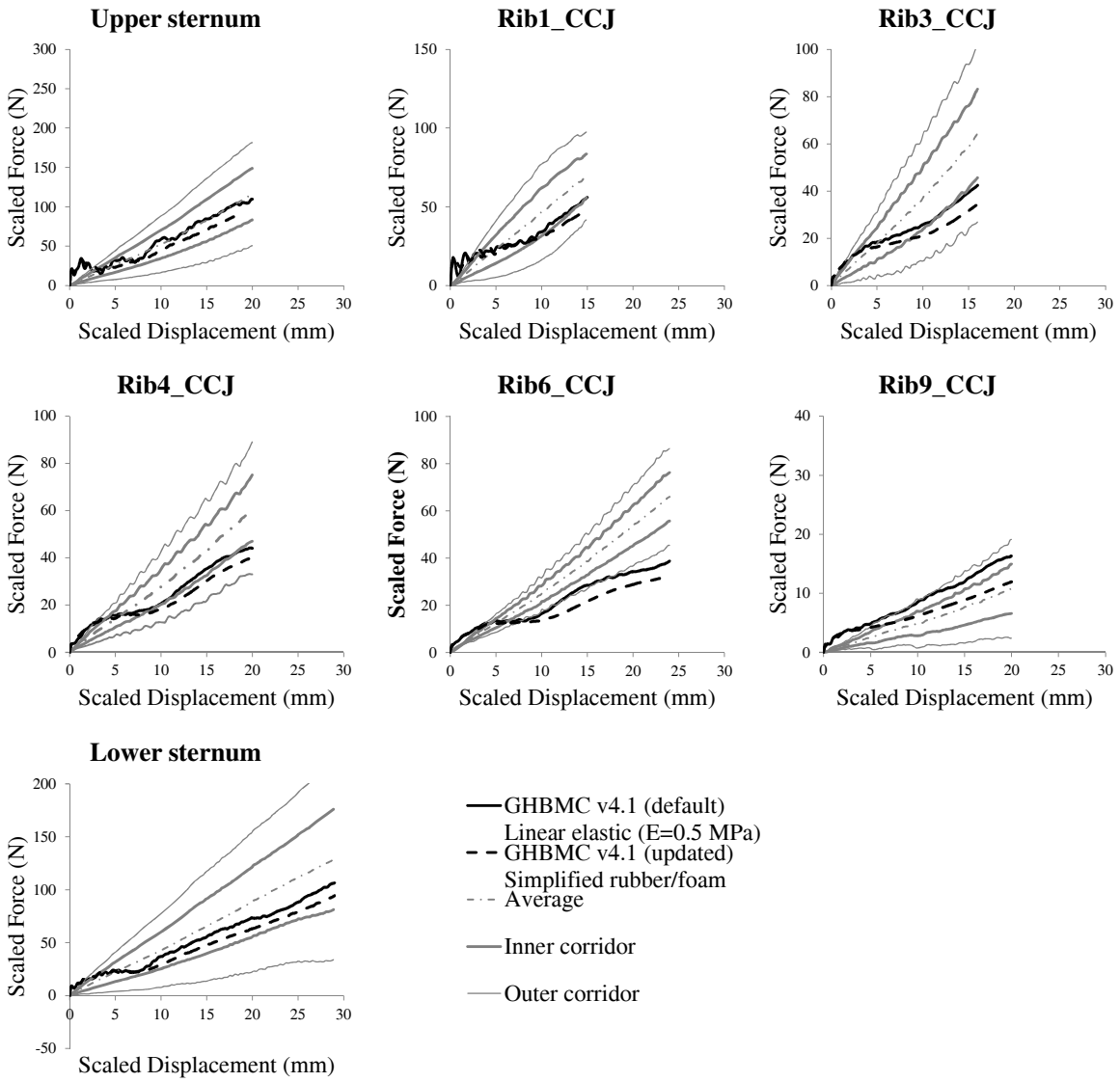

Figure6. Model performance for point loading of the denuded ribcage. Scaled Force-Scaled Displacement. Experimental corridors are adapted from [23].

Frontal and lateral pendulum tests

The reaction force versus chest deflection curves predicted by the HBM after ICM modifications was really close to the baseline model (Figure 7 and 8). CORA model scores after modifications were 0.86 in frontal and 0.89 in lateral close to the scores obtained with the baseline model (0.84 and 0.89 respectively) (Table 2).

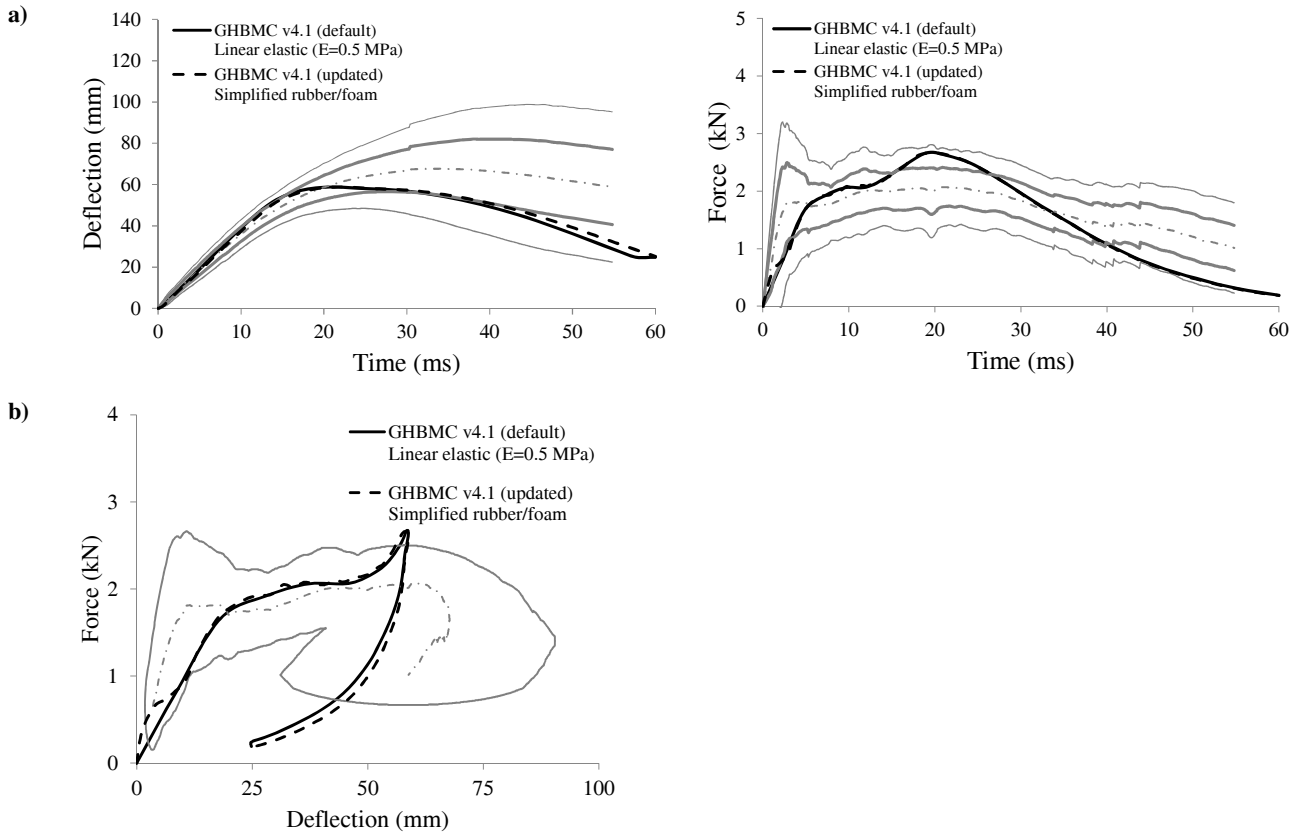

Figure7. Model performance for frontal pendulum tests. (a) Deflection-Time and Force-Time histories, (b) Force-Deflection, (c) CORA ratings. Experimental corridors are adapted from [24] and [25].

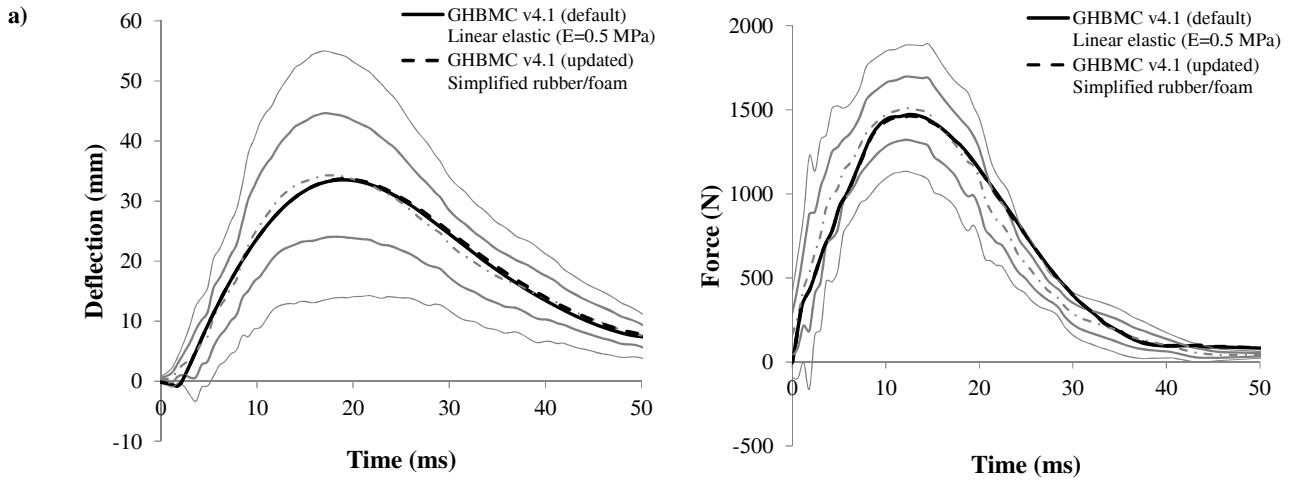

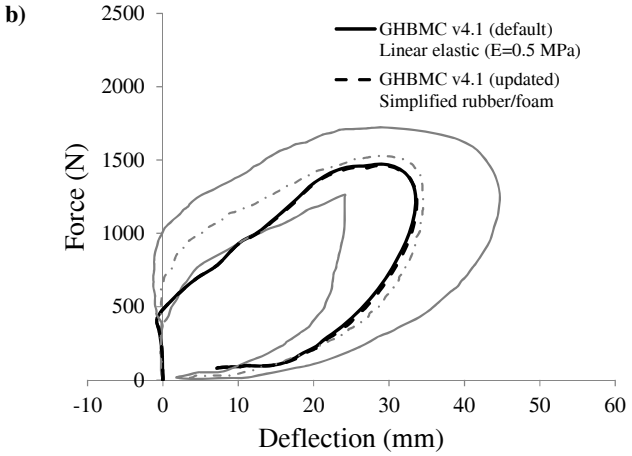

Figure8. Model performance for lateral pendulum tests: (a) Deflection-Time and Force-Time histories, (b) Force-Deflection. Experimental corridors are adapted from [26].

Table top tests

The reaction force versus chest compression curves predicted by the HBM after modifications closely agreed with the response obtained by the baseline model for all configurations (Figure9). The average CORA model score obtained by the model after modifications was 0.83 ± 0.10, slightly lower than the baseline model (0.86 ± 0.10) (Table 2).

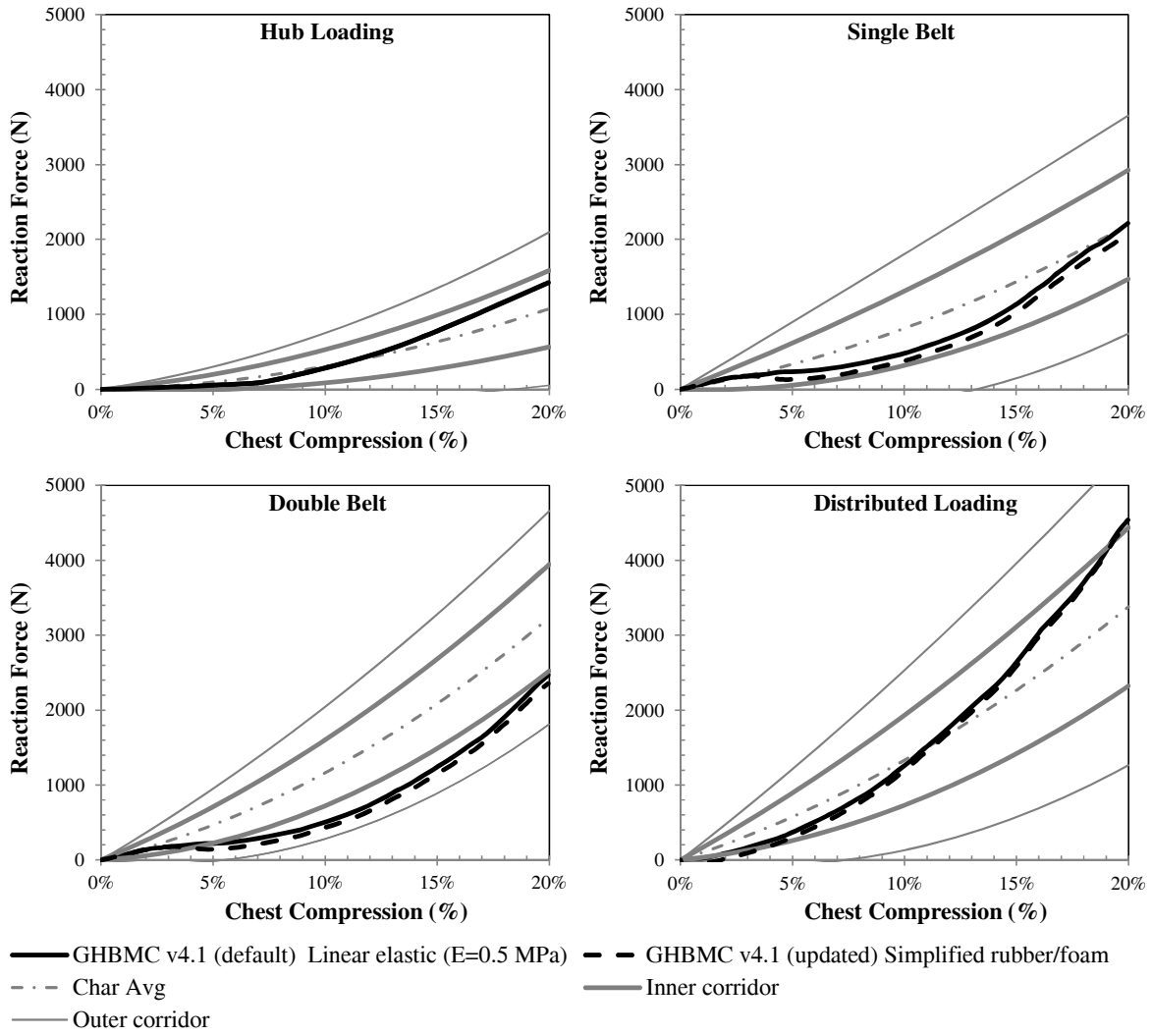

Figure9. Model performance for table top tests. (a) Reaction Force-Chest Compression, (b) CORA ratings. Experimental corridors are adapted from [27].

Table2.
CORA scores.

	Model	Subload Case	Signal	Corridor Score	Cross-correlation				Signal Score	Model Score
					Phase Score	Size Score	Progression Score	Score		
Point loading of the ribcage	1*	Lower sternum	Force	1.00	*Ignored*	0.54	1.00	0.77	0.89	0.80
		Rib1_CCJ	Force	0.89	*Ignored*	0.51	0.98	0.75	0.82	
		Rib3_CCJ	Force	1.00	*Ignored*	0.31	0.99	0.65	0.83	
		Rib4_CCJ	Force	0.93	*Ignored*	0.46	0.99	0.73	0.83	
		Rib6_CCJ	Force	0.44	*Ignored*	0.41	1.00	0.70	0.57	
		Rib9_CCJ	Force	0.44	*Ignored*	0.93	1.00	0.96	0.70	
		Upper sternum	Force	1.00	*Ignored*	0.79	1.00	0.90	0.95	
	2**	Lower sternum	Force	1.00	*Ignored*	0.44	1.00	0.72	0.86	0.73
		Rib1_CCJ	Force	0.86	*Ignored*	0.50	0.97	0.74	0.80	
		Rib3_CCJ	Force	0.85	*Ignored*	0.22	0.98	0.60	0.72	
		Rib4_CCJ	Force	0.72	*Ignored*	0.35	0.99	0.67	0.69	
		Rib6_CCJ	Force	0.15	*Ignored*	0.27	0.99	0.63	0.39	
		Rib9_CCJ	Force	0.69	*Ignored*	0.77	0.98	0.87	0.78	
		Upper sternum	Force	0.99	*Ignored*	0.56	1.00	0.78	0.88	
Frontal	1	N/A	Deflection	0.89	*Ignored*	0.68	0.99	0.84	0.86	0.84
			Force	0.67	*Ignored*	0.94	0.98	0.96	0.82	
	2	N/A	Deflection	0.93	*Ignored*	0.70	0.99	0.85	0.89	0.86
			Force	0.67	*Ignored*	0.95	0.98	0.96	0.82	
Lateral	1	N/A	Deflection	0.97	*Ignored*	0.99	1.00	1.00	0.98	0.89
			Force	0.61	*Ignored*	1.00	1.00	1.00	0.80	
	2	N/A	Deflection	0.96	*Ignored*	0.98	1.00	0.99	0.98	0.89
			Force	0.61	*Ignored*	1.00	1.00	1.00	0.80	
Table top	1	Hub loading	Force	1.00	*Ignored*	0.64	1.00	0.82	0.91	0.86
		Single belt	Force	1.00	*Ignored*	0.74	0.91	0.83	0.91	
		Double belt	Force	0.73	*Ignored*	0.40	0.99	0.70	0.71	
		Distributed loading	Force	0.98	*Ignored*	0.71	1.00	0.85	0.92	
	2	Hub loading	Force	1.00	*Ignored*	0.65	0.99	0.82	0.91	0.83
		Single belt	Force	1.00	*Ignored*	0.62	0.99	0.80	0.90	
		Double belt	Force	0.58	*Ignored*	0.36	0.99	0.67	0.63	
		Distributed loading	Force	0.89	*Ignored*	0.73	0.99	0.86	0.88	

* 1: GHBMC v4.1 (default) | Linear elastic (E=0.5 MPa). ** 2: GHBMC v4.1 (updated) | Simplified rubber/foam.

DISCUSSION

The version 4.1 of the GHBMC model was modified to include more realistic material definition of the intercostal muscles (ICM) based on recent published experiments. Its performance was evaluated qualitatively and quantitatively by comparison of the simulation results to the experiments based on signal correlation analysis. Overall, the material properties of the ICM have little effect on the externally measured impact force and chest deformation except in point loading. Sensitivy of the ICM in point loading was already observed in a previous study [20], but it is the first time such influence is studied on a thorax model at multiple length scales.

The use of a correlation method such as CORA allows to perform a multi-configuration evaluation of a FE model, and it is the first time such a method is applied to evaluate the influence of modification on a thorax model at multiple length scales. Nevertheless, not all the CORA ratings obtained for each test configuration was high, therefore a degree of caution is needed when we evaluated the influence of a specific parameter. Consequently, the relative assessment of different versions of the same model using CORA may be more pertinent that an absolute evaluation of a specific version. Thus, this method was used during this study for the different versions of the model.

As the current assessment of the model response focused on global response, its ability to predict rib fracture, a common feature in whole body FE models, was not evaluated. Fractures were reported in some tests but not in the point loading of the eviscerated ribcage which is the only load case displaying a sensitivity to a change in ICM material. An interesting contribution of this study will be to report the strain distribution within the ribcage to evaluate the influence of the ICM. Nevertheless, as no experimental data is currently available to evaluate strain distribution biofidelity, it will not possible to assess the capability of the model to appropriately predict the strain distribution in the ribs for these loading cases.

CONCLUSIONS

In the present study, an existing full body model for a seated 50th-percentile male was evaluated under five cases of loading: point loading of the denuded ribcage, frontal pendulum impact tests, lateral and oblique pendulum impact tests and table top tests. The sensitivity of the model to changes in material model of the intercostal muscles (ICM) was evaluated by using two material models: an isotropic linear elastic material model and a foam model defined by a single uniaxial load curve extracted from a recent literature. The performance of these models compared to the experiments was assessed quantitatively through a correlation analysis on the force and chest deflection time histories. The simulations found that that the material properties of the ICM have little effect on the externally measured impact force and chest deformation except in point loading suggesting that the ICM has localized effect. This localized effect may be captured by analyzing the strain distribution in the ribcage.

ACKNOWLEDGEMENTS

The funding for this study was provided by the Global Human Body Models Consortium.

REFERENCES

[1] Carroll, J., et al. 2009. “A comparison between crash test results and real-world accident outcomes in terms of injury mechanisms and occupant characteristics.”
THORAX project GA (218516).
[2] Robin, S.2001. “HUMOS: human model for safety–a joint effort towards the development of refined human-like car occupant models.”
In Proceedings of the. 17th Enhanced Safety of Vehicles Conference.
[3] Iwamoto, M., et al. 2002. “Development of a finite element model of the total human model for safety (THUMS) and application to injury reconstruction.”
In Proceedings of the International Research Council on the Biomechanics of Injury conference.
[4] Kimpara, H., et al., 2005. “Development of a Three-Dimensional Finite Element Chest Model for the 5 (th) Percentile Female”

Stapp Car Crash J. 49: p. 251-269.
[5] Zhao, J. and G. Narwani. 2005. “Development of a human body finite element model for restraint system R&D applications.”
In the 19th International Technical Conference on the Enhanced Safety of Vehicles (ESV).
[6] Song, E., Trosseille, X. and Baudrit P. 2009. “Evaluation of thoracic deflection as an injury criterion for side impact using a finite elements thorax model.”
Stapp Car Crash J, 53: p. 155-191.
[7] Ito, O., Dokko Y., and Ohashi K. 2009. “Development of adult and elderly FE thorax skeletal models.”
SAE Technical Paper.
[8] Vezin, P. and Berthet F. 2009. “Structural characterization of human rib cage behavior under dynamic loading.”
Stapp car crash journal, 53: p. 93-125.
[9] Poulard, D., et al., 2015. “Thoracic response targets for a computational model: A hierarchical approach to assess the biofidelity of a 50th-percentile occupant male finite element model.”
J Mech Behav Biomed Mater, 45C: p. 45-64.
[10] Kemper, A., et al., 2005. “Biomechanical response of the human clavicle subjected to dynamic bending. “
Biomedical sciences instrumentation, 42: p. 231-236.
[11] Duprey, S., K. Bruyere, and J.-P. Verriest, 2008. “Influence of geometrical personalization on the simulation of clavicle fractures.”
Journal of biomechanics, 41(1): p. 200-207.
[12] Charpail, E., et al., 2005. “Characterization of PMHS Ribs: A New Test Methodology.”
Stapp car crash journal, 49: p. 183-198.
[13] Li, Z., et al., 2010. “Rib fractures under anterior–posterior dynamic loads: experimental and finite-element study.”
Journal of biomechanics, 43(2): p. 228-234.
[14] Li, Z., et al. 2010. “Development of finite element model of 50th percentile male using multiblock hex meshing approach.”
In Proceedings of the 6th Annual World Congress on Biomechanics, Singapore.
[15] Guo, B.-y., et al.,2007. “Age and gender related changes in biomechanical properties of healthy human costal cartilage.”
Clinical Biomechanics, 22(3): p. 292-297.
[16] Forman, J.L., et al. 2010. “The contribution of the perichondrium to the structural mechanical behavior of the costal-cartilage. “
Journal of biomechanical engineering, 132(9): p. 094501.
[17] Yamada, H. and F.G. Evans, 1970. “Strength of biological materials.”
[18] Farkas, G.A., 1991. “Mechanical properties of respiratory muscles in primates. “
Respiration physiology, 86(1): p. 41-50.
[19] Kelly, N.G., R. McCarter, and G. Barnwell, 1993. “Respiratory muscle stiffness is age-and muscle-specific.”
Aging Clinical and Experimental Research, 5(3): p. 229-238.
[20] Kindig, M., et al., 2015. “Effect of intercostal muscle and costovertebral joint material properties on human ribcage stiffness and kinematics.”
Comput Methods Biomech Biomed Engin, 18(5): p. 556-70.
[21] Hamzah, M., et al. 2013. “An Inverse Finite Element Approach for Estimating the Fiber Orientations in Intercostal Muscles.”
In Proceedings of the Impact Research Council on the Biomechanics of Impact (IRCOBI). Gothenburg, Sweden.
[22] Gayzik, F.S., et al., 2009. “A multi-modality image data collection protocol for full body finite element model development.”
SAE Technical Paper.
[23] Kindig, M.W., et al., 2010. “Structural response of cadaveric ribcages under a localized loading: stiffness and kinematic trends.”
Stapp Car Crash J, 54: p. 337-80.

[24] Kroell, C., D. Schneider, and A. Nahum, 1971. "Impact tolerance and response of the human thorax, in biomechanics of impact injury and injury tolerances of the thorax-shoulder complex."
SAE paper 710851.
[25] Lebarbé, M. and Petit, P. 2012. "New biofidelity targets for the thorax of a 50th percentile adult male in frontal impact."
In Proceedings of the Impact Research Council on the Biomechanics of Impact (IRCOBI).
[26] Shaw, J.M., et al., 2006. "Oblique and lateral impact response of the PMHS thorax. "
Stapp Car Crash J, 50: p. 147-167.
[27] Kent, R., Lessley, D. and Sherwood, C. 2004. "Thoracic response to dynamic, non-impact loading from a hub, distributed belt, diagonal belt, and double diagonal belts. "
Stapp Car Crash J, 48: p. 495-519.
[28] Gehre, C., Gades, H. and Wernicke, P. 2009. "Objective rating of signals using test and simulation responses."
In Proceeding of the 21st International Technical Conference on the Enhanced Safety of Vehicles, Stuttgart, Germany.

IMPLEMENTATION OF NEW RIB MATERIAL MODELS TO A FE-HUMAN BODY MODEL FOR EVALUATION OF THE PRE-SAFE IMPULSE SIDE RESTRAINT SYSTEM FOR SIDE IMPACT PROTECTION

Markus Hartlieb
Christian Mayer
Julien Richert
Abdulkadir Öztürk
Florian Mayer
Daimler AG
Germany

Satyajit Pal
Ravikiran Chitteti
Mercedes-Benz Research and Development India Pvt. Ltd
India

Paper Number 15-0373

ABSTRACT

„Integrated“, „Smart“ and „Individual“ are new characteristics of future safety systems. Furthermore, side crashes are still dominant in terms of high injury risk for car occupants and are predicted to become even more relevant in future. Earlier studies on pre-conditioning the occupant during pre-crash phase have shown the potential to reduce injury risk in such accident scenarios. To evaluate and optimize such advanced safety systems to provide a high safety level for the occupant, finite element human body models were used. Especially integrated safety systems which interact with the occupant in the pre-crash phase require these new and supplementary evaluation tools.
With specific focus on the use case, the thorax and rib material of the FE human body model THUMS-D were modified and validated. Two different rib material properties have been defined for two different age groups, one for the young population and one for the elder population based on quasi static and dynamic 3-point bending test setup. Furthermore, a damage model for the rib fracture was created and implemented to the THUMS-D model. The validation process of the complete thorax followed pendulum impact standards set by GESAC 2005 and ISO/TR 9790:1999.
Finally the PRE-SAFE Impulse Side system was evaluated and optimized applying this upgraded THUMS-D model in FE car crash environment.

INTRODUCTION

As a tool for the development and also the assessment of particularly secondary safety systems, dummies have been used over the last 50 years – successively updated in terms of mechanical design, injury criteria and, slightly with respect to “individual” characters (5th female, child dummies, etc.)

As of today, numerical models of these dummies are a common technology. As a next step in the field of numerical simulation, validated human models will be used as a supplemental tool to investigate the biomechanical impact of restraint systems more in detail. Those models offer the opportunity to study effects in body parts that are currently not addressed by common anthropomorphic dummy technology, especially if the pre-crash phase has to be considered.

Analyses of the injury patterns in real crashes reveal that there is still potential to improve loads on the thorax. In order to better understand mechanisms leading to a certain injury risk, a valid representation and

characterization of material properties and injury mechanisms in this development tool is necessary to assess and optimize new restraint systems. Especially improvements in the prediction capability for risk of rib fractures in elderly population with THUMS-D motivated the experimental and simulation work which is described in the following sections. Finally, this modified THUMS-D was used to optimize an advanced pre-crash side protection system.

METHODS

Human Body Model

Mercedes-Benz is already using this integral simulation tool in the standard development process. In this study, a modified THUMS (Total Human Model for Safety) model was used. THUMS (AM50) was originally developed by Toyota Motor Corporation & Toyota Central R&D Labs, Inc. and meanwhile several THUMS base models (AF05, AM50, AM95) and derivatives are released respectively published [1]. The model used within Mercedes–Benz is based on the original THUMS versions V1.X and V3 and was continuously improved on several body parts in recent years and is therefore referred to as "THUMS-D" [2,3].

Experimental work

The entire thorax shape, bone structure and material properties of the ribs are changing over the lifespan. Several studies and research activities were published or initiated in recent years whitin this topic [4, 5]. Almost all authors agree that the stiffness of ribs decrease the older the person is. In other words, the risk for a rib fracture is increasing.

Nevertheless, age specific models which allow also a realistic modeling of a fracture behaviour are currently not existing. Therefore, an experiemental study was initated in collaboration with our scentific partner Technical University Graz to investigate and discuss relevant material properties and characteristics of human ribs for the derivation of constitutive laws and fracture modeling under FE code respectively for implemetation to THUMS-D.

1st test phase - 3-point bending – correlation bone density, age and geometrical parameters

Within a first series of experiments to derive biomechanical charcteristics of young and elderly car occupants, force-displacement curves were determined for human ribs in different areas (anterior, lateral and posterior).

Rib samples were obtained from four female and three male post-mortem human subjects (PMHS) which donated their body for reserch. One female PMHS was at the age of 32 – the male PMHS was 37 years old. All other subjects in the sample were in age range of 58 – 78 years. In this first series of experiments, the rib samples with a length of approx. 70 mm were taken from three, the anterior, lateral and posterior region of a rib. For each sample, the geometric dimensions (width, height, curvature height, cross sectional area) and the bone density was determined. Within this study the DXA method (Dual-X-Ray absorptiometry) was applied. It has to be stated, that the DXA method provides an "areal density" (mass / area, e.g g / cm^2). It does also not destinguish betrween cortical and trabecular bone structures.

The rib ends were potted in a 30mm x 30mm cylindrical sleeve (aluminum) and then tested in 3-point bending set up. Quasistatic load was applied in max. 11 cycles (hysteresis mode) starting with 30 N and complete unloading after each cycle. Results were discussed with specific focus on correlation of the geometic parameters, the bone density and age of the PMHS.

The following general findings and correlations were derived in this 1st test series. More details and an extensive discussion of the results could be found in the publication of Tomasch et.al. [6]:

- The bone density (BMD – Bone Mineral Density – g/cm^2) increases from sternum to vertebra region. (within sample a 1.39-fold increase was found on average).
- Ribs from younger PMHS showing 1.8 times higher density compared with rib samples from elderly persons on average.

- Gender specific differences are also observed: Measured bone density of male ribs were consistently higher compared with density of female ribs – but both sexes showing comparable increase of bone density values from sternum to vertebra.
- The height and cross sectional area of the ribs also increasing from anterior to posterior. These paramters decrease with age.
- Ribs samples from young, male PMHS could withstand approx. three times higher loads compared to rib samples from elderly, female persons.
- All specimen respectively tested ribs (young and elderly) showed a distinctive post-chracking behaviour. Force remains on more or less constant level until load was reduced (approx. at fourfold of the displacement of failure load).

2nd test phase - 3-point bending for failure modelling and dynamic impactor testing

28 middle ribs (mainly 3 – 6, partly 2 and 10-11) were obtained from four female PMHS. Three of them between ages of 59 and 65 – one 32 years old. Within the second series of experiments, the quasi-static 3-point bending test set up was slightly modified with regard to the length of the rib specimen and its support condition (now clamped firmly). The main focus of these experiments and especially of the further processing of the results was among the determination of the material properties on the faithful reproduction of the behavior at rupture and also the observed post-cracking mechanism of rib bones.

Figure 1 shows the test set-up of the second test phase at maximum displacement of the impactor. For the quasi-static test set up the movement speed was 100 mm/min with a total displacement range of 30mm to generate a loading on the rib until fracture. The force vs. deflection curve was collected and additional the experiment of each rib was recorded by a camera.

The force-defelction diagram in Figure 1 shows typical behaviour of elderly and yonger rib specimen as it was observed this second test phase. In principle the main characteristics of the curves are comparable with the 1st test phase. The rib bone shows a kind of elastic stiffness at the beginning of test. The curves of the yonger rib specimen are consistently steeper and e therfore indicat higher stiffness. Also in this test series rib samples from younger PMHS shown failure at approx. threefold load level compared with the sample from the elderly – also similar post-crack behavior was observed.

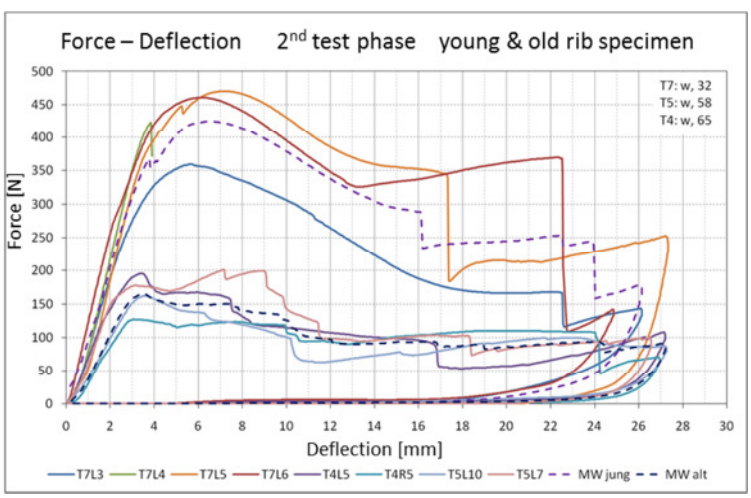

Figure 1: Typical Force-Deflection of elderly and younger rib specimen observed in this load case.

The findings of the 2nd series of experiments (quasi-static) could be summarized as follows:

- Rib specimen with similar dimensions showing quite comparable elatic behaviour – this applies for rib sample from younger and elderly.
- Ribs samples from young PMHS (female) withstand approx. two to three times higher loads compared to rib samples from elderly (female) .
- Stiffness (elastic curve section) of younger ribs is significantly higher

Based on these results and the derivation of a material model (see next pharagraph) also a validaten under dynamic loading was conducted. Focus of this study was to confirm the material model and parameters for the elastic behaviour on the one hand and for fracture on the other hand. For this, a DOE (Design Of Experiment) study was carried out based on FE-Simulation of the dynamic 3-point bending test set up. The fracture or no-fracture behavior of a rib specimen was predicted for a certain combination of test parameters respectively an impactor mass and velocity. The rib samples were as well pottet on both ends and clamped firmly in a test rig. The results were finally also plotted into the DOE diagram and corresponde well (final material properties) with the predicted behavior. Nevertheless, it has to be stated, that for this additional dynamic study only ribs from the elderly (59), female PMHS were available. So this addresses already some limitations within this study respectively for this validation.

Rib material model and failure modelling of rib fracture

The results respectively force-deflection curves from mainly the second test series were now discussed to be transferred into a constitutive law and finally a material destription to be used within the LS-Dyna code. As already described in previous paragraph, the rib bone shows an elastic stiffness at the beginning of test (Figure 2). At the end of the elastic material behavior the rib starts to get locally deformed while the test curve shows an elasto-plastic material behavior attended with a material hardening. At this point the bone starts to get a fibrous fracture at the force application point followed by an extension of the fracture along the rib in the closer area. The test curve shows a continuous elasto-plastic fracture behavior with a steady reduction of the stiffness.

To regulate the elastic range of a response curve (section a in figure 2), the Young's modulus as contributing factor had to be adjusted to the test results in terms of the Hooke's law. For adjustment of non-linear hardening in the elastic-plastic range at the peak (section b in figure 2), the effective plastic strain values (EPS) and corresponding yield stress (ES) are the parameters to control this behavior. The third part of the response curve (section c in figure 2) shows an elastic-plastic behavior combined with a softening of the bone. This softening is now realized and controlled by a modulated failure flag in the material properties which limits the maximum plastic strain at 6.8% and conduct elements deletion of the shell elements (cortical bone). It has to be noted, that the threshold respectively failure flag of 6.8% is strictly model dependant. In case of any modification in mesh or use in other models this threshold is not valid and has to be refined against the original test data. The material properties of the cortical rib bone are defined in MAT_24 similar to the current THUMSD v3.2, but with different parameter values. One of the most essential adjustments was the change of the Young's modulus from 18 GPa to 3.5 GPa (Yong Rib Material) and 1.5 GPa (Old Rib Material). Also the definition of the trabecular bone has been changed from MAT_12 to MAT_1 what is defined as elastic material behavior.

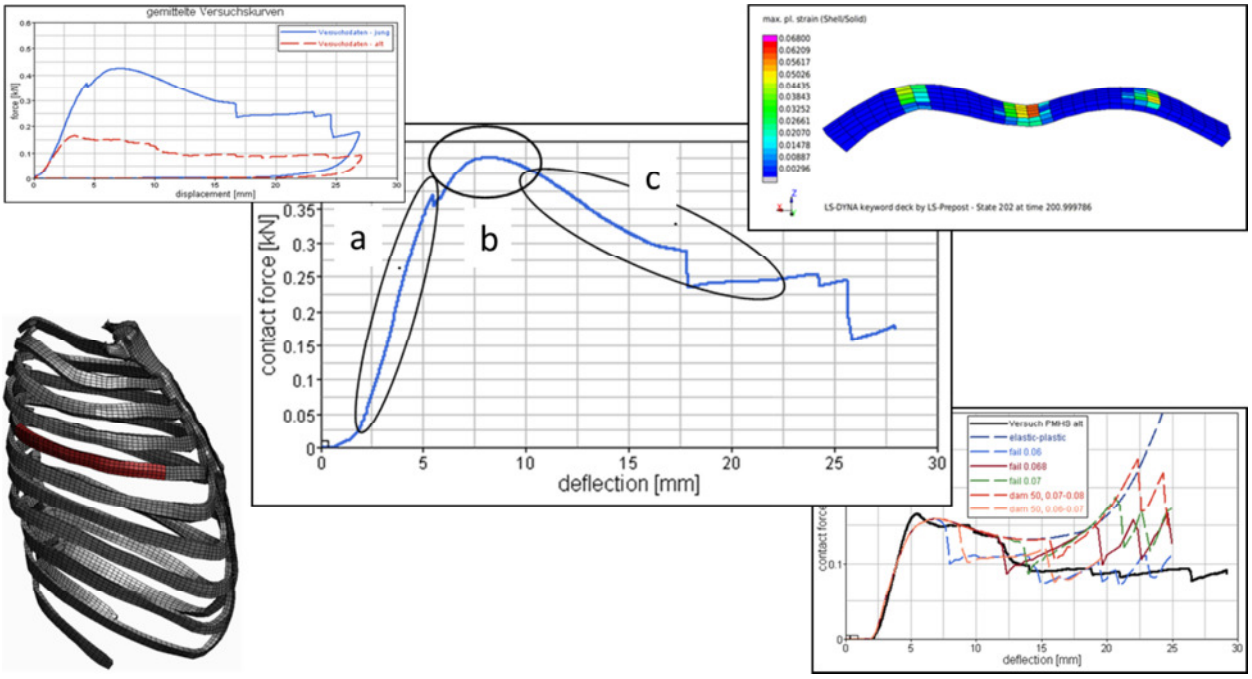

Figure 2: Rib material model and failure modelling of rib fracture – Top Left: averaged test data of elderly and younger rib specimen – Centre: characterization of test curve segments; elastic (a), elastic-plastic/hardening (b), elastic-plastic/softening (c) – Bottom Right: determination of damage parameter.

Validation against GESAC 2005 & ISO/TR 9790

The validation of the complete THUMS-D with new rib materials comprises the frontal pendulum impact tests defined by GESAC 2005 [7] and the lateral and oblique-lateral pendulum impact tests defined by ISO/TR 9790 [8].

The study on fracture mechanism showed a significant difference between the Young Rib Material (NRy) and the Old Rib Material (NRo) in terms of material behavior and predicted risk of rib fractures. The NRy performs considerably more elastic than the NRo what reflects an embrittled bone material of the elder population. A comparison with the Number of Fractured Ribs (NFR) documented in ISO/TR 9790 for lateral, low speed oblique-lateral and high speed oblique-lateral PMHS tests shows a good correlation to the predicted rib fractures given by simulatios with NRy and NRo (Figure 3).

- The NFR in 4.3 m/s lateral impact PMHS tests have a range of 0 to 7. The model with NRy predicts no risk on any rib while NRo predicts a risk on 6 ribs including 2 of them with a high fracture risk.
- For the low speed oblique-lateral impact tests on PMHS showing 0 to 2 fractured ribs on impact side and 0 fractured ribs on the opposite side. THUMSD with NRy predicts a relatively low risk for 1 rib on impact side. The model with NRo predicts 6 ribs with a risk thereof 2 to 3 with an advanced risk.
- The high speed oblique-lateral impact tests on PMHS showing 2 to 7 fractured ribs on impact side and 0 to 3 on the opposite side. The model with NRy predicts 6 ribs thereof 2 with advanced risk on the impact side. The model with NRo predicts 8 ribs thereof 6 multiple and 4 with critical risk on the impact side, additional 1 rib with an advanced risk on the opposite side.

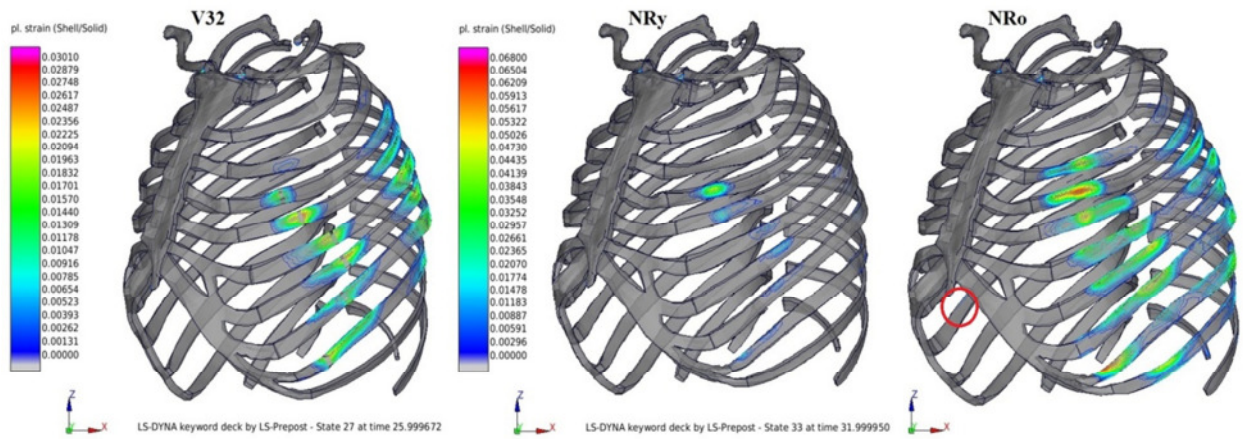

Figure 3: Fringe plots / results ISO/TR 9790 load case oblique pendulum impact 6.7 m/s; plastic strains; From left: Rib material original THUMSD (V32), Young rib material (NRy), Old rib material (NRo).

Discussion

Two new rib material models and properties, for younger population (NRy) and for elder population (NRo), were defined for the use with LS-Ddyna code based on human rib specimen tests by TU Graz. With reference to the pendulum impact results for validation, NRy and NRo are showing an improved chest response of the entire THUMSD. The outcome of this is an improved but still amendable chest response on frontal pendulum impacts, an acceptable performance on lateral pendulum impacts and a good performance in the oblique-lateral impact tests which motivated finally the application within the loadcase and system development which will be presented in the following paragraphes.

Nevertheless, it is important to note, that several limitations arise from the biomechanical testing and modelling. The biomechanical test data is limited to three elderly female and two elderly male PMHS. The data for the younger population is just based on one male and one female subject. Within the modelling and validation part no change of the thorax shape and its changes over lifespan was realised. Also the modeled fracture mechanism just reflects the results of the 3-point bending test set-up.

APPLICATION PRE-SAFE® IMPULSE SIDE:

In this chapter, the newly validated Human Body Model will be used in the development of a new generation of integral safety restraint systems: PRE-SAFE® Impulse Side.

System description PRE-SAFE® Impulse Side

Theory PRE-SAFE® Impulse Side is the very first of a new generation of pre-impacting restraint systems whose field of action will be extended prior to the collision thanks to the integration of active and passive safety [9].

The specifics of the vehicle structure in a lateral impact make it necessary to use all available space to reduce the loads to the occupants. Structural measures, the right material choice and the use of tailored side impact restraint systems like side airbags or curtain airbags describe state of the art protection measures. But what if there were more space available to take efficient mitigation countermeasures without increasing the car body dimensions? That is the idea of PRE-SAFE Impulse Side.

The new PRE-SAFE® Impulse Side restraint system aims at creating more space between occupant and car interior/structure only when needed i.e. right before a crash event occurs. As a result, the side airbag could better deploy, the contact with the intruding structure might occur later, so that more crash energy could be dissipated by the vehicle structure deformation before the gap between structure and airbag is being closed.

But PRE-SAFE® Impulse Side is not only increasing the space between occupant and side structure. Indeed, PRE-SAFE® Impulse Side also actively pre-accelerates the occupant toward the middle of the car. As a result, the occupant has already been set in motion when the collision begins, in other words the relative velocity between occupant and intruding structure has been reduced.

Maximizing the distance and reducing the relative velocity between occupant and intruding structure can significantly reduce the occupant loads especially in the thorax region.

Functional implementation Inflating a specifically designed air bladder in the seat rest side bolster creates the impulse that is needed to move the occupant.. The activation time has to be precisely calculated using information of the car surroundings gathered by camera and/or radar sensors.

Through the light impulse, the occupant is being moved towards the center of the vehicle prior to the predicted impact (Figure 4).

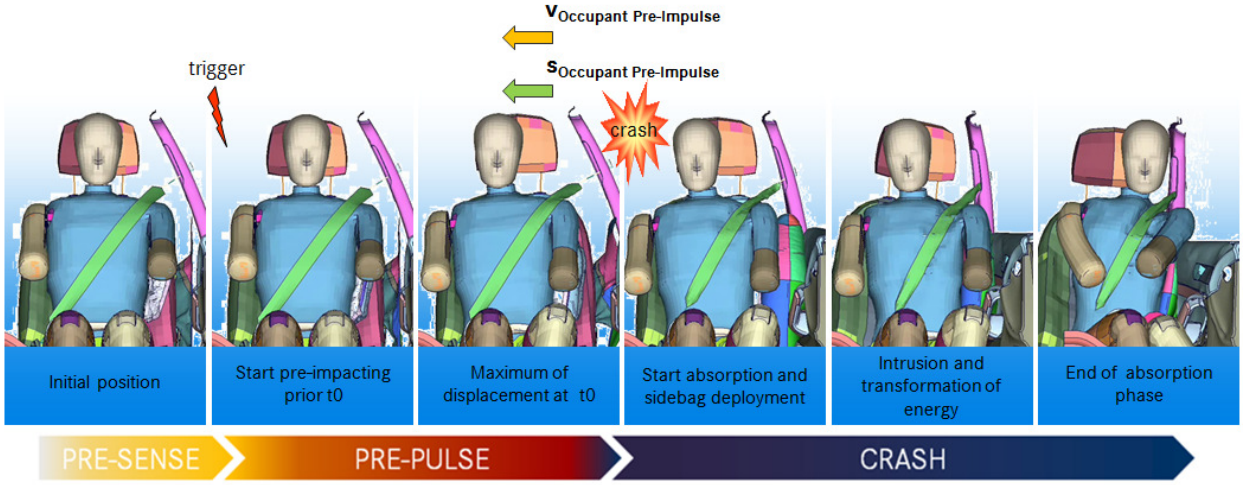

Figure4: PRE-SAFE® Impulse Side way of action

PRE-SAFE Impulse Side safeguarding

In contrast to traditional irreversible restraint systems, the deployment decision for the PRE- SAFE® Impulse Side bladder is based on surround sensing information gained from radar sensors [9]. As a result, there is a minimal chance of system activations remaining even though the collision could be avoided in the last moment. Therefore, the system characteristics were designed to meet the conflicting targets of both providing the required- impulse to the occupant and being gentle enough in the deployment not to harm any person in the seat.

The safeguarding assessment of the system was done by simulating a static deployment of PRE-SAFE® Impulse Side using THUMS-D with modified rib material representing elderly persons. After PSIS triggering, the HBM displacement as well as rib compression, stress and strain were measured (Figure 5).

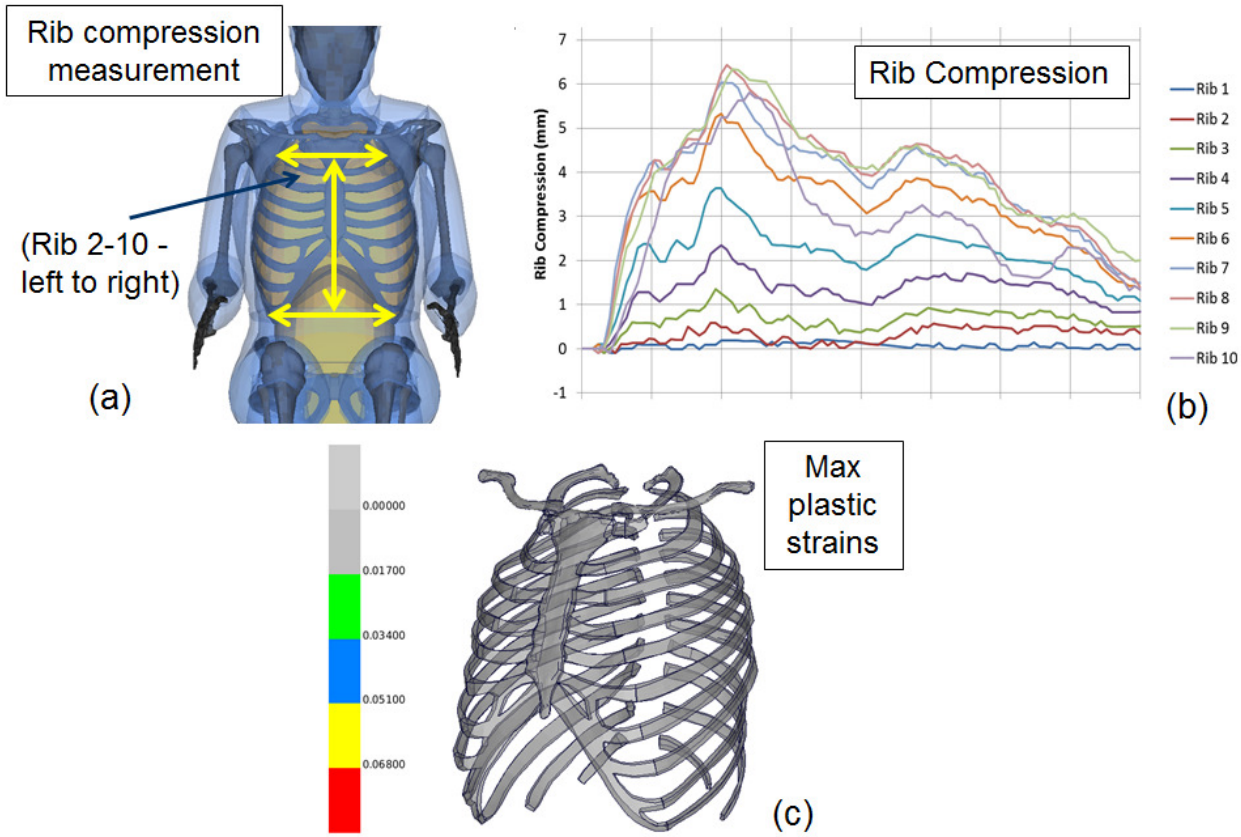

Figure 5: Definition of relative rib compression (a) relative rib compression measurement (b) and fringe plot of plastic strains(c) of the ribs

Fig.5b shows that the highest compression takes place at the lower ribs (7, 8, 9) exactly at the height of the PSIS air bladder. As can be seen on the diagram, the maximal compression does not exceed 6,5mm. Analysis of the maximal rib strains shows almost no plastic strains (c). As the fracture limit of the rib model is set to 6,8% plastic strain, the THUMS-D model is not predicting any fracture risk by an activation of PRE-SAFE® Impulse Side.

Dynamic Results

After having assessed the safeguarding of the system in a given static case, the following section describes its protection potential in a barrier load case using a full scale car crash simulation model. HBM was used to configure the system by determining the optimal time to deploy – frequently referred to as ttf (time to fire). The baseline simulation model was built using a carline achieving very good results in both European and US side crash ratings. The simulation was run with THUMS-D model with newly validated rib material (NRo).

In full scale vehicle crash tests using side impact dummy, the PSIS system has already shown the potential to reduce the measurements of the rib cage significantly with up to 20-30% decreased rib deflection values. The goal of the following CAE activity was to confirm this result using HBM. It is commonly accepted that absolute values of measurements obtained by anthropomorphic test devices cannot be directly compared to calculation results derived from HBMs. Therefore, relative values like the movement in Y direction of two nodes at the most outer position of each rib on Y-axis of each rib were used (6a). Additionally, maximal plastic strains of the ribs were estimated in order to assess the risk of rib fracture in a lateral collision with and without PSIS. The results concerning rib compression and thorax strains are plotted in Fig. 6.

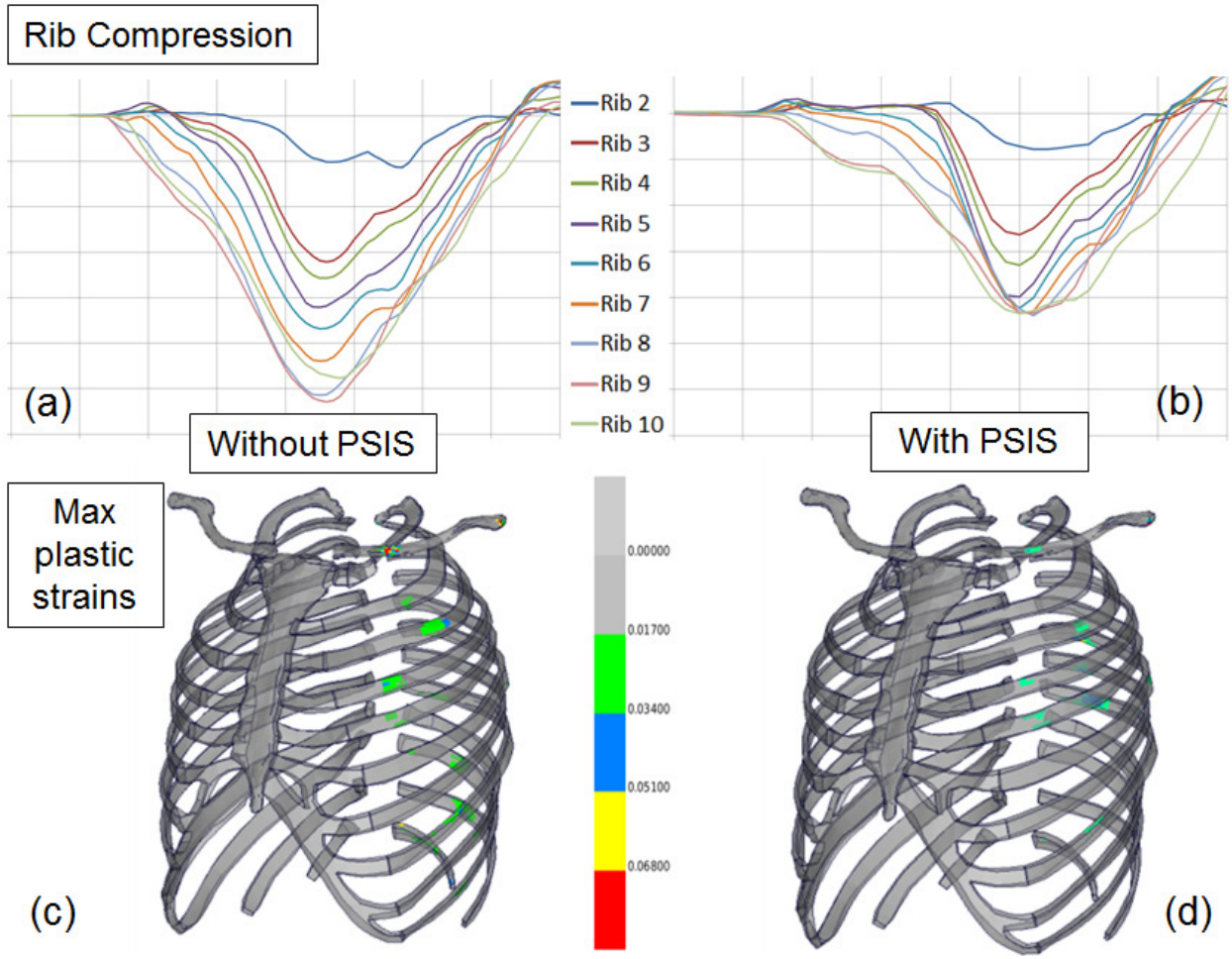

Figure 6: Rib compression measurement without (a) and with PSIS (b), maximum plastic strains without (c) and with (d) PSIS.

The calculated rib compression shows a significant reduction of the thorax load when the PSIS system is used, especially for ribs situated directly next to the air bladder. An average reduction of the rib compression by 20% was achieved.

As stated earlier in the paper, the new rib material was implemented with a failure flag when plastic strain exceeds 6,8 %. Using this limit, the simulation without PSIS indicates a possible rib fracture (red flag on Fig.6c). A reduction of the calculated max. plastic strains can be achieved while triggering PSIS system. Max. plastic strain is not exceeding 4%, leading to a significant decrease of the rib fracture risk when PSIS is used.

CONCLUSIONS

It is challenging to verify the effects and to show the whole potential of advanced restraint systems with traditional CAE tools. Therefore, the methodology shown in this paper was developed to assess the effects of a new generation of pre-impacting restraint systems. Regarding safeguarding and system optimization, a newly validated HBM with improved prediction capability for risk of rib fractures in elderly population was used to assess the PRE-SAFE Impulse Side system. The use of this new HBM was important towards the development of the system showing that the system remains harmless in case of unmotivated activation. Furthermore, the optimal triggering time of the PSIS System, found using anthropomorphic test devices, has been confirmed by

HBM simulations. In the investigated load case, both hardware tests and HBM simulations show a significant reduction of thorax load by using PSIS.

ACKNOWLEDGEMENTS

The authors wish to acknowledge our scientific partners of the Technical University Graz and the DYNAmore GmbH, which contributed to this research with their specific expertise.

REFERENCES

[1] Kitagawa, Y. and Yasuki T. "Development and Application of THUMS Version 4". Proceedings of CARHS 5th International Symposium Human Modeling and Simulation in Automotive Engineering; Oct 16th-17th, 2014; Munich.
[2] Gupta A.K., Sharma G., Shah P., Ageorges C., Mayer C. "Development of an anatomically-correct finite element model of the human shoulder". Proceedings of IRCOBI Conf. , IRC-11-58, 2011, Krakow.
[3] Doerfel S., Zhou K., Sharma G., Mayer C., Peldschus S. "Development of FE models of clavicular ligaments: quasi-static tensile test and FE simulation". Proceedings of IRCOBI Conf. , IRC-12-71, 2012, Dublin.
[4] Reporting THORAX project, "Thoracic Injury Assessment for Improved Vehicle Safety", www.thorax-project, 2009-2012, European Commission DG RTD, FP7 Theme 7,Transport-SST.2007.4.1.2.
[5] Agnew A.M., Moorhouse K., Murach M., White S.E., Kang Y-S, "Tensile Stress in Human Ribs throughout the Lifespan". Proceedings of IRCOBI Conf. , IRC-14-44, 2014, Berlin.
[6] Tomasch E., Sinz W., Kirschbichler S., Steffan H., Darok M., Patsch J., Dimai H.P., "Korrelation von Knochendichte und Rippenfrakturen"; EVU 2011-8 ; 20th EVU Conference, 2011, Graz.
[7] GESAC, Biomechanical Response Requirements of the THOR NHTSA advanced frontal Dummy. Trauma assessment device development program. 2005.1 ed: GESAC - Gerneral Engineering and Systems Analysis Company; 2005.
[8] ISO, ISO TR 9790 - Road Vehicle - Anthropomorphic side impact dummy - Lateral impact response requirements to assess the biofidelity of the dummy. vol. ISO/TR 9790:1999(E) Geneva (CH)1999. p. 145.
[9] Marica Paurevic, Prof. Dr. Rodolfo Schöneburg, Dr. Julien Richert, Ralf Bogenrieder - Daimler AG, 2014. "PRE-SAFE® IMPULSE SIDE: A PREVENTIVE PRE-IMPACTING RESTRAINT SYSTEM" In Proceedings of the 12th International Symposium and Exhibition on Sophisticated Car Occupant Safety Systems, Airbag 2014 (Karlsruhe Dec. 1-3), #14

AIMING FOR AN AVERAGE FEMALE VIRTUAL HUMAN BODY MODEL FOR SEAT PERFORMANCE ASSESSMENT IN REAR-END IMPACTS

Karin Brolin
Jonas Östh
Mats Svensson
Chalmers University of Technology
Sweden

Fusako Sato
Koshiro Ono
Japan Automotive Research Institute
Japan

Astrid Linder
Swedish National Road and Transport Research Institute, VTI
Sweden

Anders Kullgren
Folksam
Sweden

Paper Number 15- 0247

ABSTRACT

The female part of the population suffers more Whiplash Associated Disorders (WAD) in car crashes than males. Several studies have illustrated the need to consider the female population when developing and assessing the WAD prevention performance of advanced restraint systems in rear-end collisions. Presently only one crash test dummy is available, the average sized male BioRID. Recently a virtual dummy model of an average female, EvaRID, was developed and used in rear impact simulations. The results stressed the need for models representing the female part of the population, as well. Virtual crash simulations have become essential in traffic safety and with models of both an average male and female, further steps in addressing improved assessment of WAD prevention can be taken. The present paper presents a starting point of research aiming to develop an open-source average female Finite Element (FE) model with an anatomically detailed cervical spine. This paper provides a review of the literature to identify gender specific neck biomechanics and anatomical differences, followed by a review of published FE models of the cervical spine.

Data on vertebral body dimensions (height, width, depth, spinal canal diameter, facet joint angles) have been compiled from biomechanical literature. Significant gender differences exist for the vertebral body depth and width, the spinal curvature in the seated posture, and the spinal stiffness and range of motion. All have the potential to influence the outcome of an impact and should be accounted for in the development of WAD prevention.

The review of FE models of the cervical spine presented 17 models based on male geometry but only one model scaled to represent a female. An overview of the models are given with respect to the solver, geometry source, number of elements, and implementation of the facet joints, ligaments, and muscles. It is recommended that an average female model is developed with focus on; 1) the shape of the female vertebral body, especially the depth and width that provides less support area than for males, 2) defining the spinal curvature representative of seated female volunteers who generally display less lordosis than males, 3) the dimensions of the spinal ligaments, rather than the material properties, to capture the larger range of motion and less spinal stiffness of female subjects compared to males, and 4) validation to female volunteers and PMHS tests for range of motion, while failure prediction seem less gender sensitive.

KEYWORDS**:** Whiplash Associated Disorders, gender, biomechanics, finite element human body model

INTRODUCTION

Whiplash Associated Disorders (WAD) is the common denomination for a range of neck related symptoms that typically occur in vehicle collisions. During a rear-end collison, the torso of a properly restrained occupant will be accelerated while the head tends to lag behind causing inertial loading to the neck. This loading causes a so called whiplash motion of the neck in which the neck is forced into an unphysiological s-curved shape that later evolves into a c-shape (Ono et al, 1997). For example, in Sweden WADs account for ~70% of all injuries leading to disability due to vehicle crashes (Kullgren et al. 2007). The majority of victims experiencing initial WAD symptoms recover within a few weeks or months of the crash (The Whiplash Commission 2005), however, 5–10% of individuals experience different levels of medically classified permanent disabilities (Nygren 1983, Krafft 1998, The Whiplash Commission 2005). WADs occur at relatively low velocity changes, typically <25 km/h (Eichberger et al. 1996, Kullgren et al. 2003), and in impacts from all directions, although rear impacts are most frequently featured in accident statistics (Watanabe et al. 2000). Since the mid-1960s, injury statistical data have shown that females have a higher risk of sustaining WAD than males, even in similar crash conditions (Narragon 1965, Kihlberg 1969, O'Neill et al. 1972, Thomas et al. 1982, Otremski et al. 1989, Maag et al. 1990, Morris & Thomas 1996, Dolinis 1997, Temming & Zobel 1998, Richter et al. 2000, Chapline et al. 2000, Krafft et al. 2003, Jakobsson et al. 2004, Storvik et al. 2009, Carstensen et al. 2012). According to these studies, WAD risk is 1.4 to 3 times higher for females compared to males.

Currently rear impact tests are performed using the only available dummy developed for low severity testing, the Biofidelic Rear Impact Dummy, BioRID II (Davidsson et al. 1999), which represents a 50th percentile male. The BioRID II is used in test protocols, i.e. Euro NCAP, for assessing the risk of whiplash injuries when seated in the front seat. The BioRID was developed in the late 1990s to evaluate the protective performances of car seats in low severity rear impacts. However, real world accident analysis has shown that seats designed to prevent WAD are more effective for males (Kullgren et al., 2013). Therefore, there is an urgent need to better represent the whole adult population in the development and assessment of WAD prevention systems and develop models representing females, as well as males for assessing the prevention performance.

The initial step in the work towards addressing WADs in females was recently taken in the ADSEAT project (Linder et al. 2013) that adopted a broad approach when developing the world first average female virtual dummy model, EvaRID (Carlsson et al. 2014). Virtual impact simulations with seats showed, using the virtual male and female dummy models, that differences were found in the response of the BioRID II and EvaRID models for some of the seat concepts tested (Linder et al 2013). Furthermore, a prototype dummy of an average female was developed and run in the same test set-up as the Euro NCAP tests performed with the BioRID II (Schmitt et al. 2012). Four different seat types were tested and the results confirmed that the size of males and females interact differently with the seat and the head restraint. Based on the dummy responses, male and female occupants would thus obtain different levels of protection when seated in the same seat. Hence, having access to models of both an average male and female, further steps in addressing improved assessment of WAD prevention can be taken. Virtual models offer a greater variety of seated postures and the potential to evaluate a wider range of parameters, compared to what is practically possible in physical testing.

Virtual crash simulations using the Finite Element (FE) method has become an essential tool in traffic safety and with increasing computer capacity the size and complexity of the models has increased. Traditionally, FE occupant models were virtual copies of crash test dummies but more recently there has been a strong progression in the development of Human Body Models (HBMs). The latter have been designed to represent the human body rather than a dummy and have the potential to allow for much more detailed studies of injury mechanisms than physical or virtual dummies. A number of occupant HBMs have been released, primarily of the average male anthropometry, but are not widely used due to a number of reasons such as model quality, restricted availability or high licencing fees. Therefore, the need for open source models where knowledge and experience can be shared and continued improvements of the models can be provided by any user is apparent. Our overall aim is to develop an open-source FE model of an average female, with an anatomically detailed cervical spine suitable for assessment of seat performance.

This paper provides a review of the literature to identify gender specific neck biomechanics and anatomical differences followed by a review of published FE models of the cervical spine. Lastly, a short complementary discussion presents the conlusion on requirements for the development of an average female HBM. The resulting

recommendations have the potential to improve the biofidelity of female HBMs and thereby enhance the development and assessment of safety systems that can reduce the incidence of WAD in traffic accidents.

INJURY MECHANISMS

Despite much research, WAD is still one of the most poorly understood traffic injuries. Literature supports an organic basis for WADs (Siegmund et al. 2009; Curatolo et al. 2011). Several anatomical sites have been proposed, including, facet joints, spinal ligaments, intervertebral discs, vertebral arteries, dorsal root ganglia, and neck muscles. Each of these tissues is strained during a whiplash motion exposure. Two mechanisms of facet joint lesions have been proposed: pinching of the synovial fold and excessive capsule strain. The cervical vertebrae have been shown to rotate about an elevated instantaneous centre during whiplash motion in a rear-end collision. This may compress the posterior facet surfaces, pinching the synovial fold (Ono et al. 1997; Kaneoka et al. 1999). Excessive facet capsule strain has been demonstrated during rear-end collision whiplash motion experiments where, in a functional cervical spinal unit, the upper vertebrae was exposed to excessive rearward shear (Pearson et al. 2004; Yang and King 2003). Lesions to the other neck ligaments and intervertebral discs have been reported by Krakenes and Kaale (2006), for instance. Ligament lesions may cause acute neck pain and lead to chronic spinal instability. Lesion to mechanoreceptors may corrupt the normal sensory signals and can lead to abnormal muscle response patterns, decreased neck mobility and proprioception (Panjabi et al. 2006).

Chronic symptoms such as headache, blurred vision, tinnitus, dizziness, and vertigo have been proposed to be associated with altered blood flow rates due to spasm and/or narrowing of vertebral arteries in WAD patients (Reddy et al. 2002; Seric et al. 2000). Intimal tears of the vertebral artery are most common at the atlanto-axial joint. This has been hypothesized to be caused by coupled extension and axial rotation of the upper cervical spine. Also, many WAD symptoms could be explained by lesion to the dorsal root ganglia that contain the cell bodies of most peripheral sensory nerves, at each spinal level. Increased electrical activity in the spinal cord and widespread reductions in electrical and pressure thresholds after whiplash motion exposure suggest altered central pain processing (Banic et al. 2004, Curatolo et al. 2001, Kasch et al. 2001a, Scott et al. 2005). During whiplash motion, pressure transients have been registered in the spinal canal (Örtengren et al. 1996, Svensson et al. 2000). These are hypothesized to be the cause of spinal ganglion nerve cell membrane dysfunction. Direct deformation of the nerve roots is another possible cause as the diameter of the neural foramina decrease during extreme neck motions.

Muscle pain is a common WAD symptom, although evidence of direct lesions in muscles remains inconclusive. Direct muscle lesions may not be responsible for chronic pain, but may play an indirect role in modulating pain caused by injuries to other structures. The direct mechanism of muscle lesions occur due to imposed lengthening during active contraction. Both anterior and posterior muscles experience active lengthening (Brault et al. 2000; Vasavada et al. 2007). Neck muscles interact with other anatomical sites: 1) they attach to the facet capsule; 2) they indirectly load other neck structures; and 3) altered neuromuscular control may contribute to chronic pain.

For each of the above mentioned tissues, continued research is needed to help improve diagnosis and treatment. Simulations with HBMs can help shed light on the strain in different neck tissues during the multitude of different loading scenarios that occur in traffic accidents and are known to produce WADs. Also, in order to assess the protective properties of vehicle seats and other safety systems it is necessary for the HBMs to be detailed enough to provide metrics for all or at least most of the above mentioned injury mechanisms. To predict tears of the vertebral arteries and excessive strain of upper cervical ligaments, it is essential to model the complex structure of the upper cervical joints with sliding contacts between the joints and soft tissues limiting the motion. Facet joint motion and strain in the spinal ligaments are highly dependent on the vertebral kinematics and therefore it is essential the HBMs have biofidelic relative motion in the vertebral segments.

ANTHROPOMETRY AND MATERIAL PROPERTIES

There are significant differences in neck anthropometry based on gender. The female neck is more slender than the male neck, for example Harty et al. (2004) found the female neck circumference to be 84% of the male neck circumference and female neck length was 91% of the male. There is little gender differences in the head circumference while the neck circumference is smaller for females (Vasavada et al. 2001, Harty et al. 2004,

Mordaka 2004, Valkeinen et al. 2002, Vasavada et al. 2008, DeRosia 2008). Hence, females support more head mass per neck cross-sectional area. These gender differences may to some extent depend on stature and not directly on gender. To distinguish the effects of gender from stature, size matched male and female subjects were studied by Vasavada et al. (2008) and DeRosia (2008) (Table 1). It can be seen that head circumference varied by only 3%, irrespective of size matching based on neck length, seated height, or stature. On the other hand, the female neck circumference was 84 – 86 % of the male measurements for all groups. Hence, gender have significant effect on neck circumference, which is not an effect of differences in overall body dimensions. Gender differences for neck length were less than the difference for neck circumference, supporting previous findings that female necks are more slender (Vasavada et al. 2008, DeRosia 2008).

Table 1. Body Dimensions for Size Matched Volunteers

F = Females, M = Males, No. = Number of subjects, Circumf. = Circumference.

*Neck length measure: C7 spinous process - tragus of the ear (Vasavada 2008), C2-C6 length (DeRosia 2008).

		average ± SD				
References		Schneider et al. 1983	Vasavada et al. 2008	DeRosia 2008	DeRosia 2008	DeRosia 2008
Size Matched		50th percentiles	neck length	seated height	head circumf.	stature
No. F			14	11	19	11
No. M			14	17	15	10
Head Circumf.	F		562 ± 15	561 ± 14	559 ± 7	548 ± 15
[mm]	M		577 ± 13	580 ± 15	561 ± 8	564 ± 21
	F/M		97%	97%	100%	97%
Neck Circumf.	F		331 ± 20	324 ± 12	322 ± 14	318 ± 22
[mm]	M		394 ± 22	376 ± 16	379 ± 20	379 ± 23
	F/M		84%	86%	85%	84%
Neck length*	F		107 ± 5	88 ± 6	86 ± 6	86 ± 7
[mm]	M		108 ± 5	95 ± 6	97 ± 6	97 ± 6
	F/M		99%	94%	88%	89%
Stature	F	1618	1690 ± 30	1677 ± 60	1645 ± 69	1687 ± 18
[mm]	M	1753	1690 ± 30	1745 ± 44	1785 ± 92	1693 ± 18
	F/M	92%	100%	96%	92%	100%
Seated height	F	844		879 ± 10	859 ± 24	851 ± 19
[mm]	M	901		886 ± 9	900 ± 41	875 ± 18
	F/M	94%		99%	95%	97%
Mass	F	62	66 ± 9	64 ± 6	61 ± 6	60 ± 12
[kg]	M	77	74 ± 9	76 ± 8	79 ± 14	75 ± 7
	F/M	81%	89%	84%	77%	80%

Vertebral body dimensions are smaller for females than males (Table 2), irrespecitve if measured on skeletal bone specimen or from medical images of patients and volunteers. This is expected as the female population is overall smaller than the male population. Frobin et al. (2002) found that the vertebral body height divided by depth ratio was smaller for females than males, indicating that the female cervical spine has less support area. When this ratio was calculated for other studies where both depth and height were reported, similar trends were seen (Table 2, last three columns). Vasavada et al. (2008) matched volunteers with regards to seated height and neck length, and found the female dimensions to be 86-98% of the male dimensions. Gender differences were most prominent for the C3-C5 vertebral bodies. DeRosia (2008) and Stemper et al. (2008, 2009) pusblished results with size matched volunteers in three groups based on either seated height, head circumference, or stature. They found that the female dimensions were 86-95% of the male dimensions and significantly smaller with regards to width and depth for females among the head circumference matched volunteers. The results from the head circumference matched group compare well with a large survey without size matching by Parenteau et al. (2014), which is likely because the head circumference matching provides a large spread in stature and other dimensions. Hence, even when size-matched, females have smaller vertebral bodies than males, which is most prominent for the vertebral depth.

A narrow spinal canal could possibly increase the risk of nervous tissue lesions. Significant gender differences in spinal canal dimensions have been found in studies of skeletal specimens and patients (Table 3). The spinal canal was widest in the upper cervical spine and narrowest at the C4-C6 levels. The largest gender differences were found at the C4-C5 level, where the spinal diameter was 4-6% narrower for females (Tatarek 2005 and Evangelopoulos et al. 2012, Parenteau et al. 2014). On the other hand, differences of less than 2% were reported for all levels (Hukuda and Kojima 2002) and for C4 and above (Parenteau et al. 2014). None of these studies comprised size-matched subjects and the gender differences may stem from a difference in overall size rather than gender.

Table 2. Vertebral Body Dimensions

F = females, M = males, No. = number of, skel. = skeletal specimen, vol = volunteers.

	Height*			Depth**									Width***					Height by Depth		
	average ± SD [mm]			average ± SD [mm]									average ± SD [mm]					[mm/mm]		
References	Boyle et al. 1996	Hukuda and Kojima 2002	Vasavada et al. 2008	Milne 1991	Kasai et al. 1996	Ebraheim et al. 1998	Hukuda and Kojima 2002	Vasavada et al. 2008	DeRosia 2008	Stemper et al. 2009	Stemper et al. 2009	Parenteau et al. 2014	Milne 1991	Vasavada et al. 2008	DeRosia 2008	Stemper et al. 2009	Stemper et al. 2009	Frobin et al. 2002	Hukuda and Kojima 2002	Vasavada et al. 2008
Size Matched	no	no	neck length	no	no	no	no	neck length	stature	sitting height	head circumf.	no	no	neck length	stature	sitting height	head circumf.	no	no	neck length
Subjects	skel.	skel.	vol.	skel.	skel.	skel.	skel.	vol.	vol.	vol.	vol.	patients	skel.	vol.	vol.	vol.	vol.	skel.	skel.	vol.
No. F	25	114	14	21	10	11	114	14	11	11	18	176	21	14	11	11	18	100	114	14
No. M	26	105	14	40		16	105	14	10	17	9	251	40	14	10	17	9	35	105	14
C1 F								45,1 ± 1,9												
M								47,6 ± 4,5												
F/M								95%												
C2 F						13,7 ± 1,3		13,1 ± 1,0	15,7 ± 1,1	15,9 ± 1,2	15,4 ± 0,9	14,4 ± 1,4			19,6 ± 2,3	20,4 ± 2,4	20,2 ± 1,7			
M						14,6 ± 1,2		14,2 ± 1,0	16,8 ± 0,9	17,5 ± 0,9	17,0 ± 0,8	16,7 ± 1,6			21,8 ± 1,0	22,3 ± 1,3	21,9 ± 1,0			
F/M						94%		92%	93%	91%	91%	86%			90%	91%	92%			
C3 F		13,0 ± 1,2	12,0 ± 0,9	13,8 ± 0,2		13,6 ± 1,4	16,0 ± 1,2	12,8 ± 0,8	15,4 ± 1,0	15,7 ± 0,8	15,1 ± 0,9	15,0 ± 1,6	18,2 ± 0,3	14,6 ± 2,6	20,4 ± 1,8	20,9 ± 1,9	20,7 ± 1,7	0,94	0,81	0,94
M		14,6 ± 1,5	13,5 ± 0,9	15,3 ± 0,2		14,6 ± 1,2	18,1 ± 1,3	14,2 ± 1,6	16,6 ± 1,0	16,8 ± 1,1	16,9 ± 1,2	17,2 ± 1,9	19,1 ± 0,3	16,9 ± 1,6	22,0 ± 1,3	22,9 ± 1,4	22,2 ± 1,9	0,91	0,81	0,95
F/M		89%	89%	90%		93%	88%	90%	93%	93%	89%	87%	95%	86%	93%	91%	93%	103%	101%	99%
C4 F		12,7 ± 1,2	11,6 ± 0,9	14,4 ± 0,3		13,5 ± 1,4	15,7 ± 1,3	13,0 ± 1,0	15,3 ± 0,9	15,7 ± 0,8	15,2 ± 1,0	15,3 ± 2,0	20,9 ± 0,3	16,9 ± 1,2	20,6 ± 2,0	21,9 ± 1,7	21,3 ± 1,5	0,88	0,81	0,89
M		14,2 ± 1,4	12,6 ± 0,8	16,0 ± 0,3		14,8 ± 1,6	17,6 ± 1,4	14,8 ± 1,2	16,9 ± 1,0	16,8 ± 1,1	17,1 ± 1,6	17,5 ± 2,1	19,3 ± 0,3	17,8 ± 2,1	22,2 ± 1,6	23,2 ± 1,3	22,7 ± 1,3	0,84	0,81	0,85
F/M		89%	92%	90%		91%	89%	88%	91%	93%	89%	87%	108%	95%	93%	94%	94%	105%	100%	105%
C5 F		12,7 ± 1,2	11,3 ± 0,7	14,0 ± 0,2	17,1 ± 0,6	13,4 ± 1,3	15,3 ± 1,3	13,0 ± 0,9	15,5 ± 0,9	15,8 ± 0,8	15,6 ± 1,2	16,6 ± 2,5	20,4 ± 0,3	18,3 ± 1,5	21,1 ± 1,5	22,1 ± 1,3	21,6 ± 1,8	0,85	0,83	0,87
M		13,9 ± 1,4	12,2 ± 0,6	16,2 ± 0,3	18,2 ± 0,5	14,6 ± 1,4	17,4 ± 1,4	15,2 ± 1,1	17,7 ± 1,2	16,9 ± 0,8	17,6 ± 1,2	18,7 ± 2,6	21,6 ± 0,2	19,0 ± 2,0	23,5 ± 1,7	23,8 ± 2,2	23,2 ± 1,5	0,81	0,80	0,80
F/M		91%	93%	86%	94%	92%	88%	86%	88%	93%	89%	89%	94%	96%	90%	93%	93%	104%	104%	108%
C6 F	11,1 ± 1,1	12,8 ± 1,3	11,6 ± 0,8	14,9 ± 0,5		13,3 ± 1,0	15,9 ± 1,3	14,0 ± 1,0	15,9 ± 0,9	16,3 ± 1,0	16,2 ± 1,0	16,9 ± 2,2	22,1 ± 0,4	19,8 ± 1,6	24,5 ± 1,8	24,7 ± 1,3	24,1 ± 1,8	0,83	0,81	0,83
M	11,8 ± 0,9	13,7 ± 1,2	12,0 ± 0,7	16,6 ± 0,3		14,8 ± 1,3	18,1 ± 1,4	15,6 ± 1,0	18,4 ± 2,0	18,0 ± 1,3	18,8 ± 2,0	19,0 ± 2,4	23,7 ± 0,3	20,9 ± 2,3	27,0 ± 1,6	26,0 ± 2,0	27,0 ± 1,2	0,85	0,76	0,77
F/M	94%	93%	97%	90%		92%	88%	90%	86%	91%	86%	89%	93%	95%	91%	95%	89%	99%	106%	108%
C7 F	12,9 ± 1,2	14,1 ± 1,2	12,8 ± 0,6	14,7 ± 0,3		12,9 ± 0,7	16,6 ± 1,3	13,7 ± 1,2				15,6 ± 1,7	23,4 ± 0,3	22,6 ± 2,4				0,91	0,85	0,93
M	13,3 ± 1,3	15,6 ± 1,5	13,0 ± 1,0	16,5 ± 0,3		14,3 ± 1,0	18,7 ± 1,2	15,5 ± 1,3				17,7 ± 1,9	25,2 ± 0,2	24,6 ± 2,7				0,92	0,83	0,84
F/M	97%	90%	98%	89%		90%	89%	88%				88%	93%	92%				98%	102%	111%
T1 F	14,3 ± 1,3			14,4 ± 0,3									23,4 ± 0,3							
M	15,3 ± 1,1			16,2 ± 0,2									25,2 ± 0,3							
F/M	94%			88%									93%							

* Height was measured at the middle of the vertebral body or the average of anterior and posterior height. ** Depth was measured at the middle of the vertbral body or the average of the superior and inferior surfaces, except for Milne 1991 (superior surface), Parenteau et al. 2014 (inferior surface), Stemper et al. 2009 and DeRosia 2008 (maximum measurement). *** Width was measured at the superior surface by Milne 1991, average of superior and inferior surface in Vasavada et al. 2008, and the maximum measurement in Stemper et al. 2009 and DeRosia 2008.

The facet joints are important for the biomechanical response. Gender differences in facet joint angles have been hypothesized as one explanation to the increased WAD risk for females. Measured relative to the vertebral body, very small and contradictory gender differences have been reported by Milne (1991), Boyle et al. (1996), Kasai et al. (1996), and Parenteau et al. (2013) (Table 3). Any difference in facet joint angle must thus stem from a difference in posture and/or spinal curvature. The variations in cervical spine alignment have been investigated extensively. For a majority of the population lordosis of the cervical spine is normal. The proportions of non-lordosis (straight or kyphosis) were 36% (Matsumoto et al. 1998) and 38% (Takeshima 2002) for an asymptomatic population measured in a seated position. Matsumoto et al. (1998) showed that females more frequently presented non-lordosis than males and that gender was an independent factor significantly associated with non-lordosis. Likewise, Helliwel et al .(1994) reported that the cervical spine was more likely to be straight in females than in males. Haedacker et al. (1997) observed that statistically cervical lordosis in males was more pronounced than in females. Additionally, Lee et al. (2014) focused on the cervicothoracic junction. Females had a thinner thoracic cage than males and males had a more forward-inclined thoracic inlet (angle between lines drawn from the top of the manubrium to the centroid of the cranial T1 end plate and the horizontal plane) than females. They concluded that a small anteroposterior diameter in the upper most thoracic cage was associated with cervical hypolordosis, whereas an inclined thoracic inlet was associated with pronounced cervical lordosis. Klinich et al. (2004) investigated the relationship between stature and type of cervical spine alignment. Tall females were more likely to have a straight cervical spine than short females. On the other hand, there was no significant relationship between stature and curvature for males. Hence, accounting for the spinal curvature, less lordosis will give a more horizontal orientation of the facet joint surfaces. An average female occupant HBM should include a seated posture with less lordosis than the average male models, based on these data. Also, the height of the female HBM should be considered when the seated lordosis is defined.

Dynamic response of occupants in rear impacts have been analysed with volunteer and post mortem human subject (PMHS) tests in order to understand the biomechanics of whiplash motion. In volunteer tests (Siegmund et al. 1997), females had greater head and neck kinematics compared to males in the overall motion analysis. In addition, cervical vertebral kinematics were also greater for females compared to males, when analysing sequential cineradiography images of cervical spines (Ono et al. 2006, Sato et al. 2014). Likewise, in rear impact sled tests with PMHS head-neck complexes, cervical vertebral kinematics were significantly greater for the female specimens than for the male specimens (Stemper et al. 2003, 2004). Initial alignment of cervical vertebrae has been considered as one of possible causes of the experimental gender difference seen. The alignment influences load transmission between the head and trunk of the body through the cervical spine, and can affect vertebral kinematics. Previous experimental studies (Maiman et al. 1983, Maiman et al. 2002, Yoganandan et al. 1986, Yoganandan et al. 1999, Liu and Dai 1989, Pintar et al. 1995) showed that changes in the initial alignment of the cervical spine had an influence on the severity of injury. Ono et al. (1997) conducted rear impact sled tests with a volunteer and quantified the effect of the initial alignment of the cervical spine on vertebral kinematics. They reported that rotational angles of cervical vertebrae were significantly greater in kyphotic alignment than in lordosis. Hence, as females are more likely to present with non-lordosis this implies that females inherently will suffer greater vertbral rotations. Likewise, Stemper et al. (2005) and Frechede et al. (2006) investigated elongation of the facet joint capsular ligaments (CL) in lordotic, straight and kyphotic cervical alignment with a FE head/neck model and reported that facet joint ligament elongations increased with kyphotic cervical alignment and concluded that kyphosispresented a higher risk for WAD than lordosis or straight spinal aligment.

Alongside anthropometry and spinal alignment, gender differences in material properties can influence the risk of lesions. Nightingale et al. (2002, 2007) tested upper and lower cervial spine specimen (4 female, 7 male) in flexion and extension bending load to failure. They found the mean upper cervical flexion and extension strength to be greater for males than females, however only significantly for flexion. The mean angle at failure were not significantly different for the genders. The female upper cervical spine was significantly less stiff than the male. Hence, the male range of motion was significantly greater than the female. Similar differences were seen also for the lower cervical spine. This, could be because of gender differences in cross sectional area of the ligaments or in the material properties. In sports, female athletes sustain more anterior cruciate ligament lesions (Elliot 2010), and some studies indicate that the influence of sex hormones on the material properties of the ligament may provide part of the explanation to increased risk (Wild 2012). Osakabe et al. (2001) studied the elastin and collagen content of lumbar ligaments with aging and found gender difference. The elastin content decreased with age for males but not for females. They suggested that sex steroid hormones may regulate the metabolism and thus effect how the elastin and collagen contents change with age. Stemper et al. (2010) tested thoracic specimen and found gender to influence the

elastic modulus in tension and compression, with female specimen having significantly greater moduli. Contrary, Bass et al. (2007) did not find any gender dependence for the failure true stress and failure true strain in cervical specimen (6 male, 5 female) tested for anterior longitudinal ligament (ALL), posterior longitudinal ligament (PLL), and ligamentum flavum (LF). Mattucci et al. 2012 tested the ALL, PLL, LF, CL, and interspinous ligament (ISL) from 8 male and 8 female cadavers in quasi-static (0.5 s-1) and dynamic (up to 250 s-1) load rates. Stiffness and strength were consistently lower for female specimen, although significant gender differences were only found for the Young's modulus of the ALL and the failure force of the CL (Mattucci 2012). Hence, it seems likely that the gender difference due to anthropometry have a larger influence than gender difference in the material properties of the ligaments.

Table 3. Spinal Canal Diameter and Facet Joint Angles

None of these studies included size matched subjects. F = Females, M = Males, No. = Number of, skel. = skeletal specimen.
* Spinal canal anterior-posterior diameter in the sagittal plane. For Parenteau et al. 2014 the diameter was recalculated by doubling the reported radius. Tatarek 2005 values are the average of the two reported groups. ** The angle of the superior facet to the plane of the end plate, except for Parenteau et al. 2013 (inferior facet). Data from Kasai et al. 1996 was recalculated from the angle to the posterior vertebral line by adding 90 degrees.

		Spinal Canal Diameter *				**Facet Joint Angles ****			
		average ± SD [mm]				average ± SD [degrees]			
References		Hukuda and Kojima 2002	Tatarek 2005	Evangelopoulos et al. 2012	Parenteau et al. 2014	Milne 1991	Boyle et al. 1996	Kasai et al. 1996	Parenteau et al. 2013
Subjects		skel.	skel.	patients	patients	skel.	skel.	patients	patients
No. F		114	321	100	176	21	25	10	173
No. M		105			251	40	26		250
C1	F			16,3 ± 1,6					
	M			16,6 ± 1,9					
	F/M			98%					
C2	F		15,9 ± 1,4	13,3 ± 1,3	13,7 ± 1,6				126,5 ± 14,0
	M		16,6 ± 1,4	13,6 ± 1,6	13,7 ± 1,9				122,1 ± 12,3
	F/M		95%	97%	100%				104%
C3	F	16,8 ± 1,7	13,9 ± 1,4	12,9 ± 1,3	12,9 ± 1,5	126,2 ± 1,2		128,4 ± 3,8	127,0 ± 11,4
	M	16,6 ± 1,5	14,7 ± 1,3	13,3 ± 1,7	13,0 ± 1,7	122,8 ± 1,2		129,5 ± 4,2	124,1 ± 9,1
	F/M	101%	94%	97%	99%	103%		97%	102%
C4	F	15,8 ± 1,7	13,4 ± 1,4	12,5 ± 1,5	12,7 ± 1,5	124,8 ± 1,23		129,7 ± 2,8	128,4 ± 11,5
	M	15,8 ± 1,4	14,3 ± 1,3	13,1 ± 1,0	13,0 ± 1,9	124,5 ± 0,81		131,2 ± 4,1	129,0 ± 8,8
	F/M	100%	94%	96%	98%	100%		96%	100%
C5	F	15,7 ± 1,6	13,4 ± 1,3	12,7 ± 1,7	12,3 ± 1,7	125,7 ± 1,5		131,7 ± 3,0	128,0 ± 11,3
	M	15,9 ± 1,3	14,3 ± 1,3	13,4 ± 1,2	13,0 ± 1,6	127,6 ± 0,8		132,3 ± 2,5	129,3 ± 10,2
	F/M	99%	94%	94%	95%	99%		99%	99%
C6	F	15,6 ± 1,6	13,5 ± 1,1	12,5 ± 1,8	12,7 ± 1,5	124,8 ± 1,42	124,4 ± 5,7	125,3 ± 2,7	120,9 ± 11,9
	M	15,9 ± 1,3	14,3 ± 1,3	13,3 ± 1,9	13,3 ± 1,7	126 ± 0,89	125,7 ± 5,5	126,1 ± 4,5	124,5 ± 9,3
	F/M	98%	95%	94%	96%	99%	99%	98%	97%
C7	F	15,5 ± 1,6	13,5 ± 1,1		13,6 ± 1,5	116,0 ± 1,1	115,8 ± 5,7	115,2 ± 2,8	124,2 ± 14,4
	M	15,8 ± 1,4	14,4 ± 1,2		14,2 ± 1,4	115,6 ± 0,9	118,7 ± 5,1	117,4 ± 4,0	125,4 ± 11,4
	F/M	98%	94%		96%	100%	98%	92%	99%
T1	F					111,1 ± 1,13	108,5 ± 6,1		
	M					112,2 ± 1,05	112,2 ± 6,6		
	F/M					99%	97%		

FINITE ELEMENT HUMAN BODY MODELS

A number of whole body FE occupant models have been released, primarily of the 50th percentile male anthropometry as defined by Schneider et al. 1983. A first generation of models developed in the late 1990s and early 2000s are the THUMS v3 (Iwamoto et al. 2002), HUMOS (Robin 2001), and the JAMA model (Sugimoto and Yamazaki 2005). In the THUMS v3, 7 400 elements of the total 143 000 are located in the cervical region. However, quite substantial simplifications such as the the facet joints being represented by single hexahedral elements in shear, rather than a sliding contact, makes soft tissue injury prediction difficult. A second generation of whole body HBMs have more recently been released, with an increased number of elements by an order of

magnitude; the THUMS v4 (Watanabe et al. 2011) includes 1.7 million elements and the GHBMC model (Vavalle et al. 2013) 2.2 million elements to represent a 50th percentile male occupant. To date, the most advanced cervical model in a whole body HBM appears to be the GHBMC model, that includes sliding contact facet joints with articular cartilage, failure criteria for the interverterbral discs to represent disc avulsion, failure criteria for 1D cervical ligaments and bone, and 3D musculature with superimposed active 1D elements. For the GHBMC, 12% of the elements are located in the cervical region, while in the THUMS v4 only 1.6 % is used. For some of the models mentioned above, 95th percentile male and 5th percentile female versions have been developed and released. However, to the best of our knowledge, no 50th percentile female whole body HBM has been released to date.

Many models of the isolated cervical spine have been developed and used to study impact biomechanics problems. The first models employed multibody dynamics modelling techniques (de Jager 1996, Deng and Goldsmith 1987, van der Horst 2002), and were used to show the importance of musculature in capturing volunteer responses in multi-directional impacts (de Jager 1996, van der Horst 2002). The multibody approach is numerically more efficient than FE simulations, an important property for early models. When applied to whiplash motion, one major drawback of the multi body models is that the spinal joints were modelled with kinematic joints instead of facet surfaces restrained by soft tissues. One of the first FE models to inlude the complex joints of the upper cervical spine with sliding surfaces between the occiput and second cervical vertebra was Brolin and Halldin (2004), illustrating the benefit of this modelling approach when studying how material properites of ligaments influence kinematics. More recent studies have successfully been used to study the effect of cervical muscle activity, using optimisation (Chancey et al. 2003, Brolin et al. 2005, Dibb et al. 2013) or neuromuscular control schemes (de Bruijn 2014) for the cervical musculature. In order to capture the response of live human subjects through numerical simulation, detailed representation of the cervical musculature and at least a basic muscle activation scheme are necessary (Brolin et al. 2008, Hedenstierna and Halldin 2008). For rear-end impacts the importance of cervical muscle activation has also been confirmed through numerous experimental studies, e.g. by Siegmund et al. 2003.

The overwhelming majority of the developed impact biomechanics FE cervical spine models, summarised in Table 4, are based on the average male anthropometry. In general no stringent definition of the average male subject used for model development appear to have been used, such as defined for the GHBMC model (Gayzik et al. 2011), but rather a male volunteer or PMHS of arbitrary average size has provided the template geometry for the models. Interesting exceptions are the Duke University models, which have been scaled to represent the cervical spine of 6 and 10 year old children (Dibb et al. 2013), and the Nottingham Trent University model which was scaled to an average female size (Mordaka 2004). Although a limited number of publications were made with the average female model, it was concluded that scaling alone is not sufficient to capture gender differences in head-neck kinematics during rear-end impact simulations (Mordaka 2004). Furthermore, an expected trend of increasing number of elements with later years can be found, with the exception of the parametric model of Laville et al.(2009). By parameterizing and simulating 16 different individual cervical spine geometries, almost all variation present in experimental moment-rotation corridors for the C5–C6 spinal unit was captured, although material properties were kept constant (Laville et al. 2009). As shown by the review of female anthropometry in this paper, significant differences between female and male cervical vertebral geometry exist; hence, the findings of Laville et al. 2009 support the need for HBMs based on female anthropometry.

The strength of the FE method for impact biomechanics modelling is that it allows for localised injury prediction, rather than using global kinematic and force criteria, as used for assessment with anthropomorphic test devices. In about half of the publications included in Table 4, no assessment of soft tissue injury has been considered. For the rest, the most commonly assessed parameter is ligament strain, which can either be relative between simulations (Brolin et al. 2008, Kitagawa et al. 2008), or compared with experimentally recorded failure levels (Cronin et al. 2012, DeWit and Cronin 2012, Fice and Cronin 2012, Fice et al. 2011, Panzer et al. 2011). Peak intervertebral annulus fibrosus strain has been considered (Panzer et al. 2011), as well as shear deformation of the disc (Fice et al. 2011), the change in intervertebral disc pressure and cross-sectional force between simulations (Brolin et al. 2008), and disc avulsion by tied contact failure (Cronin et al. 2012). For the hard tissues, bone fracture simulation by element elimination is quite common (Cronin et al. 2012, DeWit and Cronin 2012, Halldin et al. 2000, Panzer et al. 2011, Zhang et al. 2005), although some questions about post failure response accuracy have been raised (DeWit and Cronin 2012). Furthermore, global injury criteria that have been suggested, or used as complements to local criteria, were the neck injury criterion (Kitagawa et al. 2008) and cervical spine tensile or compressive forces (Camacho et al. 1997, Dibb et al. 2013).

Table 4. Summary of FE Cervical Spine Models for Impact Biomechanics

Anthrop. = Anthropometry, No. Elem. = Number of elements, M50 = average male, F50 = average female, PMHS = Post Mortem Human Subject. CT = Computed Tomography. MRI = Magnetic Resonance Imaging. 1,2,3D = One, two, or three dimensional elements. *Only elements in the cervical spine are reported here. The number of elements may vary with different versions of the models.

References	Anthrop.	Skeletal geometry	No. Elem.*	Solver	Facet Joints	Ligaments	Muscles
Camacho et al. 1997 Chancey et al. 2003 Dibb et al. 2013	M50 6-year-old 10-year-old	Visible Human Database. Child models scaled based on anatomical literature.	1137	LS-DYNA	Non-linear kinematic joints govern intervertebral joint motion, soft tissues not modelled individually.		Active 1D
Yang et al. 1998	M50	Volunteer MRI data.	14700	PAM-CRASH	Sliding contact	Non-linear 1D and 2D	Not included
Halldin et al. 2000 Brolin and Halldin 2004 Brolin et al. 2005 Brolin et al. 2008 Hedenstierna et al. 2008	M50	Volunteer CT data.	8400	LS-DYNA	Sliding contact	Non-linear 1D	Active 1D and 3D
Jost and Nurick 2000	M50	Anatomical literature.	3000	ABAQUS	Not included	2D	Passive 2D
Gentle et al. 2001 Mordaka 2004	M50 F50	Visible Human Database. F50 scaled from M50 based on anatomical literature.	Not reported	LS-DYNA	Not reported	Non-linear 1D and 3D	Passive 1D
Meyer et al. 2004	M50	Volunteer CT data.	73185	RADIOSS	Sliding contact	1D	Passive 3D
Zhang et al. 2005 Zhang et al. 2006	M50	Volunteer external measurements.	22094	LS-DYNA	Sliding contact	Non-linear 1D	Not included
Eijima et al. 2005	M50	JAMA model [x] and volunteer MRI scan	14300	LS-DYNA	Solid elements	2D	Passive 3D
Panzer 2006 Panzer and Cronin 2009 Fice et al. 2011 Panzer et al. 2011 Cronin et al. 2012 DeWit and Cronin 2012 Fice and Cronin 2012	M50	Commercial geometry package.	108300	LS-DYNA	Sliding contact with synovial fluid	Non-linear 1D with failure	Active 1D
Wheeldon et al. 2008	M50	PMHS CT data and cryomicrotome data.	Not reported	ABAQUS	Sliding contact with synovial fluid	Non-linear 1D	Not included
Kitagawa et al. 2008	M50	From THUMS v.4 (Watanabe et al. 2011)	80000	LS-DYNA	Sliding contact with synovial fluid	2D	Passive 1D
Laville et al. 2009	Subject specific	Volunteer CT	5350	RADIOSS	Sliding contact	Non-linear 1D	Not included
Cervical spine models in whole human body models							
Iwamoto et al. 2002 THUMS v3	M50	Commercial geometry package.		LS-DYNA,PAM-CRASH	Solid element in shear	Linear 2D	Passive 1D
Watanabe et al. 2011 THUMS v4	M50	CT Scan data set.		LS-DYNA, PAM-CRASH	Solid element in shear	Linear 2D	Passive 1D
Robin et al. 2001 HUMOS/HUMOS2	M50	Photos of PMHS slices.		MADYMO, RADIOSS, PAM-CRASH	Sliding contact	Non-linear 1D	Passive 1D
Vavalle et al. 2013 GHBMC	M50	Volunteer CT and MRI data sets.		LS-DYNA	Sliding contact	Non-linear 1D with failure	Active 1D
Sugimoto and Yamazaki 2005, JAMA	M50	Based on other FE models.		LS-DYNA, PAM-CRASH	Unknown	Unknown	Unknown

In relation to proposed injury mechanisms for WAD, summarised in the Injury Mechanisms section, synovial fold pinching, tension of dorsal root ganglia or vertebral arteries, and musculoskeletal injury appear not to have been covered in detail in studies with FE impact biomechanics models of the cervical spine. It is likely that further model development is nescessary to assess these mechanisms. Another mechanism not investigated by the models summarised in Table 4 is cervical canal pressure transients that may load and deform nerve tissue such as the spinal ganlia, which require coupled fluid dynamic and solid mechanics simulations in the HBM or in a submodel that use the output from the HBM as input in order to model local phenomena.

SUMMARY AND CONCLUSIONS

Real-world data has identified the female occupant to be at more risk for WAD in traffic accidents and many studies illustrate important differences in the kinematic response of male and female subjects, volunteers and PMHSs. The review of FE models of the cervical spine presented 17 models based on male geometry but only one model that was scaled to represent a female. It is obvious that current tools are not adequate for assessing seat performance or develop protection against WAD with the female population in focus. An average female HBM has the potential to improve WAD prevention and assessment of seat performance to reduce traffic injuries in the population most at risk of these injuries. When the EvaRID model was developed, the average female was defined on the anthropometric measures of the 50th percentile female from the UMTRI study (stature 161.8 cm, mass 62.3 kg, Schneider et al. 1983) as it was considered a reasonable representation of the worldwide population at risk (Carlsson 2014). Another advantage of using the data by Schneider et al. (1983) for the average female HBM is that it would be consistent with several of the average male models developed based on the 50th percentile male (stature 175.3 cm, 77.3 kg, , Schneider et al. 1983). This approach would provide stronger comparisons between average male and female responses for seat assessment and other safety applications.

The literature review leaves no doubt that female HBMs should be developed directly based on female anthropometry and not scaled from male data because females have more slender necks and less muscle mass than males. Gender significantly influences the shape of the vertebral body, with the female vertebral body being less deep and not as wide. There was no or very little influence of gender on the height of the vertebral bodies and the diameter of the spinal canal. The facet joint angles compared to a reference in the vertebral body did not seem to depend on gender. Instead, gender significantly influenced the spinal alignment in the seated posture, where females on average present a straighter spine and males show more lordosis. There may be an effect of gender on the material properties of the ligaments in the cervical spine; however it is probably less important than gender differences in the cross sectional area of ligaments. In future studies on gender dependence, using size matched male and female subjects based on neck length or seated height rather than head circumference is recommended to distinguish the effect of gender from size.

To conclude, we recommend that average female HBMs are developed with focus on;

- The shape of the female vertebral body, especially the depth and width that provides less support area than for males,
- Defining a spinal curvature representative of seated female volunteers that on average present with less lordosis than males,
- The dimensions of the spinal ligaments, rather than the material properties, to capture the larger range of motion and less spinal stiffness of female subjects compared to male, and
- Validation of female volunteers and PMHS tests for range of motion, while failure prediction seem to be less gender sensitive.

ACKNOWLEDGEMENT

The work presented in this paper was partly funded by VINNOVA, the Swedish Governmental Agency for Innovation Systems and the Strategic Area of Advance (Transport), Chalmers. The work was conducted within the SAFER Vehicle and Traffic Safety Centre at Chalmers, Gothenburg, Sweden and it was also partly performed by the Advanced Research Project, the Safety Research Division at JARI, Japan Automobile Research Institute, Tsukuba, Japan.

REFERENCES

Banic B, Petersen-Felix S, Andersen O, Radanov B, Villiger P, Arendt-Nielsen L, Curatolo M. (2004) Evidence for Spinal Cord Hypersensitivityin Chronic Pain after Whiplash Injury and in Fibromyalgia. Pain 107: 7–15.

Bass CR, Lucas SR, Salzar RS, Oyen ML, Planchak C, Shender BS, Paskoff G (2007) Failure Properties of Cervical Spinal Ligaments under Fast Strain Rate Deformations. Spine 32(1): E7–13.

Boyle J, Singer K, Milne N. (1996) Morphological survey of the cervicothoracic junctional region. Spine 21(5): 544-548

Brault JR, Siegmund GP, Wheeler JB. (2000) Cervical Muscle Response during Whiplash: Evidence of a Lengthening Muscle Contraction. Clin. Biomech. 15: 426–435.

Brolin K, Halldin P. (2004). Development of a Finite Element Model of the Upper Cervical Spine and a Parameter Study of Ligament Characteristics, Spine 29(4): 376-385.

Brolin K, Halldin P, Leijonhufvud I. (2005) The Effect of Muscle Activation on Neck Response, Traffic Inj Prev. 6(1): 67–76.

Brolin K, Hedenstierna S, Halldin P, Bass C, Alem N. (2008). The Importance of Muscle Tension on the Outcome of Impacts with a Major Vertical Component. International Journal of Crashworthiness 13(5): 487–498.

Camacho D, Nightingale R, Robinette J, Vanguri S, Coates D, Myers B. (1997). Experimental Flexibility Measurements for the Development of a Computational Head-Neck Model Validated for Near-Vertex Head Impact, In Proceedings of the 41st Stapp Car Crash Conference (Orlando, FL, USA). Paper no. 973345.

Carlsson A, Chang F, Lemmen P, Kullgren A, Schmitt KU, Linder A, Svensson M. (2014) Anthropometric Specifications, Development, and Evaluation of EvaRID - A 50th Percentile Female Rear Impact Finite Element Dummy Model. Traffic Inj Prev. 15(8): 855-865.

Carstensen T, Frostholm L, Oernboel E, Kongsted A, Kasch H, Jensen T, Fink P (2012) Are There Gender Differences in Coping with Neck Pain Following Acute Whiplash Trauma? A 12-Month Follow-Up Study, Eur J Pain. 16(1): 49–60.

Chancey V, Nightingale R, Van Ee C, Knaub K, Myers B. (2003) Improved Estimation of Human Neck Tensile Tolerance: Reducing the Range of Reported Tolerance Using Anthropmetrically Correct Muscles and Optimized Physilogic Initial Conditions, Stapp Car Crash J. 47: 135–153.

Chapline J, Ferguson S, Lillis R, Lund A, Williams A (2000) Neck Pain and Head Restraint Position Relative to the Driver's Head in Rear-End Collisions, Accid Anal Prev. 32(2): 287–297.

Cronin D, Fice J, DeWit J, Moulton J. (2012) Upper Cervical Spine Kinematic Response and Injury Prediction, In Proceedings of the IRCOBI Conference (Dublin, Ireland, Sept. 12–14), 225–234.

Curatolo M, Bogduk N, Ivancic P, McLean S, Siegmund G, Winkelstein B (2011) The role of tissue damage in whiplash associated disorders: Discussion paper 1. Spine. 36(25 Suppl): S309–315.

Curatolo M, Petersen-Felix S, Arendt-Nielsen L, Giana C, Zbinden AM, Radanov BP. (2001) Central Hypersensitivity in Chronic Pain after Whiplash Injury. Clin J Pain. 17(4): 306–315.

Davidsson, J., Lövsund, P., Ono, K., Svensson, M. Y., & Inami, S. (1999). A comparison between volunteer, BioRID P3 and Hybrid III performance in rear impacts. In Proceedings of the International Research Council on the Biomechanics of Injury conference (Vol. 27, pp. 165-178). International Research Council on Biomechanics of Injury.

de Bruijn E. (2014) Isometric and Dynamic Control of Neck Muscles – Reflexive Contributions and Muscle Synergies, Doctoral Thesis, Delft University of Technology, Delft, the Netherlands.

de Jager M. (1996) Mathematical Head-Neck Models for Acceleration Impacts, Doctoral Thesis, Eindhoven University of Technology, Eindhoven, the Netherlands.

Deng Y-C, Goldsmith W. (1987) Response of a Human Head/Neck/Upper-Torso Replica to Dynamic Loading – II. Analytical/Numerical Model, J Biomech. 20(5): 487–497.

DeRosia J (2008) Role of Gender and Size in Biomechanics of Rear Impact. Doctoral Dissertation, Marquette University, USA, UMI Number: 3357947.

DeWit J, Cronin D (2012) Cervical Spine Segment Finite Element Model for Traumatic Injury Prediction, J Mech Behav Biomed Mater. 10: 138–150.

Dibb A, Cox C, Nightingale R, Luck J, Cutcliffe H, Myers B, Arbogast K, Seacrist T, Bass C. (2013) Importance of Muscle Activation for Biofidelic Pediatric Neck Response in Computational Models", Traffic Inj Prev. 14 Suppl: S116–127.

Dolinis J (1997) Risk Factors for "Whiplash" in Drivers: a Cohort Study of Rear-End Traffic Crashes, Injury 28(3): 173–179.

Ebraheim N, Fow J, Xu R, Yeasting R. (1998) The Vertebral Body Depths of the Cervical Spine and Its Relation to Anterior Plate-Screw Fixation. Spine 23(21): 2299-2302.

Eichberger A, Geigl BC, Moser A, Fachbach B, Steffan H. (1996) Comparison of Different Car Seats Regarding Head-Neck Kinematics of Volunteers During Rear End Impact. Proceedings of the International Research Conference on the Biomechanics of Impact, IRCOBI, Dublin (Ireland).

Ejima S, Ono K, Kaneoka K, Fukushima M. (2005) Development and Validation of the Human Neck Muscle Model Under Impact Loading, In Proceedings of the IRCOBI Conference (Prague, Czech Republic, Sept. 21–23), 245–255.

Elliot D, Goldberg L, Kuehl K. (2010) Young Women's Anterior Cruciate Ligament Injuries An Expanded Model and Prevention Paradigm. Sports med 40(5): 367-376.

Evangelopoulos D, Kontovazenitis P, Kouris S, Zlatidou X, Benneker L, Vlamis J, Korres D, Efstathopoulos N. (2012) Computerized Tomographic Morphometric Analysis of the Cervical Spine. Open Orthop J. 6: 250-254.
Fice J, Cronin D. (2012) Investigation of Whiplash Injuries in the Upper Cervical Spine using a Detailed Neck Model, J Biomech. 45(6): 1098–1102.
Fice J, Cronin D, Panzer M. (2011) Cervical Spine Model to Predict Capsular Ligament Response in Rear Impact, Ann Biomed Eng. 39(8): 2152–2162.
Frechede B, Bertholon N, Saillant G, Lavaste F, Skalli W (2006) Finite Element Model of the Human Neck during Omni-directional Impacts. Part II: Relation between Cervical Curvature and Risk of Injury. Comput Methods Biomech Biomed Engin. 9(6): 379-386.
Frobin W, Leivseth G, Biggemann M, Brinckmann P. (2002) Vertebral height, disc height, posteroanterior displacement and dens–atlas gap in the cervical spine: precision measurement protocol and normal data. Clin Biomech. 17: 423-431.
Gayzik F, Moreno D, Geer C, Wuertzer S, Martin R, Stitzel J. (2011). Development of a Full Body CAD Dataset for Computational Modeling: A Multi-Modality Approach, Ann Biomed Eng. 39(10): 2568–2583.
Gentle, C.R., Golinski, W.Z., and Heitplatz, F. (2001) Computational Studies of 'Whiplash' Injuries, Proc Inst Mech Eng H. 215(2): 181–189.
Haedacker JW, Shuford RF, Capicoto PN, Pryor PW (1997) Radiographic Standing Cervical Segmental Alignment in Adult Volunteers without Neck Symptoms. Spine. 22(13): 1472-1480.
Halldin P, Brolin K, Kleiven S, von Holst H, Jakobsson L, Palmertz C. (2000) Investigation of Conditions that Affect Neck Compression-Flexion Injuries Using Numerical Techniques, In Proceedings of the 44th Stapp Car Crash Conference (Atlanta, GA, USA, Nov. 6–8). Paper no. 2001-01-SC10.
Harty J, Quinlan J, Kennedy J, Walsh M, O'Byrne J. (2004) Anthropometrical analysis of cervical spine injuries. Injury 35(3): 249-252.
Hedenstierna S, Halldin P. (2008) How Does a Three-Dimensional Continuum Muscle Model Affect the Kinematics and Muscle Strains of a Finite Element Neck Model Compared to a Discrete Muscle Model in Rear-End, Frontal, and Lateral Impacts, Spine. 33(8): E236–245.
Helliwel PS, Evans PF, Wright V (1994) The Straight Cervical Spine: Does it Indicate Muscle Spasm? J Bone Joint Surg Br. 76(1): 103-106.
Hukuda S, Kojima Y. (2002) Sex Discrepancy in the Canal/Body Ratio of the Cervical Spine Implicating the Prevalence of Cervical Myelopathy in Men. Spine 27(3): 250-253.
Iwamoto M, Kisanuki Y, Watanabe I, Furusu K, Miki K. (2002) Development of a Finite Element Model of the Total Human Model for Safety (THUMS) and Application to Injury Reconstruction, In Proceedings of the IRCOBI Conference (Munich, Germany, Sep. 18–20)
Jakobsson L, Norin H, Svensson M. (2004) Parameters Influencing AIS 1 Neck Injury Outcome in Frontal Impacts. Traffic Inj Prev. 5(2): 156–163.
Jost R, Nurick G. (2000) Development of a Finite Element Model of the Human Neck Subjected to High G-Level Lateral Deceleration, International Journal of Crashworthiness, 5(3): 259–269.
Kaneoka K, Ono K, Inami S, Hayashi K (1999) Motion analysis of cervical vertebrae during whiplash loading. Spine. 24(8): 763-769.
Kasai T, Ikata T, Katoh S, Miyake R, Tsubo M. (1996) Growth of the Cervical Spine With Special Reference to Its Lordosis and Mobility. Spine 21(18): 2067-2073.
Kasch H, Stengaard-Pedersen K, Arendt-Nielsen L, Staehelin Jensen T. (2001) Pain Thresholds and Tenderness in Neck and Head Following Acute Whiplash Injury: A Prospective Study. Cephalalgia 21(3): 189–197.
Kihlberg JK (1969) Flexion-Torsion Neck Injury in Rear Impacts. Proceedings of the 13th Association for the Advancement of Automotive Medicine (AAAM) Conference, pp. 1–16.
Kitagawa Y, Yasuki T, Hasegawa J. (2008) Research Study on Neck Injury Lessening with Active Head Restraint Using Human Body FE Model", Traffic Inj Prev. 9(6): 574–582.
Klinich KD, Ebert SM, Van Ee CA, Flannagan CAC, Prasad M, Reed MP, Schneider LW (2004) Cervical Spine Geometry in the Automotive Seated Posture: Variations with Age, Stature , and Gender. Stapp Car Crash J. 48: 301-330.
Krafft M. (1998). Non-fatal injuries to car occupants, Injury assessment and analysis of impacts causing short- and long-term consequences with special reference to neck injuries. Doctoral thesis, Karolinska Institutet, Stockholm, Sweden.
Krafft M, Kullgren A, Lie A, Tingvall C. (2003) The Risk of Whiplash Injury in the Rear Seat Compared to the Front Seat in Rear Impacts, Traffic Inj Prev. 4(2): 136–140.
Krakenes J, Kaale BR. (2006) Magnetic Resonance Imaging Assessment of Craniovertebral Ligaments and Membranes after Whiplash Trauma. Spine. 31(24): 2820–2826.
Kullgren A, Krafft M, Tingvall C, Lie A. (2003) Combining crash recorder and paired comparison technique: Injury risk functions in frontal and rear impacts with special reference to neck injuries. Proc. 18th ESV Conf, Paper No. 404, Nagoya (Japan).
Kullgren A, Krafft M, Lie A, Tingvall C (2007) The Effect of Whiplash Protection Systems in Real-Life Crashes and Their Correlation to Consumer Crash Test Programmes, Proc. 20th ESV Conf. (07-0468), Lyon (France).

Kullgren A, Stigson H, Krafft M (2013) Development of Whiplash Associated Disorders for Male and Female Car Occupants in Cars Launched Since the 80s in Different Impact Directions. Proceedings of the International Research Conference on the Biomechanics of Impact, IRCOBI, pp 51-62.
Laville A, Laporte S, Skalli W. (2009) Parametric and Subject-Specific Finite Element Modelling of the Lower Cervical Spine. Influence of Geometrical Parameters on the Motion Patterns. J Biomech. 42(10): 1409–1415.
Lee JH, Park YK, Kim JH (2014) Chronic Neck Pain in Young Adults: Perspectives on Anatomic Differences. Spine J. 14(11): 2628-2638.
Linder A, Schick S, Hell W, Svensson M, Carlsson A, Lemmen P, Schmitt K-U, Gutsche, A, Tomasch E. (2013) ADSEAT – Adaptive Seat to Reduce Neck Injuries for Female and Male Occupants, Accid Anal Prev. 60: 334-343.
Liu YK, Dai QG (1989) The Second Stiffest Axis of a Beam-Colum: Implications for Cervical Spine Trauma. J Biomech Eng. 111(2): 122-127.
Maag U, Desjardins D, Bourbeau R, Laberge-Nadeau C (1990) Seat Belts and Neck Injuries, Proceedings of the IRCOBI Conference, Bron (France), pp. 1–14.
Maiman D, Sances A Jr, Myklebust J, Larson S, Houterman C, Chilbert M, El-Ghatit A (1983) Compression Injury of the Cervical Spine. Neurosurgery. 13(3): 254-260.
Maiman D, Yoganandan N, Pintar F (2002) Preinjury Cervical Alignment Affecting Spinal Trauma. J Neurosurg. 97(1 Suppl): 57-62.
Matsumoto M, Fujimura Y, Suzuki N, Toyama Y, Shiga H (1998) Cervical Curvature in Acute Whiplash Injures: Prospective Comparative Study with Asymptomatic Subjects. Injury. 29(10): 775-778.
Mattucci S, Moulton J, Chandrashekar N, Cronin D. (2012) Strain rate dependent properties of younger human cervical spine ligaments. J Mech Behav Biomed Mater. 10: 216-226.
Meyer F, Bourdet N, Deck C, Willinger R, Raul J. (2004) Human Neck Finite Element Model Development and Validation against Original Experimental Data, Stapp Car Crash J. 48, Paper no. 2004–22–0008.
Milne N. (1991) The role of zygapophysial joint orientation and uncinated processes in controlling motion in the cervical spine. J. Anat. 178: 189-201.
Mordaka J. (2004) Finite Element Analysis of Whiplash Injury for Women, Doctoral Thesis, Nottingham Trent University, Nottingham, UK.
Morris AP, Thomas PD (1996) Neck Injuries in the UK Co-operative Crash Injury Study, Proc. 40th Stapp Car Crash Conf., SAE 962433), pp. 317–329.
Narragon EA (1965) Sex Comparisons in Automobile Crash Injury, Cornell Aeronautical Laboratory (CAL) Report No. VJ 1823-R15.
Nightingale R, Chancey C, Ottaviano D, Luck J, Tran L, Prange M, Myers B. (2007) Flexion and extension structural properties and strengths for male cervical spine segments. J Biomech 40(3): 535-542.
Nightingale R, Winkelstein B, Knaub K, Richardson W, Luck J, Myers B. (2002) Comparative strengths and structural properties of the upper and lower cervical spine in flexion and extension. J Biomech 35(6): 725-732.
Nygren, Å. (1983). Injuries to Car Occupants - Some Aspects of the Interior Safety of Cars. Acta Oto-Laryngologica. 95(s395): 1-135, doi: 10.3109/00016488309139642.
O'Neill B, Haddon W Jr, Kelley AB, Sorenson WW (1972) Automobile Head Restraints: Frequency of Neck Injury Claims in Relation to the Presence of Head Restraints. Am J Public Health. 62(3): 309–406.
Ono K, Ejima S, Suzuki S, Kaneoka K, Fukushima M, Ujihashi S. (2006) Prediction of Neck Injury Risk based on the Analysis of Localized Cervical Vertebral Motion of Human Volunteers during Low-speed Rear Impacts. Proceedings of IRCOBI Conference, Madrid, Spain.
Ono K, Kaneoka K, Wittek A, Kajzer J. (1997) Cervical Injury Mechanism Based on the Analysis of Human Cervical Vertebral Motion and Head-Neck-Torso Kinematics during Low-speed Rear Impacts. Proc.41st Stapp Car Crash Conference, pp. 339–356.
Örtengren T, Hansson HA, Lövsund P, Svensson MY, Suneson A, Säljö A. (1996) Membrane Leakage in Spinal Ganglion Nerve Cells Induced by Experimental Whiplash Extension Motion: A Study in Pigs. J Neurotrauma. 13(3): 171–180.
Osakabe T, Hayashi M, Hasegawa K, Okuaki T, Ritty T, Mecham R, Wachi H, Seyama Y. (2001) Age- and Gender-Related changes in ligament components. Ann Clin Biochem. 38(Pt 5): 527- 532.
Otremski I, Marsh JL, Wilde BR, McLardy Smith PD, Newman RJ (1989) Soft tissue cervical injuries in motor vehicle accidents. Injury. 20(6): 349–351.
Panjabi MM. (2006) A Hypothesis of Chronic Back Pain: Ligament Subfailure Injuries Lead to Muscle Control Dysfunction. Eur Spine J. 15(5): 668–676.
Panzer M. (2006) Numerical Modeling of the Human Cervical Spine in Frontal Impact. Master Thesis, University of Waterloo, Waterloo, ON, Canada.
Panzer M, Cronin D. (2009) C4–C5 Segment Finite Element Model Development, Validation, and Load-Sharing Investigation, J Biomech. 42(4): 480–490.
Panzer M, Fice J, Cronin D. (2011) Cervical Spine Response in Frontal Crash, Med Eng Phys. 33(9): 1147–1159.
Parenteau C, Wang N, Zhang P, Caird M, Wang S. (2014) Quantification of Pediatric and Adult Cervical Vertebra—Anatomical Characteristics by Age and Gender for Automotive Application. Traffic Inj Prev. 15(6): 572-582.

Parenteau C, Zuby D, Brolin K, Svensson M, Palmertz C, Wang S. (2013) Restrained Male and Female Occupants in Frontal Crashes: Are We Different? International IRCOBI Conference on the Biomechanics of Impact, September 11-13, Gothenburg, Sweden.

Pearson AM, Ivancic PC, Ito S, Panjabi MM. (2004) Facet Joint Kinematics and Injury Mechanisms during Simulated Whiplash. Spine. 29(4): 390–397.

Pintar F, Yoganandan N, Voo L, Cusick JF, Maiman DJ, Sances A Jr (1995) Dynamic Characteristics of the Human Cervical Spine. 39th Stapp Car Crash Conference Proceedings, pp. 195-202.

Reddy M, Reddy B, Schoggl A, Saringer W, Matula C. (2002) The Complexity of Trauma to the Cranio-Cervical Junction: Correlation of Clinical Presentation with Doppler Flow Velocities in the V3- Segment of the Vertebral Arteries. Acta Neurochir (Wien). 144(6): 575–580.

Richter M, Otte D, Pohlemann T, Krettek C, Blauth M (2000) Whiplash-Type Neck Distortion in Restrained Car Drivers: Frequency, Causes and Long-Term Results, Eur Spine J. 9(2): 109–117.

Robin S. (2001) HUMOS: Human Model for Safety – A Joint Effort Towards the Development of Refined Human-like Car Occupant Models. 17th ESV Conference (Amsterdam, the Netherlands, June 4–7). Paper no. 297.

Sato F, Nakajima T, Ono K, Svensson M, Brolin K, Kaneoka K (2014) Dynamic Cervical Vertebral Motion of Female and Male Volunteers and Analysis of its Interaction with Head/Neck/Torso Behavior during Low-speed Rear Impact. Proceedings of IRCOBI Conference, Berlin, Germany.

Schmitt K-U, Weber T, Svensson M, Davidsson J, Carlsson A, Björklund M, Jakobsson L, Tomasch E, Linder A (2012) Seat testing to investigate the female neck injury risk - preliminary results using a new female dummy prototype, Proceedings of the International Research Conference on the Biomechanics of Impact, IRCOBI, Dublin (Ireland).

Schneider LW, Robbins DH, Pflüg MA, Snyder RG. (1983) Development of Anthropometrically Based Design Specifications for an Advanced Adult Anthropomorphic Dummy Family, Final Report, UMTRI-83-53-1, University of Michigan Transportation Research Institute, Ann Arbor, Michigan, USA.

Scott D, Jull G, Sterling M. (2005) Widespread Sensory Hypersensitivity Is a Feature of Chronic Whiplash-Associated Disorder but Not Chronic Idiopathic Neck Pain. Clin J Pain. 21(2): 175–181.

Seric V, Blazic-Cop N, Demarin V. (2000) Haemodynamic Changes in Patients with Whiplash Injury Measured by Transcranial Doppler Sonography (TCD). Coll Antropol. 24(1): 197–204.

Siegmund GP, King DJ, Lawrence JM, Wheeler JB, Brault JR, Smith TA (1997) Head/neck kinematic response of human subjects in low-speed rear-end collisions, Proceedings of 41th Stapp Car Crash Conference, Lake Buena Vista, FL, USA, SAE paper 973341.

Siegmund G, Winkelstein B, Ivancic P, Svensson M, Vasavada A (2009) The anatomy and biomechanics of acute and chronic whiplash injury. Traffic Inj Prev. 10(2): 101-112.

Siegmund G, Sanderson D, Myers B, Inglis J. (2003) Rapid Neck Muscle Adaptation Alters the Head Kinematics of Aware and Unaware Subjects Undergoing Multiple Whiplash-Like Perturbations. J Biomech. 36(4): 473–482.

Stemper B, Board D, Yoganandan N, Wolfla C. (2010) Biomechanical properties of human thoracic spine disc segments. J Craniovertebr Junction Spine 1(1): 18-22.

Stemper B, DeRosia J, Yogananan N, Pintar F, Shender B, Paskoff G (2009) Gender Dependent Cervical Spine Anatomical Differences in Size-Matched Volunteers. 46th International ISA Biomedical Science Instrumentation Symposium, Milwaukee WI, 17-19 April, 149-154.

Stemper B, Yoganandan N, Pintar F. (2005) Effects of Abnormal Posture on Capsular Ligament Elongations in a Computational Model Subjected to Whiplash Loading. J Biomech. 38(6): 1313–1323.

Stemper B, Yoganandan N, Pintar FA. (2004) Gender- and Region- Dependent Local Facet Joint Kinematics in Rear Impact. Spine 29(16): 1764–1771.

Stemper B, Hallman J, Pintar F, Maiman D. (2012) Gender and Aging: Considerations for Orthopaedics. In Orthopaedic Biomechanics, Editor: Beth A. Winkelstein, Published: December 18, 2012 by CRC Press

Stemper B, Yoganandan N, Pintar FA, Maiman DJ, Meyer MA, DeRosia J, Shender BS, Paskoff G (2008) Anatomical Gender Differences in Cervical Vertebrae of Size-Matched Volunteers. Spine. 33(2): E44–E49.

Stemper B, Yoganandan N, Pintar F. (2003) Gender Dependent Cervical Spine Segmental Kinematics during Whiplash. J Biomech. 36(9): 1281–1289.

Storvik S, Stemper B, Yoganandan N, Pintar F. (2009) Population-Based Estimates of Whiplash Injury Using NASS CDS Data, Biomed Sci Instrum. 45: 244–249.

Sugimoto T, Yamazaki K. (2005). First Results from the JAMA Human Body Model Project. 19th ESV Conf. (Washington D.C., US), Paper no. 05–0291.

Svensson MY, Boström O, Davidsson J, Hansson H-A, Håland Y, Lövsund P, Suneson A, Säljö A. (2000) Neck Injuries in Car Collisions—A Review Covering a Possible Injury Mechanism and the Development of a New Rear-Impact Dummy. Accid Anal Prev. 32(2): 167–175.

Takeshima T, Omokawa S, Takaoka T, Araki M, Ueda Y, Takakura Y (2002) Sagittal Alignment of Cervical Flexion and Extension. Spine. 27(15): E348–355.

Tatarek N. (2005) Variation in the human cervical neural canal. Spine J. 5(6): 623-631.

Temming J, Zobel R (1998) Frequency and Risk of Cervical Spine Distortion Injuries in Passenger Car Accidents: Significance of Human Factors Data, Proceedings of the IRCOBI Conference, Göteborg, Sweden, pp. 219–233.

The Whiplash Commission (2005) *Final Report* http://www.whiplashkommissionen.se/pdf/WK_finalreport.pdf.

Thomas C, Faverjon G, Hartemann F, Tarriere C, Patel A, Got C (1982) Protection Against Rear-End Accidents, Proceedings of the IRCOBI Conference, Cologne, Germany, pp. 17–29.
Valkeinen H, Ylinen J, Malkia E, Alen M, Hakkinen K. (2002) Maximal force, force/time and activation /coactivation characteristics of the neck muscles in extension and flexion in healthy men and women at different ages. Eur J Appl Physiol. 88(3): 247–254.
van der Horst M. (2002) Human Head Neck Response in Frontal, Lateral, and Rear End Impact Loading – Modelling and Validation, Doctoral Thesis, Eindhoven University of Technology, Eindhoven, the Netherlands.
Vasavada A, Brault J, Siegmund G. (2007) Musculotendon and Fascicle Strains in Anterior and Posterior Muscles during Whiplash Injury. Spine 32(7): 756–765.
Vasavada A, Danaraj J, Siegmund G. (2008) Head and neck anthropometry, vertebral geometry and neck strength in height-matched men and women. J Biomech. 41(1): 114-121.
Vasavada A, Li S, Delp S. (2001) Three-Dimensional Isometric Strength of Neck Muscles in Humans. Spine. 26(17): 1904-1909.
Vavalle N, Moreno D, Rhyne A, Stitzel J, Gayzik F. (2013) Lateral Impact Validation of a Geometrically Accurate Full Body Finite Element Model for Injury Prediction, Ann Biomed Eng. 41(3): 497–512.
Watanabe Y, Ichikawa H, Kayama O, Ono, K, Kaneoka K, Inami S (2000) Influence of Seat Characteristics on Occupant Motion in Low-Velocity Rear-End Impacts, Accid Anal Prev 32(2): 243–250.
Watanabe R, Miyazaki H, Kitagawa Y, Yasuki T. (2011) Research of Collision Speed Dependency of Pedestrian Head and Chest Injuries Using Human FE Model (THUMS Version 4). 22nd ESV Conf. (Wasington D.C., June 13–16). Paper no. 11–0043.
Wheeldon J, Stemper B, Yoganandan N, Pintar F. (2008) Validation of a Finite Element Model of the Young Normal Lower Cervical Spine, Ann Biomed Eng. 36(9): 1458–1469.
Wild CY, Steele JR, Bridget J, Munro BJ (2012) Why Do Girls Sustain More Anterior Cruciate Ligament Injuries Than Boys? A Review of the Changes in Estrogen and Musculoskeletal Structure and Function During Puberty. Sports Med. 42(9): 733–749.
Yang K, King A. (2003) Neck Kinematics in Rear-end Impacts. Pain Res Manag. 8(2): 79–85.
Yang K, Zhu F, Luan F, Zhao L, Begeman, P. (1998) Development of a Finite Element Model of the Human Neck. In Proceedings of the 42nd Stapp Car Crash Conference (Tempe, AZ, USA). Paper no. 983157.
Yoganandan N, Pintar F, Gennarelli T, Eppinger R, Voo L.(1999) Geometrical Effects on the Mechanism of Cervical Spine Injury due to Head Impact. Proceedings of IRCOBI Conference, Sitges, Spain.
Yoganandan N, Sances A Jr, Maiman DJ, Myklebust JB, Pech P, Larson SJ (1986) Experimental Spinal Injuries with Vertical Impact. Spine. 11(9): 855–860.
Zhang Q, Teo E, Ng H. (2005) Development and Validation of a C0–C7 FE Complex for Biomechanical Study, J Biomech Eng. 127(5): 729–735.
Zhang Q, Teo E, Ng H, Lee V. (2006) Finite Element Analysis of a Moment-Rotation Relationship for Human Cervical Spine, J Biomech., 39(1): 189–193.

MUSCLE ACTIVATION STRATEGIES IN HUMAN BODY MODELS FOR THE DEVELOPMENT OF INTEGRATED SAFETY

Jonas Östh
Karin Brolin
Jóna Marín Ólafsdóttir
Johan Davidsson
Chalmers University of Technology
Bengt Pipkorn
Autoliv Research
Lotta Jakobsson
Volvo Car Corporation and Chalmers University of Technology
Fredrik Törnvall
Volvo Group Trucks Technology
Mats Lindkvist
Umeå University
Sweden

Paper Number 15-0345

ABSTRACT
Human Body Models (HBMs) have been used in crash safety research for some time, and are now emerging as tools for the development of restraints systems. One important challenge in the development of advanced restraint systems is to integrate sensory information about the pre-crash phase (time to collision, impact speed and direction, occupant position) to alter restraint activation parameters. Restraint activation can begin even before the beginning of an impact, providing additional time to reposition or restrain the occupant. However, any such pre-crash intervention would invoke a muscle response that needs to be taken into account in HBMs used in simulation of integrated restraints.

The objective of this paper is to provide an update on state-of-the-art modeling techniques for active musculature in HBMs. Examples of applications are presented, to illustrate future challenges in modeling of car occupants muscle responses to restraint activation.

The most common approach for modeling active muscle force in HBMs is to use Hill-type models, in which the force produced is a function of muscle length, shortening velocity, and activation level. Active musculature was first implemented in cervical spine models. These models were applied to study occupant kinematic responses and injury outcome in rear-end, lateral, and frontal impacts; it was found that active musculature is essential for studying the response of the cervical spine. One approach utilized to represent muscle activity in HBMs is to use experimentally recorded muscle activities or activity levels acquired through inverse optimization in open-loop. More recently, in order to represent car occupant muscle responses in pre-crash situations, closed-loop control has been implemented for multibody and finite element HBMs, allowing the models to maintain their posture and simulate reflexive responses. Studies with these models showed that in addition to feedback control, anticipatory postural responses needs to be included to represent driver actions such as voluntary braking.

Current HBMs have the capacity to model (utilizing closed-loop control) active muscle responses of car occupants in longitudinal pre-crash events. However, models have only been validated for limited sets of data since as high quality volunteer data, although it exists, is scarce. Omni-directional muscle responses have been implemented to some extent, but biofidelity of the simulated muscle activation schemes has not been assessed. Additional experimental volunteer muscle activity measurements (with normalized electromyogram recordings) in complex 3D-loading scenarios are needed for validation and to investigate how muscle recruitment depends on occupant awareness and varies between individuals. Further model development and validation of muscle activations schemes are necessary, for instance startle responses, and individual muscle control. This could improve assessment of restraint performance in complex accident scenarios, such as multiple impacts, far-side impacts and roll-over situations.

INTRODUCTION
Human Body Models (HBMs) have been used in crash safety research for some time. Compared to Anthropomorphic Test Devices (ATDs) they can be made more humanlike, and usually incorporates an omnidirectional design; which makes them suitable for a wider range of crash situations. Future safety development challenges include more oblique and complex crash scenarios, in contrast to standardized crash test scenarios (usually pure lateral, frontal, or rear-end impacts) with ATDs in upright seated postures. Recently, small overlap

frontal crashes have been included in the standardized test procedures (IIHS 2012) and one of the challenges identified is the ATDs' limitations in recreating occupant kinematics within these crashes, with a combination of longitudinal and lateral movement (Jakobson et al. 2013). Small overlap frontal crashes are an example of crash situations where the benefit of an omnidirectional HBM is clear. Other situations include oblique or angled impacts, multiple events, rollover, and run off road events. In a run off road event, the vehicle kinematics is complex and posing significant challenges for occupant simulation (Jakobsson et al. 2014). During run off road events not only the directions of impact can vary, but also the occurrence of multiple impacts connected with low acceleration amplitude events influencing occupant posture during the events. Such scenarios could perhaps be viewed as the ultimate challenge from an occupant simulation perspective. Developing HBMs to address this challenge would be beneficial from a real world safety perspective.

Pre-crash maneuvers can influence occupant posture prior to an impact (Heiter et al. 2005; Hault-Dubrulle et al. 2011). In an analysis of accident data in Japan for 1993–2004, Ejima et al. (2009) reported that approximately 50% of drivers made an evasive maneuver in the form of braking or combined braking and steering before an impact. The development of Collision Avoidance Systems (CASs) is likely to increase the occurrence of pre-crash braking, by adding autonomous braking to the cases where drivers did not brake prior to the accident. CASs help drivers avoid or mitigate collisions through warnings and/or interventions, based on information about the traffic environment (Ljung-Aust et al. 2015). This information can be obtained by radar, laser, camera and other sensors. Intervention can include automatic braking and/or steering as well as means for improving occupant protection by triggering/adapting restraints. The development of CAS has been rapid over the last decade. While quite exotic 10 years ago, today most vehicle manufacturers offer some form of CAS in their vehicles, at least as an extra option. This has been made possible through developments in sensing and threat assessment, as well as improved actuators in production vehicles like steering control and differential wheel braking. The first generation systems were introduced in early 2000 with functionality restricted to provide brake support by tracking objects moving in the same direction as the host vehicle (Coelingh et al. 2006). In 2015, the state of the art systems includes tracking of cyclists, pedestrians and vehicles in front of the host vehicle as well as a first step into addressing intersection situations (when turning in front of an oncoming vehicle) (Ljung-Aust et al. 2015). The results from the few available real world follow-up studies indicate that CAS provide a substantial safety benefit (IIHS 2011; Isaksson-Hellman and Lindman 2012; IIHS 2013; Rizzi et al. 2014). The development of CAS creates a need for tools to evaluate the occupant response during the pre-crash phase, combined with possible subsequent impacts.

To improve restraint functionality, and prepare occupants for impact, reversible pre-tension systems have also been used together with CAS (Schöneburg et al. 2011); this allows the occupant to be more tightly coupled to the seat during autonomous braking, and has the potential to reduce forward displacement of occupants as a result of the pre-crash braking (Antona et al. 2010). Advanced restraint systems, that utilize reversible pre-tensioning of seat belts during the pre-crash phase, are emerging and some studies on the effect of pre-tensioning on occupant kinematics have been published, using either volunteers (Mages et al. 2003; Good et al. 2008a; Schöneburg et al. 2011; Östh et al. 2013; Ólafsdottir et al. 2013; Develet et al. 2013; Ito et al. 2013) or ATDs (Good et al. 2008b; Woitsch and Sinz 2014). However, extending these studies to also assess the injury reduction potential of restraints active in both the pre- and in-crash phase is difficult. Volunteers cannot be subjected to injurious loads while ATDs, developed to predict injury in high energy impacts, are too stiff to represent relaxed vehicle occupants under low loading conditions (Beeman et al. 2012).

The limitations associated with ATD and volunteer testing can be addressed with mathematical HBMs that can represent occupant responses in pre-crash as well as crash loading conditions (Schöneburg et al. 2011, Mages et al. 2011). To represent an attentive occupant and the influence of the occupant's muscle reaction on the kinematic response during the pre-crash phase, active muscle response and a human-like control strategy of the muscles must be included in future HBMs. In the past, several models with one dimensional or solid elements only representing the passive elastic and damping response of the neck musculature have been developed (Jost and Nurick 2000; Robin 2001; Ejima et al. 2005; Toyota 2008). However, the active force generated by muscles has a different order of magnitude than the passive muscle stiffness and damping at physiological muscle lengths. Early implementation of active muscle properties in HBMs were made in cervical spine models (Deng and Goldsmith 1987; de Jager 1996; Wittek 2000; Brolin et al. 2005). Since then, models with active musculature have been included in numerous HBMs, summarized in Table 1. The most common method for implementing active muscle properties in HBMs is to utilize 1D Hill-type muscle elements. In some models 1D Hill-type elements have been super-positioned with a passive bulk material to provide 3D muscles geometry with existing material models in the FE solvers (Behr et al.

2006; Hedenstierna et al. 2008; Iwamoto et al. 2009; 2011; 2012). Another study implemented the Hill-model with local fiber directions in a continuum FE material model (Khodaei et al. 2013).

The aim of this paper is to provide an update on state-of-the-art modeling techniques for simulation of muscle activity in HBMs, and to highlight future challenges and benefits with modeling of car occupants muscle responses to restraint activation.

REVIEW OF ACTIVE MUSCLE CONTROL IN HBM

Several methods for regulating muscle activity in HBMs have been proposed. These methods can be divided into two main categories: open-loop control, where muscle activation functions are defined prior to simulation, and closed-loop control, where muscle activities are regulated based on sensory information about the current state of the model, for instance the position of a limb.

Table 1. Summary of HBM studies that have included active musculature. MB = Multibody; FE = Finite Element; 1D = 1 dimensional; 3D = 3 dimensional. EMG = Electromyogram; PID = Proportional, Integral, and Derivative; T1 = First thoracic vertebra.

***Model* Type / Solver**	**Reference**	**Body part**	**Actuators[1]**	**Control**	**Activation scheme**	**Application**
TNO Active Human Model	Cappon et al. 2007	Spine	Torque actuators	Closed-loop	PID controllers	Reversible belt pre-tension, roll-over
	Budziszewski et al. 2008	Upper extremity	1D muscles	Closed-loop	PID controllers	Elbow flexion
MB / MADYMO	Meijer et al. 2008	Spine, left arm and legs	Torque actuators, 1D muscles	Open and closed-loop	PID controllers, engineering judgment	Far-side impact
	Fraga et al. 2009	Cervical spine	1D muscles	Closed-loop	PID controllers	Motorcycle braking and cornering
	Nemirovsky and van Rooij 2010	Cervical spine	1D muscles	Closed-loop	PID controllers	Rear-end impacts
	van Rooij 2011	Spine	Torque actuators, 1D muscles	Closed-loop	PID controllers	Autonomous braking
	Meijer et al. 2012	Whole body	1D muscles, torque actuators	Closed- and open-loop co-contraction	PID controllers, variable co-contraction	Autonomous braking, frontal, lateral, and rear-end impact
	Meijer et al. 2013b	Whole body, hip and elbow added	1D muscles, torque actuators	Closed- and open-loop (co-contraction)	PID controllers, variable co-contraction and reaction time	Pendulum impacts, car braking, sled impacts
	Meijer et al. 2013a	Whole body, new neck and elbow	1D muscles, torque actuators	Closed- and open-loop (co-contraction)	PID controllers, varied levels of co-contraction	Anterior-posterior T1 perturbations, elbow flexion impulses, and autonomous braking.
	de Bruijn 2014	Cervical spine	1D muscles	Closed-loop	Vestibular and muscle spindle feedback	Anterior-posterior T1 perturbations

Table 1. Continued.

***Model* Type / Solver**	**Reference**	**Body part**	**Actuators[1]**	**Control**	**Activation scheme**	**Application**
SAFER A-HBM	Östh et al. 2012b	Upper extremity	1D muscles	Closed-loop	PID controller	Elbow flexion-extension impulse load and posture maintenance
FE / LS-DYNA	Östh et al. 2012a	Cervical and lumbar spine	1D muscles	Closed-loop	PID controllers	Autonomous braking for car passengers
	Östh et al. 2014a	Cervical and lumbar spine, upper extremities	1D muscles	Closed-loop	PID controllers	Autonomous braking with reversible pre-tension
	Östh et al. 2014b	Cervical and lumbar spine, upper and lower extremities	1D muscles	Closed-loop with anticipatory component, and open-loop	PID controllers and based on normalized EMG (lower extremities)	Driver maximal emergency braking postural response
Active THUMS	Sugiyama et al. 2007	Lower extremity	1D muscles	Open-loop	Inverse dynamics model	Brake pedal impacts
FE / LS-DYNA	Iwamoto et al. 2009	Upper extremity	3D muscles	Open-loop	engineering judgment	Lateral impact to elbow
	Iwamoto et al. 2011	Whole body	3D muscles	Open-loop	Normalized EMG	Frontal impact
	Iwamoto et al. 2012	Whole body	3D muscles	Open-loop	Reinforcement learning model	Frontal and rear-end impacts
	Iwamoto and Nakahira 2014	Whole body	3D muscles	Open-loop	Normalized EMG, engineering judgment	Pedestrian impacts
FE /PAM-CRASH	Wittek 2000	Cervical spine	1D muscles	Open-loop	Reflex activation	Rear-end impacts
FE / LS-DYNA	Brolin et al. 2005; 2008	Cervical spine	1D muscles	Open-loop	Reflex activation, optimization	Frontal and lateral impact, helicopter crash
FE / LS-DYNA	Hedenstierna 2008	Cervical spine	3D muscles	Open-loop	Reflex activation, Optimization	Frontal, lateral and rear-end impacts
MB / LS-DYNA	Chancey et al. 2003; Dibb et al. 2013	Cervical spine	1D muscles	Open-loop	optimization	Tensile neck loading, frontal impact, child HBM
FE/LS-DYNA	Chang et al.2008; Chang et al. 2009	Lower extremity	1D muscles	Open-loop	Normalized EMG	Knee impacts

[1] In all HBMs which used muscle elements as actuators, the active behavior was modeled with a Hill-type material model. All models with 3D muscles employ the super-position of a passive continuum bulk material and Hill-type line muscle elements (Hedenstierna et al. 2008).

Muscle Models with Open-loop Control

In models that use open-loop control, muscle activities are defined as a function of time prior to the simulation, based on know-how from previous simulations, experimental data, or optimization in static load cases. The outcome is observed afterwards, and the activation function may be iteratively adjusted to achieve a more biofidelic model response in upcoming simulations.

Reflex Activation

Several cervical spine models (de Jager 1996; Wittek 2000; van der Horst 2002; Brolin et al. 2005; Stemper et al. 2006) have accounted for the influence of active behavior by the application of a maximum activity starting at a specified time in the simulation. With this approach in a multibody (MB) neck model, de Jager (1996) showed the importance of active muscles to capture the human head-neck response in frontal and lateral impacts; the same model was later refined and employed in rear-end impacts, and yet again the importance of active muscles was shown by van der Horst (2002). Brolin et al. (2005) found that including muscle activity for an FE neck model, with 1D Hill-type muscle elements, improved the kinematic correlation with volunteer data for frontal and lateral impacts. The muscle activation properties, i.e. the shape of the curve defining muscle activity, were varied and the best correlation with experimental data was found when neck flexors and extensors were assigned different activity levels. In addition, Brolin et al. (2005) also found altered injury patterns as an effect of neck muscle activity with respect to cervical ligament strain.

Maximum muscle activation at a specified time in the simulation is a straightforward way to introduce the effect of reflexive muscle responses and that of eccentric muscle lengthening. If simultaneous activation of all muscles is modeled, the implicit assumption is that a reflexive startle response is present. A startle response is a rapid response to stimulation of mechanoreceptors, acoustic stimuli, visual stimuli, or a combination thereof. It is characterized as a bilateral response which includes closing of the eyes, extension of the neck, elevation of the shoulders, and extension of the lumbar back (Yeomans et al. 2002). This might very well be present in many impact-like scenarios, and this method may suffice for short duration impacts with a clear loading direction, but not for more complex scenarios or for scenarios in which posture must be maintained for a period of time (Brolin et al. 2008).

Optimization of Static Posture-Maintaining Activities

Chancey et al. (2003) developed an MB neck model with detailed muscles and studied the effect of muscle activity on tensile loading of the neck for two sets of muscle activities. The muscle activities evaluated were determined with an optimization scheme that gave initial stable postures for low-level and maximal muscle activation. More recently the same method was applied to find posture maintaining muscle activation schemes for six and ten-year-old pediatric cervical spine models (Dibb et al. 2013). The neck stabilizing muscle activity levels reported by Chancey et al. (2003) were used as a starting point to find load case specific stabilizing activities in a study with an FE neck model conducted by Brolin et al. (2008). The model was thereafter applied to evaluate the influence of tensed muscles on spinal injuries for helicopter pilots, and it was found that stabilizing neck muscle activation reduced the risk of ligamentous injuries. Bose and Crandall (2008) and Bose et al. (2010) used an MB HBM which was varied in size from the approximate 20th to 80th percentile male anthropometry, nine different initial postures, and 0–100% muscle co-contraction activity in 1D Hill-type elements. They performed optimization simulations to generate static stabilizing co-contraction activity levels and evaluated the influence of initial muscle co-contraction on a whole body injury metric in a simulated 57 km/h impact. They found that the initial posture was the most significant factor in determining the injury outcome, although the initial muscle co-contraction also had some influence. In particular, an increased risk for injury in the lower extremities with increasing muscle co-contraction was reported.

In open-loop control, optimization is a systematic way to balance a set of muscle activity levels. However, actual stabilizing activity levels are difficult to achieve. For instance, Chancey et al. (2003) defined posture maintenance as less than 5° rotation or 10 mm translation of the head over a period of 100 ms and Brolin et al. (2008) used a similar criteria in combination with a threshold of ±1 mm and 0.01 radians head motion for the subsequent 300 ms as a requirement for postural stability. In addition, any reflex responses due to the perturbation are not accounted for in an impact scenario.

Optimization of Dynamic Activities

Iwamoto et al. (2012) presented a version of the THUMS HBM with a detailed 3D representation of muscles for all body parts. For the head and neck, a simplified model using 1D Hill-type elements was also developed. Using the simplified neck model and an optimization process called reinforcement learning, tabulated muscle control functions that account for both joint angles and velocities were derived. The optimization provided individual muscle activation functions that were applied in the detailed model in a rear-end impact test case. With the reinforcement learning muscle activities the THUMS with 3D muscles appeared to perform better than with deactivated muscles in the initial phase of the impacts compared with volunteer data, but then it overestimated the effect of the muscle activity on kinematics.

Multi-dimensional, pre-determined, activity tables can resemble actual human motor control, as the joint angles and velocities would correspond to stretch and rate of change of muscle lengths and correlate with input to the vestibular organs. If the model is accurate in reproducing the muscle activity for a wide range of combinations of angles and velocities, the resulting activation patterns could be compared with experimental data and the muscle response of the model would be human-like. However, a drawback of the study performed by Iwamoto et al. (2012) appears to be the large number of simulations (660) needed to generate the dynamic activity tables, and that these tables were derived for a simplified model, that potentially have different dynamic properties than the actual active HBM.

Estimation based on Experimental Data

Behr et al. (2006), Sugiyama et al. (2007), and Chang et al. (2008; 2009) all modeled emergency braking with active muscles in the lower extremities. The muscle activity levels were taken from normalized electromyogram (EMG) measurements in emergency braking experiments. They studied the injury risk in frontal impacts (Behr et al. 2006), brake pedal impacts (Sugiyama et al. 2007) and knee impacts (Chang et al. 2008), and concluded that the inclusion of active musculature changes the injury risk in these situations. Chang et al. (2008) predicted that the external force producing a fracture in the knee-thigh-hip area decreases when muscle tension is taken into account, although a limitation of the study was the lack of detailed muscle activity data for the lower extremities. Therefore, a second study was made (Chang et al. 2009), in which an inverse dynamics musculoskeletal model was used to derive detailed individual muscle activity levels from experimental data. The same approach applying inverse optimization was used by Choi et al. (2005), i.e. an optimization in which muscle activity levels are derived using a musculoskeletal model, measured forces, and limb positions, together with hypothesized optimization constraints. They simulated occupant bracing in sled impacts with active muscles in the upper and lower extremities. Iwamoto and Nakahira (2014) simulated pedestrian impacts with a whole body HBM with 3D musculature without muscle activity, with relaxed activity and 20% activity in all muscles, as well as only neck muscle activity based on volunteer data. They concluded that muscle activity affected pedestrian kinematics and could have an influence on the injury outcome predicted in such simulations.

If maximum voluntary contractions are performed for the specific experimental setup, it is possible to derive muscle activity levels for measured muscles under experimental conditions. These levels can then be used in simulations, such as in the studies summarized in the present section, either directly or through optimization with inverse dynamics models. This approach will generate muscle activities in the model which are in good temporal agreement and of the right magnitude, if the EMG is appropriately processed. However, for each scenario simulated, volunteer experiments must be performed and the models would not be able to predict occupant responses in other conditions. Therefore, this practical approach has limited applicability for safety restraint development, since interaction with new restraint systems may change muscle activity, as will more severe loading than what can be used in volunteer experiments.

Muscle Models with Closed-loop Control

In closed-loop applications the response of the controlled system is continuously monitored and the control signal is adjusted in accordance with the actual model response. In the human body the reflex arc, is the simplest closed-loop structure in the neuromuscular control system. In current active HBMs, closed-loop control has mainly been implemented with proportional, integral, and derivative (PID) controllers defined as:

$$e(t) = r(t) - y(t) \tag{1}$$

$$u(t) = k_p \cdot e(t) + k_i \cdot \int_0^t e(\tau)d\tau + k_d \cdot \frac{de(t)}{dt}. \tag{2}$$

The current state of the system, *y(t)*, is compared with the reference, *r(t)*, and the control signal, *u(t),* is proportional to the difference between the two according to Equation (2). The characteristics of the PID controller are determined by the proportional gain, k_p, integral gain, k_i, and derivative gain, k_d. The PID feedback control can be applied to model human postural responses; the proportional and derivative feedback then models the effect of muscle spindle and vestibular reflexive stabilization, while the integrative controller removes any steady state error due to constant loads such as gravity.

Closed-Loop Postural Control with Torque Actuators

One of the first implementations of closed-loop control to model occupant postural responses was realized by Cappon et al. (2007) who utilized PID controllers to apply torque at each individual vertebral joint in a MB HBM.

The model was applied to study the phase preceding a roll-over accident and a static application of a reversible pre-tensioned restraint. The addition of the active spine improved the model kinematics in the roll-over scenario but was less successful in capturing the volunteer response to the reversible pre-tensioned restraint. The spine with active torque actuators was later utilized in several publications on the *TNO Active Human Model* (Meijer et al. 2008; van Rooij 2011; Meijer et al. 2012; Meijer et al. 2013a; 2013b). In addition, the torque actuator approach was used to simulate child kinematics with a 6-year old MB child model (Brolin et al. 2014). Torque actuators with closed-loop control are suitable for modeling scenarios where kinematic responses are of primary interest, but less so for crash events or study of injury outcome.

Closed-loop Postural Control with 1D Muscle Elements

Budziszewski et al. (2008) implemented closed-loop control of 1D Hill-type elbow flexor and extensor muscles in a MB arm model. A PID controller was implemented for the elbow joint angle and the muscles were grouped into flexors and extensors and assigned equal activity levels from the controller. The model was tested and compared with experimental data of voluntary elbow flexion and extension; it was concluded that the kinematic performance of the model matched that of the volunteers but that predicted muscle activity levels were over-estimated. Fraga et al. (2009) used feedback PID control of line muscle elements to stabilize the head of a motorcycle rider in lateral and longitudinal maneuvers for MB simulations. They concluded that their model appeared to capture resulting head kinematics of a volunteer with average awareness who applied the brakes on a motorcycle. Furthermore, they stated that the model was promising for the development of advanced restraint systems for motorcycle riders, and that it was a step towards active whole body HBMs.

The head-neck model used by Fraga et al. (2009) was further developed by Nemirovsky and van Rooij (2010) by the implementation of a postural controller for the head-neck complex, with the aim of regulating flexion-extension, lateral flexion, and rotation of the head. The motions were decoupled by a muscle recruitment strategy, which would ensure that only one degree of freedom was influenced by each controller; however, only the model response in flexion-extension was evaluated. Along with three PID controllers for the three head rotational degrees of freedom, a variable co-contraction ratio was implemented. The co-contraction ratio was important for the resulting closed-loop response, as muscular co-contraction makes a significant contribution to the damping of the closed-loop system. The model was later used by van Rooij (2011), who hypothesized that the attentiveness of drivers is reflected by the gains used in the control model. He simulated the influence of different levels of awareness on driver kinematics in autonomous braking interventions.

Meijer et al. (2012) combined and extended the work presented in the previous publications on the *TNO Active Human Model* (Cappon et al. 2007; Meijer et al. 2008; Fraga et al. 2009; Nemirovsky and van Rooij 2010; van Rooij 2011) to form an active whole body model. The feedback loop was complemented with a reaction time for events that produce a larger controller error than the preceding ones in the simulation. A low-pass filter function representing the neural transmission time from the CNS to the distal muscles was also added. The signal from each controller was converted to the muscles or torque actuators through multiplication by a constant defined in a recruitment table, to ensure that only the degree of freedom being regulated was affected (Nemirovsky and van Rooij 2010). Furthermore, muscle co-contraction was defined prior to the simulations, i.e. open-loop control, to generate muscle tension without any net moment around the joints, contributing to the intrinsic stiffness. Kinematic responses of the model were evaluated for autonomous braking, frontal, lateral, and rear-end impacts. It was concluded that both feedback control and muscle co-contraction is needed to predict volunteer responses in these types of events.

In Meijer et al. (2013b), feedback controlled elbow and hip muscles were introduced and a muscle recruitment approach similar to that described by Nemirovsky and van Rooij (2010) was used to decouple hip flexion-extension, medial-lateral rotation and abduction-adduction. Utilizing 50% co-contraction of the muscle actuators, the model was reasonably well able to capture forward displacements of the chest and neck in 1 g driver braking events, and in 3.8 g, and 15 g volunteer impact tests. Meijer et al. (2013a) introduced new and more biofidelic neck muscle geometry in the TNO Active Human Model, and evaluated the response of the head-neck complex to low level random perturbations of the T1 vertebra. Furthermore, force pulse perturbations were applied to the hand, inducing flexion and extension of the elbow and the model response was compared with that of one volunteer. Finally, the difference between a braced state and a relaxed state for the model was evaluated by simulating a braking event. It was concluded that the model response for the relaxed condition is different from the braced condition.

The head-neck complex from *TNO Active Human Model* was taken a step further by modeling muscle spindle and vestibular feedback in more detail (de Bruijn 2014). The controller included a model of the dynamics of each reflex loop and their respective neural delays. Muscle activity regulation was based on inputs on muscle length and lengthening velocity (spindle feedback) and head angular velocity and gravitational force (vestibular feedback). Each muscle was activated individually based on a muscle recruitment scheme obtained from isometric optimization simulations. Although the model was not used to simulate the head-neck response in vehicle impact scenarios it has potential to be applied in such studies in the future.

Östh et al. (2012b) implemented PID control for the elbow joint of the THUMS v3 (Toyota 2008) FE HBM, actuated by 1D Hill-type muscles. This study showed the feasibility of using closed loop muscle activation with FE HBM. In this particular case the PID controller was implemented in LS-DYNA with use of the solution control subroutine (Erhart 2010) in LS-DYNA, which allows for users to program their own material models and element formulations, Figure 1. The model was able to maintain its posture in a field of gravity. With 5 % extensor and 3 % flexor co-contraction and experimentally determined controller gains the model was able to reproduce the response of one volunteer to a 15 N force impulse. Furthermore, it was concluded that the detail of the original contact based joints in the THUMS v3 did not provide biofidelic passive joint properties and had to be replaced with revolute joints. An alternative approach for performing feedback control in LS-DYNA was presented by Prüggler et al. (2011), who used external software for the feedback control algorithm coupled to the FE solver for simulations with a simplified FE HBM.

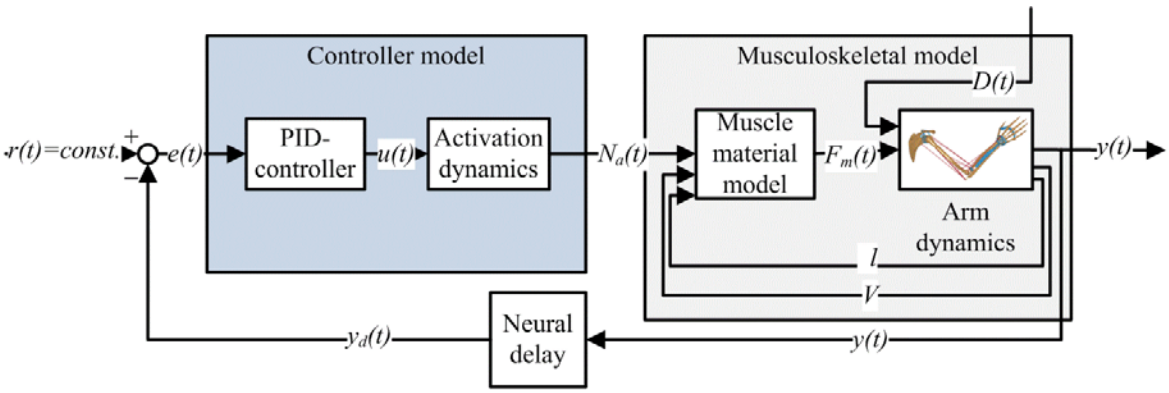

Figure 1. Illustration of the neuromuscular feedback control loop used for the elbow joint by Östh et al. (2012b). Reprinted with permission from Taylor and Francis.

The work by Östh et al. (2012b) was continued by adding 1D Hill-type muscles to the cervical and lumbar region and three PID controllers for the angles of the head, neck, and lumbar spine relative to the vertical axis. The model was used to study passenger forward head displacements in autonomous brake interventions of 6 m/s^2 compared with volunteer data (Östh et al. 2012a). It was reported that for passengers wearing a three-point seat belt, the support of the belt reduced the importance of the lumbar controller to match volunteer kinematics. Hence, to validate a lumbar controller experimental data from volunteers not wearing a shoulder belt is needed; instead wearing a lap belt or travelling unrestrained is needed. Moreover, in order to be able to simulate driver postural responses to autonomous braking, feedback control and linked 1D Hill-type muscles were added to the shoulders and combined with the previously developed elbow, trunk, and neck controllers (Östh et al. 2014b). This version of the model, denoted the *SAFER A-HBM* (Table 1), was then validated for four loading conditions: in driver and passenger positions for autonomous braking of 11 m/s^2 with two different three-point seat belt configurations. A seat belt with a reversible pre-tensioned retractor that provided 170 N of pre-tension to the shoulder belt prior to the braking was compared to a belt with a standard inertia reel retractor. The model compared well for kinematics, timing, and boundary forces between the occupant and vehicle, and reasonably for muscle activity levels. The validated model was employed in a parameter study of belt activation parameters, which showed that the largest reduction of peak head displacement was found for 570N pre-tension 0.15 s before deceleration onset, for both the driver and passenger positions.

Lastly, lower extremity muscles were added to the *SAFER A-HBM* (Östh et al. 2014a) and maximum driver braking was simulated. Based on experimental observations, an anticipatory postural response was hypothesized and implemented by changing the reference angles of the PID controllers for the head, neck, elbows and lumbar spine proportionally to the deceleration pulse. In general, most drivers will have extensive experience from braking events of varying magnitude, and, hence, will have inherent knowledge of the acceleration pulse that will follow after voluntary brake application. Without the anticipatory postural response the model predicted 100 mm longer forward displacements and 16° greater head rotations than were measured for braking volunteer drivers. With the anticipatory postural response, the model head displacement was within the volunteer corridors. Therefore, the hypothesized approach seems feasible and has the potential to be enhanced for other loading modes.

DISCUSSION

HBMs will play an important role in future safety development of vehicles. Although certification procedures most likely will take a number of years to include virtual testing, it is not unlikely that it will become part of consumer information testing to a greater extent than today. Robustness and repeatability are important requirements for HBMs to be used for verification, with or without simulated muscle activity. This will be a challenge for HBMs with muscle control that changes their response with the level and direction of loading. From a real world safety development perspective there is a considerable need for active HBMs. Maneuvers prior to an impact are a reality (Ejima et al. 2009; Bohman et al. 2011) and are necessary to simulate in order develop protective systems for these situations. Evasive braking as well as steering maneuvers, represent the first priorities. However, ultimately HBMs should be designed to simulate a whole event of combined intensity, such as multiple impacts or run off road events. We would like to stress the importance of developing active HBMs that can be used to study both the pre-crash and crash in one or coupled simulations in a straight forward and simple methodology, preferably with the same HBM.

To date, one FE (Östh et al. 2014b) and one MB (Meijer et al. 2013b) whole body occupant HBM with muscle activity regulated by closed loop control, have been developed to simulate driver and passenger kinematics in pre-crash and emergency events. Both of these models are of average male anthropometry. They have been evaluated with respect to volunteer data in longitudinal loading situations. Future needs for safety development require HBMs with omnidirectional biofidelity and therefore there is a need to further enhance and validate these HBMs for oblique loading with lateral components. Also, to study long duration and complex crash scenarios FE HBMs are particularly needed for the crash simulations, as explicit FE is the industry standard. Furthermore, FE HBMs have the ability to predict injuries in more detail than MB HBMs. MB HBMs have the main strength for kinematics simulation, which is why they can have a benefit for applications like motorcycle events, pedestrian impacts, and for studying how design of sensors and signals and their systems will influence occupant kinematics in autonomous events without subsequent impacts. To conclude, FE HBMs are needed to study small overlap frontal crashes, oblique/angled impacts, multiple events, rollover, and run off road events, for example.

Future Development of the *SAFER A-HBM*

The next step in the development of the *SAFER A-HBM* (Östh 2014a; 2014b) will be to implement muscle activity control for lateral and oblique load cases. The muscle activity varies between individual muscles and with the direction of loading (Ólafsdóttir et al. 2015). Therefore, refined recruitment strategies are needed, especially for the head-neck complex to capture head motion in various loading events. This means regulating the activity of each muscle individually. One of the major challenges in developing a controller for individual neck muscle regulation is the definition of load sharing and muscle recruitment patterns. So far this has been based on optimization in simulation of isometric conditions (Nemirovsky and van Rooij 2010, de Bruijn 2014) and not based on in vivo data from dynamic events, because such data has not been available previously. This year, Ólafsdóttir et al. (2015) published the first study providing such data by analyzing volunteer neck EMG data during seated perturbations and presenting spatial patterns of muscle recruitment for acceleration pulses in 45 degree intervals from 0 to 315 degrees.

More physiological muscle activity control in HBMs can be developed for many reasons; which are to be prioritized based on the simulation requirements for development of safety systems. Postural control by the central nervous system, for example of the head on the torso, can either be relative to space or relative to the torso depending on the loading conditions, low and high frequency perturbations respectively (de Bruijn 2014). We speculate that muscle control is modulated differently during driving (high frequency) and in autonomous interventions (low frequency). With these two postural control strategies muscle activity can be triggered by feedback from either muscle spindle, i.e. either stretch of the muscle, or from the vestibular system, i.e. balance in space. For vehicle occupants both

systems are likely important and should ideally be implemented in active HBMs. For instance, during an emergency event or a long-duration crash, where an occupant tries to maintain a posture while interacting with advanced restraint systems that may cause local high muscle stretch (repositioning for example), both control loops are likely triggered. Future active HBMs might therefore benefit from including both reflex loops. Furthermore, as the contribution of the two control strategies varies with perturbation bandwidth (de Bruijn 2014) the controller parameters in the HBM need to be modulated depending on the simulated loading condition. In addition, safety systems activated before the event, whether by a crash or avoidance maneuver, can trigger startle-like responses (Östh et al. 2013; Ólafsdóttir et al. 2013). Omnidirectional HBMs with detailed neuromuscular control models that can simulate the startle reflex would be useful to further study how increased muscle activity due to startle affects the injury risk. Further, enhanced models for anticipatory postural response for driver initiated maneuvers, provide the potential to study how drivers interact with autonomous systems and how that changes the occupant response.

Validation Data for Future Active HBM

The evaluation of the biofidelity of active HBMs requires experimental data from volunteers in scenarios that replicate pre-crash conditions. In these tests a non-injurious, but representative, acceleration pulse is applied to seated volunteers whose muscle activity can be measured through EMG, the kinematics can be recorded with a camera, a motion capturing system, and/or accelerometers, and the boundary conditions can be recorded with load cells mounted to the steering wheel, seat, pedals, etc. The experimental data obtained in these experiments can also provide an estimate of the muscle activation schemes adopted by occupants in actual pre-crash events, aiding the development of methods for simulating muscle recruitment strategies, as outlined in the previous section. Hence, future volunteer experiments should be prepared and carried out carefully in order to generate useful data on muscle activity, the kinematic response, and boundary conditions.

Scenarios

Volunteer data that represent the effect of autonomous braking are readily available. Ejima et al. (2007; 2008) measured EMG, kinematics, and boundary conditions in volunteers in frontal loading conditions with a sled configuration and accelerations ranging from 0.2 – 1.0 g. In addition, a number of volunteer experiments with autonomous braking events using passenger cars and driving in regular traffic are available (Carlsson and Davidsson 2011; Östh et al. 2013; Ólafsdóttir et al. 2013). By driving or riding in a regular vehicle on regular roads the experimental conditions mimicked the targeted scenario to a higher degree than sled tests conditions; it was expected that these experiments provided data more representative of a scenario for which brake systems are autonomously activated.

Systems that avoid a collision by steering are being researched (e.g. Eidehall et al. 2007) and therefore there is an urgent need for validated omnidirectional active HBMs that can mimic the human response in these scenarios. Volunteer experiments with lateral and oblique loading have so far received less attention than longitudinal loading. Volunteer kinematic responses and EMG data during pure lateral and lane change type loading have been provided by van Rooij et al. (2013) and Ejima et al. (2012). In both these studies the volunteers were seated in a rigid seat and the experiments were carried out inside a laboratory. Huber et al. (2012) presented upper torso, arm and head kinematics, activation timings and absolute EMG levels during 1 g lane change maneuvers for front row vehicle passengers. Future volunteer experiments are to be carried out in conditions that more closely resemble an actual driving event.

Other scenarios for which volunteer test data will be required are multiple events, rollover, and run off road events. These scenarios include complex vehicle kinematics and are difficult to simulate on a test track using a regular passenger car. Instead they could be replicated in advanced vehicle simulators or robot test rigs

EMG

EMG signals from various muscle groups were recorded and normalized to the maximum EMG value recorded during the event for several muscle groups in the experiments conducted by Ejima et al. (2007; 2008) and van Rooij et al. (2013). These experiments provided a valuable insight into which muscle group is activated during pre-crash braking and steering events, the respective activation timings and overall kinematics. The magnitude of the EMG signals, however, cannot be used to directly compare the level of muscle activity between different muscles or volunteers nor with the simulated muscle activity in active HBMs; hence, their applicability for model development are limited. EMG signals normalized to maximum voluntary contractions (MVCs), as were provided by Östh et al. (2013) and Ólafsdóttir et al. (2013), are more appropriate for active HBM development and validation where the signals are represented as a percentage of a maximum activation, which can more easily be compared to or defined

in an active HBM. For the simulation of test scenarios that result in lateral occupant motions there is a need for muscle data for the muscles surrounding the pelvis, legs and for the muscles stabilizing the lower spine. Few studies have yet presented such data; one study has presented leg muscle activations when the volunteer was performing emergency braking (Behr et al. 2010).

Several studies have measured the activation levels of deep muscles in the spine using intra-muscular EMG when the volunteer were subjected to perturbations (Siegmund et al. 2007; Ólafsdóttir et al. 2015). Such data provide neuromuscular parameters, muscle synergies and an understanding of neck stabilization in dynamic events and are essential for the development of muscle recruitment models for the head-neck complex. However, additional data is required for loading conditions matching those that would occur in vehicles fitted with systems that employ active steering.

In conclusion, access to MVC normalized EMG data from various loading conditions is imperative for development of muscle recruitment strategies and as validation data for active HBMs. Future studies should preferably include measurements of deep muscles activity and include muscles that stabilize the trunk.

Kinematic response

Proper recording of kinematics in volunteer experiments are a necessity for the development and evaluation of active HBMs. Recording volunteer kinematics with traditional video recordings in regular passenger vehicles when longitudinal acceleration is deployed have been carried out successfully (Carlsson and Davidsson 2011; Östh et al. 2013; Ólafsdóttir et al. 2013). The visibility of targets has sometimes been limited; targets mounted to the lower neck region can be obstructed by the seat and chest targets can be obstructed by clothing and other occupants. Motion capturing systems have also been successfully adopted (Huber et al. 2012) although these systems encounter similar visibility limitations as traditional video recordings. For scenarios including lateral vehicle acceleration, the volunteer response would be more complex and would require multiple video cameras or other systems to capture occupant kinematics. Although traditional video system and motion capturing systems can be adopted and installed we encourage the development of new methods to measure occupant kinematics during dynamic events.

Boundary conditions

It is important to measure boundary conditions, such as restraint, pedal, and steering wheel forces and seat contacts, as the occupants will be interacting with their environment. In past volunteer studies the boundary conditions have been recorded (Ejima et al. 2007; 2008; 2012 Östh et al. 2013; Ólafsdóttir et al. 2013) while in others the main purpose of volunteer studies has not been to provide validation data (Carlsson and Davidsson 2011) and boundary conditions have thus been omitted. Such boundary conditions are important in validations of active HBMs and should be recorded in future studies.

ACKNOWLEDGEMENT

The work presented in this paper was carried out at SAFER, the Vehicle and Traffic Safety Centre, at Chalmers, Gothenburg, Sweden. It was funded by VINNOVA, the Swedish Governmental Agency for Innovation Systems, as part of the FFI Vehicle and Traffic Safety research program and by the industrial partners. The authors would like to thank Elisabet Agar for language editing of the manuscript.

REFERENCES

Antona J, Ejima S, Zama Y (2010) Influence of the Driver Conditions on the Injury Outcome in Front Impact Collisions. *Proceedings of the JSAE Conference*; Tokyo, Japan.

Beeman SM, Kemper AR, Madigan ML, Franck CT, Loftus SC (2012) Occupant Kinematics in Low-speed Frontal Sled Tests: Human Volunteers, Hybrid III ATD, and PMHS. *Accident Analysis and Prevention* 47:128–139.

Behr M, Arnoux PJ, Serre T, Thollon L, Brunet C (2006) Tonic Finite Element Model of the Lower Limb. *Journal of Biomechanical Engineering* 128:223–228.

Bohman K, Arbogast KB, Boström O (2011) Head Injury Causation Scenarios for Belted, Rear-Seated Children in Frontal Impacts. *Traffic Injury Prevention* 12:62–70.

Bose D, Crandall JR (2008) Influence of Active Muscle Contribution on the Injury Response of Restrained Car Occupants. *Proceedings of the Annals of Advances in Automotive Medicine Conference*.

Bose D, Crandall JR, Untaroiu CD, Maslen EH (2010) Influence of Pre-Collision Occupant Parameters on Injury Outcome in a Frontal Collision. *Accident Analysis and Prevention* 42:1398–1407.

Brolin K, Gras L, Stockman I (2014) Active Spine Modeling Representing a 6 Year-Old Child. Presentation at the 7th World Congress of Biomechanics; Boston, USA.

Brolin K, Halldin P, Leijonhufvud I (2005) The Effect of Muscle Activation on Neck Response. *Traffic Injury Prevention* 6:67–76.

Brolin K, Hedenstierna S, Halldin P, Bass C, Alem N (2008) The Importance of Muscle Tension on the Outcome of Impacts with a Major Vertical Component. *International Journal of Crashworthiness* 13(5):487–498.

Budziszewski P, van Nunen E, Mordaka JK, Kędzior K (2008) Active Controlled Muscles in Numerical Model of Human Arm for Movement in Two Degrees of Freedom. *Proceedings of the IRCOBI Conference*; Bern, Switzerland.

Cappon H, Mordaka J, van Rooij L, Adamec J, Praxl N, Muggenthaler H (2007) A Computational Human Model with Stabilizing Spine: A Step Towards Active Safety. SAE Technical Paper No. 2007–01–1171; SAE International. Warrendale, PA, USA.

Carlsson S and Davidsson J (2011) Volunteer Occupant Kinematics during Driver Initiated and Autonomous Braking when Driving in Real Traffic Environments. *Proceedings of the IRCOBI Conference*; Krakow, Poland.

Chancey VC, Nightingale RW, Van Ee CA, Knaub KE, Myers BS (2003) Improved Estimation of Human Neck Tensile Tolerance: Reducing the Range of Reported Tolerance using Anthropometrically Correct Muscles and Optimized Physiologic Initial Conditions. *Stapp Car Crash Journal* 47:135–153.

Chang CY, Rupp JD, Kikuchi N, Schneider LW (2008) Development of a Finite Element Model to Study the Effects of Muscle Forces on Knee-Thigh-Hip Injuries in Frontal Crashes. *Stapp Car Crash Journal* 52:475–504.

Chang CY, Rupp JD, Kikuchi N, Schneider LW (2009) Predicting the Effects of Muscle Activation on Knee, Thigh, and Hip Injuries in Frontal Crashes Using a Finite-Element Model with Muscle Forces from Subject Testing and Musculoskeletal Modeling. *Stapp Car Crash Journal* 53:291–328.

Choi HY, Sah SJ, Lee B, Cho HS, Kang SJ, Mun MS, Lee I, Lee J (2005) Experimental and Numerical Studies of Muscular Activations of Bracing Occupant. *Proceedings of the 19th ESV Conference*; Washington, D.C., USA. Paper no. 05–0139.

Coelingh E, Lind H, Wolfgang B, Wetterberg D (2006) Collision Warning with Auto Brake, *FISITA World Congress*; Yokohama, Japan. Paper No. F2006V130.

de Bruijn E (2014) *Isometric and Dynamic Control of Neck Muscles*. Ph.D. Thesis; Delft University of Technology, Delft, the Netherlands.

de Jager MKJ (1996) *Mathematical Head-Neck Models for Acceleration Impacts*. Ph.D. Thesis; Eindhoven University of Technology, Eindhoven, the Netherlands.

Deng YC, Goldsmith W (1987) Response of a Human Head/Neck/Upper-Torso Replica to Dynamic Loading – II. Analytical/Numerical Model. *Journal of Biomechanics* 20(5):487–497.

Develet J-A, Carlsson A, Svensson M, Fredriksson R, Bråse D, Holcombe S (2013) Evaluation of the Biofidelity of the BioRID-II and THOR-NT Anthropometric Test Devices under Seatbelt Pre-Pretensioner Loading in Stationary Conditions. *Proceedings of the Ohio State University Injury Biomechanics Seminar*; Columbus, OH, USA.

Dibb AT, Cox CA, Nightingale RW, Luck JF, Cutcliffe HC, Myers BS, Arbogast KB, Seacrist T, Bass CR (2013) Importance of Muscle Activations for Biofidelic Pediatric Neck Response in Computational Models. *Traffic Injury Prevention* 14(Sup1):S116–S127.

Eidehall A, Pohl J, Gustafsson F, Ekmark J (2007) Toward Autonomous Collision Avoidance by Steering. *IEEE Transactions on Intelligent Transportation Systems* 8(1):84–94.

Ejima S, Ito D, Satou F, Mikami K, Ono K, Kaneoka K, Shiina I (2012) Effects of Pre-Impact Swerving/Steering on Physical Motion of the Volunteer in the Low-Speed Side-Impact Sled Test. *Proceedings of the IRCOBI Conference*; Dublin, Republic of Ireland.

Ejima S, Ono K, Holcombe S, Kaneoka K, Fukushima M (2007) A Study on Occupant Kinematics Behaviour and Muscle Activities during Pre-Impact Braking based on Volunteer Tests. *Proceedings of the IRCOBI Conference*; Maastricht, the Netherlands.

Ejima S, Ono K, Kaneoka K, Fukushima M (2005) Development and Validation of the Human Neck Muscle Model under Impact Loading. *Proceedings of the IRCOBI Conference*; Prague, Czech Republic.

Ejima S, Zama Y, Ono K, Kaneoka K, Shiina I, Asada H (2009) Prediction of Pre-Impact Occupant Kinematic behavior Based on the Muscle Activity during Frontal Collision. *Proceedings of the 21st ESV Conference*; Stuttgart, Germany. Paper no. 09–0913.

Ejima S, Zama Y, Satou F, Holcombe S, Ono K, Kaneoka K, Shiina I (2008) Prediction of the Physical Motion of the Human Body based on Muscle Activity during Pre-Impact Braking. *Proceedings of the IRCOBI Conference*; Bern, Switzerland.

Erhart T (2010) An Overview of User Defined Interfaces in LS-DYNA. Paper presented at the LS-DYNA Forum; Bamberg, Germany.

Fraga F, van Rooj L, Symeonidis I, Peldschus S, Happee R, Wismans J (2009) Development and Preliminary Validation of a Motorcycle Rider Model with Focus on Head and Neck Biofidelity, Recurring to Line Element Muscle Models and Feedback Control. *Proceedings of the 21st ESV Conference*; Stuttgart, Germany. Paper no. 09–0244.

Good CA, Viano DC, Ronsky JL (2008a) Biomechanics of Volunteers Subject to Loading by a Motorized Shoulder Belt Tensioner. *Spine* 33:E225–E235.

Good CA, Viano DC, Ronsky JL (2008b) The Hybrid III Dummy Family Subject to Loading by a Motorized Shoulder Belt Tensioner. *SAE International Journal of Passenger Cars-Mechanical Systems* 1(1):383–395.

Hault-Dubrulle A, Robach F, Pacaux M-P, Morvan, H (2011) Determination of Pre-Impact Occupant Postures and Analysis of Consequences on Injury Outcome. Part I: A Driving Simulator Study. *Accident Analysis and Prevention* 43:66–74.

Hedenstierna S (2008) *3D Finite Element Modeling of Cervical Musculature and its Effect on Neck Injury Prevention*. Ph.D. Thesis; Royal Institute of Technology, Stockholm, Sweden.

Hedenstierna S, Halldin P, Brolin K (2008) Evaluation of a Combination of Continuum and Truss Finite Elements in a Model of Passive and Active Muscle Tissue. *Computer Methods in Biomechanics and Biomedical Engineering* 11(6):627–639.

Hetier M, Wang X, Robache F, Autuori B, Morvan H (2005) Experimental Investigation and Modeling of Driver's Frontal Pre-crash Postural Anticipation. *Proceedings of the Digital Human Modeling for Design and Engineering Symposium*; Iowa City, Iowa, USA.

IIHS (2011) Status Report. *Insurance Institute for Highway Safety Status Report* 46(6).

IIHS (2012) Status Report – Small Overlap Crashes: New Consumer-test Program Aims for Even Safer Vehicles. *Insurance Institute for Highway Safety Status Report* 47(6).

IIHS (2013) Status Report. *Insurance Institute for Highway Safety Status Report* 48(3).

Isaksson-Hellman I, Lindman M (2012) The Effect of a Low-speed Automatic Brake System Estimated from Real Life Data. *Annals of Advances in Automotive Medicine* 56:231–240.

Ito D, Ejima S, Kitajima S, Katoh R, Ito H, Sakane M, Nishino T, Nakayama K, Ato T, Kimura T (2013) Occupant Kinematic Behavior and Effects of a Motorized Seatbelt on Occupant Restraint of Human Volunteers during Low Speed Frontal Impact: Mini-sled Tests with Mass Production Car Seat. *Proceedings of the IRCOBI Conference*; Gothenburg, Sweden.

Iwamoto M, and Nakahira Y (2014) A Preliminary Study to Investigate Muscular Effects for Pedestrian Kinematics and Injuries Using Active THUMS. *Proceedings of the IRCOBI Conference*; Berlin, Germany.

Iwamoto M, Nakahira Y, Kimpara H, Sugiyama T (2009) Development of a Human FE Model with 3-D Geometry of Muscles and Lateral Impact Analysis for the Arm with Muscle Activity. SAE Technical Paper No. 2009–01–226; Society of Automotive Engineers, Warrendale, PA, USA.

Iwamoto M, Nakahira Y, Kimpara H, Sugiyama T (2012) Development of a Human Body Finite Element Model with Multiple Muscles and their Controller for Estimating Occupant Motions and Impact Responses in Frontal Crash Situations. *Stapp Car Crash Journal* 56:231–268.

Iwamoto M, Nakahira Y, Sugiyama T (2011) Investigation of Pre-impact Bracing Effects for Injury Outcome using an Active Human FE Model with 3D Geometry of Muscles. *Proceedings of the 22nd ESV Conference*; Washington, D.C., USA. Paper no. 11–0150.

Jakobsson L, Kling A, Lindman M, Wågström L, Axelson A, Broberg T, McInally G (2013) Severe Partial Overlap Crashes – A Methodology Representative of Car to Car Real World Frontal Crash Situations. *Proceedings of the 23rd ESV Conference*; Seoul, South Korea. Paper no. 13-0294.

Jakobsson L, Lindman M, Axelson A, Lokensgard B, Petersson M, Svanberg B, Kovaceva J (2014) Addressing Run Off Road Safety. *Proceedings of the SAE Congress*; Detroit, MI. SAE Technical Paper 2014–01–0554.

Jost R, Nurick GN (2000) Development of a Finite Element Model of the Human Neck Subjected to High g-Level Lateral Deceleration. *International Journal of Crashworthiness* 5(3):259–270.

Khodaei H, Mostofizadeh S, Brolin K, Johansson H, Östh J (2013) Simulation of Active Skeletal Muscle Tissue with a Transversly Isotropic Viscohyperelastic Continuum Material Model. *Journal of Engineering in Medicine* 227(5):571–580.

Ljung-Aust M, Jakobsson L, Lindman M, Coelingh E (2015) Collision Avoidance Systems – Advancements and Efficiency. *Proceedings of the SAE Congress*; Detroit, MI. SAE Technical Paper 2015–01–1406.

Mages M, Seyffert M, Class U (2011) Analysis of the Pre-Crash Benefit of Reversible Belt Pre-pretensioning in Different Accident Scenarios. *Proceedings of the 22nd ESV Conference*; Washington, D.C., USA. Paper no. 11–0442.

Meijer R, Broos J, Elrofai H, de Bruijn E, Forbes P, Happee R (2013a) Modelling of Bracing in a Multi-Body Active Human Model. *Proceedings of the IRCOBI Conference*; Gothenburg, Sweden.

Meijer R, Elrofai H, Broos J, van Hassel E (2013b) Evaluation of an Active Multi-Body Human Model for Braking and Frontal Crash Events. *Proceedings of the 23rd ESV Conference*; Seoul, South Korea. Paper no. 13–0163.

Meijer R, Rodarius C, Adamec J, van Nunen E, van Rooij L (2008) A First Step in Computer Modelling of the Active Human Response in a Far-side Impact. *International Journal of Crashworthiness* 13(6):643–652.

Meijer R, van Hassel E, Broos J, Elrofai H, van Rooij L, van Hooijdonk P (2012) Development of a Multi-Body Human Model that Predicts Active and Passive Human Behavior. *Proceedings of the IRCOBI Conference*; Dublin, Republic of Ireland.

Nemirovsky N, van Rooij L (2010) A New Methodology for Biofidelic Head-Neck Postural Control. *Proceedings of the IRCOBI Conference*; Hannover, Germany.

Olafsdottir J, Brolin K, Blouin J, Siegmund G (2015) Dynamic Spatial Tuning of Cervical Muscle Reflexes to Multidirectional Seated Perturbations. *Spine* 40(4):E211–E219.

Ólafsdóttir JM, Östh JKH, Davidsson J, Brolin K (2013) Passenger Kinematics and Muscle Responses in Autonomous Braking Events with Standard and Reversible Pre-tensioned Restraints. Proceedings of the IRCOBI Conference; Gothenburg, Sweden, pp. 602–617.

Östh J, Brolin K, Bråse D (2014a) A Human Body Model with Active Muscles for Simulation of Pre-Tensioned Restraints in Autonomous Braking Interventions. *Traffic Injury Prevention* 16(3):304–313.

Östh J, Brolin K, Carlsson S, Wismans J, Davidsson J (2012a) The Occupant Response to Autonomous Braking: A Modeling Approach that Accounts for Active Musculature. *Traffic Injury Prevention* 13(3):265–277.

Östh J, Brolin K, Happee R (2012b) Active Muscle Response using Feedback Control of a Finite Element Human Arm Model. *Computer Methods in Biomechanics and Biomedical Engineering* 15(4):347–361.

Östh J, Eliasson E, Happee R, Brolin K (2014b) A Method to Model Anticipatory Postural Control in Driver Braking Events. *Gait and Posture* 40(4):664–669.

Östh J, Ólafsdóttir JM, Davidsson J, Brolin K (2013) Driver Kinematic and Muscle Responses in Braking Events with Standard and Reversible Pre-tensioned Restraints: Validation Data for Human Models. Stapp Car Crash Journal 57:1–41.

Prüggler A, Huber P, Rieser A, Steiner K, Kirschbichler S, Eichberger A (2011) Implementation of Reactive Human Behavior in a Numerical Human Body Model using Controlled Beam Elements as Muscle Element Substitutes. *Proceedings of the 22nd ESV Conference*; Washington, D.C., USA. Paper no. 11–0154.

Rizzi M, Kullgren A, Tingvall C (2014) The Injury Crash Reduction of Low-Speed Autonomous Emergency Braking (AEB) on Passenger Cars. *Proceedings of the IRCOBI Conference;* Berlin, Germany.

Robin S (2001) Humos: Human Model for Safety – A Joint Effort Towards the Development of Refined Human-like Car Occupant Models. *Proceedings of the 17th ESV Conference*; Amsterdam, the Netherlands. Paper no. 291.

Schöneburg R, Baumann K-H, and Fehring M (2011) The Efficiency of PRE-SAFE® Systems in Pre-braked Frontal Collision Situations. *Proceedings of the 22nd ESV Conference*; Washington, D.C., USA. Paper no. 11–0207.

Siegmund GP, Blouin J-S, Brault JR, Hedenstierna S, Inglis JT (2007) Electromyography of Superficial and Deep Neck Muscles during Isometric, Voluntary, and Reflex Contractions. *Journal of Biomechanical Engineering* 129(1): 66–77.

Stemper BD, Yoganandan N, Pintar FA, Rao RD (2006) Anterior Longitudinal Ligament Injuries in Whiplash May Lead to Cervical Instability. *Medical Engineering & Physics* 28:515–524.

Sugiyama T, Kimpara H, Iwamoto M, Yamada D, Nakahira Y, Masatoshi H (2007) Effects of Muscle Tense on Impact Responses of Lower Extremity. *Proceedings of the IRCOBI Conference*; Maastricht, the Netherlands.

Toyota (2008) *Users' Guide of Computational Human Model THUMS® – AM50 Occupant Model: Version 3.0–080225*. Toyota Motor Corporation, Toyota Central Labs Inc, Toyota City, Aichi, Japan.

van der Horst M (2002) *Human Head Neck Response in Frontal, Lateral and Rear End Impact Loading – Modeling and Validation*. Ph.D. Thesis; Eindhoven University of Technology, Eindhoven, the Netherlands.

van Rooij L (2011) Effect of Various Pre-Crash Braking Strategies on Simulated Human Kinematic Response with Varying Levels of Driver Attention. *Proceedings of the 22nd ESV Conference*; Washington, D.C., USA. Paper no. 11–0306.

van Rooij L, H Elrofai M, Philippens MGM, Daanen HAM (2013) Volunteer Kinematics and Reaction in Lateral Emergency Maneuver Tests. *Stapp Car Crash Journal* 57:313–42.

Wittek A (2000) *Mathematical Modeling of the Muscle Effects on the Human Body Responses under Transient Loads – Example of Head-Neck Complex*. Ph.D. Thesis; Chalmers University of Technology, Gothenburg, Sweden.

Woitsch G, Sinz W (2014) Influences of Pre-Crash Braking Induced Dummy – Forward Displacements on Dummy Behaviour during EuroNCAP Frontal Crashtest. *Accident Analysis and Prevention* 62:268–275.

Yeomans JS, Li L, Scott BW, Frankland PW (2002) Tactile, Acoustic and Vestibular Systems Sum to Elicit the Startle Reflex. *Neuroscience and Biobehavioural Reviews* 26: 1–11.

ABDOMINAL CHARACTERIZATION UNDER LAP BELT LOADING

Taewung Kim
Gwansik Park
Salvador Montesinos
Damien Subit
James Bolton
Brian Overby
Jason Forman
Jeff Crandall
University of Virginia Center for Applied Biomechanics
USA

Hyungjoo Kim
Hyundai Motor Group
South Korea

Paper Number 15-0312

ABSTRACT

The phenomenon of submarining is of major interest in the design and optimization of restraint systems. A biofidelic finite element human body model can be more useful for investigating this phenomenon than the existing dummy. For the validation of finite element human body models, belt pull tests were performed to characterize thoracic and abdominal regions of the PMHS, and the 50%tile male Hybrid III dummy was tested for comparison with the PMHS. The spines of subjects were rigidly mounted to a test fixture through a mounting system to minimize the influence of the spinal motion during the test. The pelvis of the subjects were positioned close to the normal driving posture, but the torso angle was more reclined than the average driving posture due to the difficulty of adjusting the torso angle during the mounting process. This torso angle led to the belt being positioned more rearward with respect to anterior superior iliac spine (ASIS) in the longitudinal direction. The subjects were loaded under lap belt only configurations with two levels of load limits, 1 kN and 3 kN. The lap belt was positioned in various vertical offsets with respect to ASIS and belt angles. The vertical offset of the belt from ASIS was determined based on volunteer test data. Belt pulling distance, belt cable force, spine reaction force, and belt kinematics were documented for the human body model validation. During the lap belt tests, both belt sliding over the pelvis and belt staying in front of the pelvis were observed, and a large amount of abdominal compression was observed during the submarining cases. After finishing the test series, autopsies were performed on the PMHS, and both PMHS showed no injuries in the abdominal region. One of the PMHS also showed a pelvic fracture at the iliac crest, but the PMHS had a pre-existing healed pelvic fracture at the same location. It was believed that this pre-existing fracture had not healed completely prior to death. Note that its ASIS region was intact so it should not have affected the occurrence of the submarining-like belt kinematics. Although only two PMHS were tested, the biomechanical responses collected through the belt pull test can be used to validate the computational human body model for further investigation on the submarining phenomenon.

INTRODUCTION

Submarining is one of the major concerns in restraint system design. Lamielle et al. (2006) showed grown relative importance of abdominal injury due to the greater reduction in severe or fatal injuries in head and thorax than in the abdominal region. Poplin et al. (2014) showed that increased speed and the resulting crash delta V increases risk of AIS 2+ injuries to the hollow organs of the abdomen and suggested that direct loading from lap belts into lower abdomen seems to be one of the mechanisms of the abdominal injuries. Adomeit and Hegar (1975) pointed out that the occurrence of submarining harmfult to an occupant during a vehicular crash not only because the belt directly loads the abdominal region but also it can increase the risk of the thoracic injury and the lower extremity injury due to greater pelvic motion and loading the lower torso by shoulder belt due to reclined posture of an occupant, respectivley.

Abdominal characterization tests have been performed focusing on the abdominal region but initial lap belt to pelvis interaction or the driving posture of PMHS were not given much consideration during those tests (Foster et al., 2006, Lamielle et al., 2008). The subjects were positioned the belt at mid-umbilicus and pulled horizontally by only engaging the abdominal region. While the biomechanical test data collected from these two studies provide rich information to validate the abdominal region, it does not provide information on the initial interaction between the belt and the pelvis.

Uriot et al. (2006) studied the interaction between the lap belt and the pelvic region using a component level belt pull test by rotating the pulling direction. This study characterized the behavior of the pelvic region under lap belt loading conditions, but the belt was initially positioned below the ASIS. Note that Reed et al. (2013) found that out-of-position belt fit, which means wearing the lap belt over the ASIS, was prevalent from their volunteer belt fit study. This suggests the importance of characterizing the lap belt to abdominal and pelvic region interation under out-of-position belt fit.

The finite element human body model has the potential to investigate the submarinig phenominon since the current anthropomorphic test devices showed substantial difference in behavior while interacting with a lap belt under submarining at risk conditions (Uriot et al., 2006, Luet et al., 2012).

In the current study, an abdomonial characterization test using a lap belt was performed with for the average pelvic angle of driving posture. The belt was positioned around and above the ASIS based on the volunteer belt fit study (Reed et al., 2013) The spine was fixed to isolate the chracteristics of the abdominal region from other body regions. Belt force, belt displacement, and belt kinematics in 3-dimensional space were documented to aid computational model validation.

METHOD

Specimen and Specimen Preparation

Two female PMHS with similar statures but different weights, a health weight and an obese, were subjected to lap belt loading (Table 1). It was hyphothesized that females has higher risk of submarining due to their lower pelvis height compared to males. In addition to the PMHS, the 50th percentile male Hybrid III dummy was tested for comparison.

Table 1.
PMHS information

PMHS No.	683	700
Age	83	67
Gender	Female	Female
Height (cm)	168	165
Weight (kg)	68.0	84.4
Body Mass Index (BMI)	24.1 (Normal range)	31.0 (obese)
Spine mount location	Upper spine mount: C6, T2, T6, T8, T10, and T11-12 Lower spine mount: L2, L4, and sacrum	Upper: T1, T4, T7, T9, T11, and L1 Lower spine mount: L3, L5, sacrum

All PMHS specimens were screened for Hepatitis A, B, C, and HIV, as well as for pre-existing pathologies with the potential to influence thoracic properties. Pre-test radiographs and CT scans were taken to verify that specimens with acute or healed rib fractures or other pre-existing thoracic trauma were excluded from this study. All test procedures were approved by the University of Virginia cadaver institutional review board.

Test Rig

The test rig consisted of seat and seat back to support a subject, which was mounted onto the upper and lower spine mounts, and belt pull system (Figure 1 and Table 2). The design objectives for the test rig were to consider the shape of the abdominal skin of a typical driving situation during the interaction between the lap belt and the skin and to isolate the characteristics of the abdomen and pelvis from spinal motion for model validation purposes. The test fixture had 3 degrees of freedom to accommodate various sizes of subjects and to control belt angles. To prevent a parallel path for the vertical component of the belt force, the seat plate was positioned forward so that it did not support the pelvis. Since the hip joints of the PMHS were compliant in flexion and extension of the thigh, the seat load cell did not experience a substantial amount of vertical force.

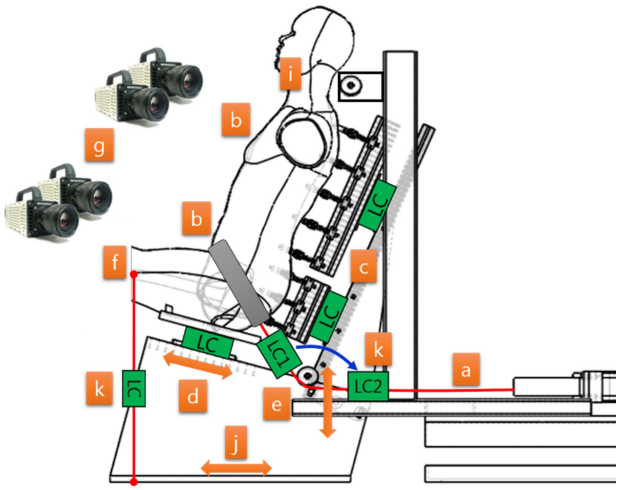

Figure 1. Schematic of belt pull test rig

Table 2.
Description of a belt pull test set-up

Item	Description
a	The belt cables attached to the belt ends were pulled by a pneumatic cylinder. A honeycomb was used to prevent excessive force applied to the PMHS.
b	A custom rigidized belt was placed on the abdomen and connected to the steel belt cables (see Custom rigidized belt).
c	Almost every other vertebra were mounted onto the upper and lower spine mounts. Six-axis loadcells (Model 2554AJ) were installed between the upper and lower spine mounts and the seat base. (see Spine mount)
d	A five-axis load cell was mounted under the seat to measure the reaction forces and moments.
e	The height of the anchor was adjusted to control the angle of the belt. The belt cable goes through a pulley to transmit the tensile force from the pneumatic cylinder to the belt. The distance between the left and right pulley was 560 mm.
f	The femurs were amputated and constrained to the seat bottom to prevent any upward motion of them.
g	Two Aramis optical displacement and strain mapping systems were used to track the 3-dimensional motion of the belt and deformation of the skin.
h	A uniaxial loadcell was placed in the cable that connected the femur and the seat base to measure tensile force in the cable.
i	Neck support was used to support the head due to the inactivity of the neck muscle.
j	The distance between the seat and seat back was adjustable to accommodate different sizes of subjects.
k	Belt cable loadcells were installed in the steel belt cable. It was moved from LC1 location fo LC2 location for the PMHS700 and the dummy tests.

Both ends of the belt was pulled by a pneumatic cylinder at the same speed (Figure 2), and the belt pulling force was measured using uniaxial belt cable loadcells on each end of the belt. Note that the belt cable loadcells were placed right next to the belt ends (LC1 in Figure 1) to exclude inertial and frictional force from pulleys for PMHS683 but it was moved to after the first pulley (LC2 in Figure 1) to resolve an initial slack problem in the belt. The belt pulling force was limited using a force limiting device by placing honeycomb between piston disk and belt pulling disk (Figure 2).

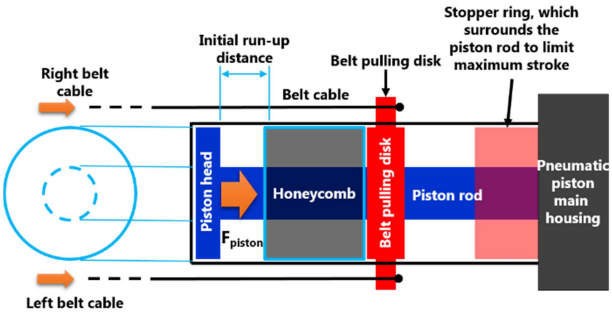

Figure 2. Load limiting device (top view)

<u>Spine mount</u> The spine mounts (Salzar et al., 2013), which were used for table-top tests, were installed to fix alternating vertebrae to the seat back (Figure 3). The thoracic spines were mounted to the upper spine mount column and the lumbar spine and sacrum, except L1 of PMHS700, were mounted to the lower spine mount column (Figure 1 and Table 2). Each spine mount had two degrees of freedom to adjust the pelvic angle and spine posture of the subject.

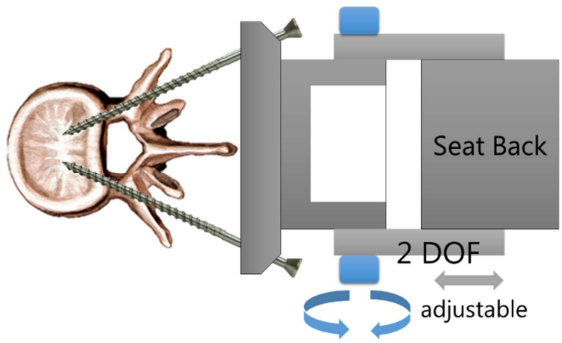

Figure 3. Spine mount (top view)

<u>Custom rigidized belt</u> The belt used in the current study was made of a polyethylene fiber-reinforced composite (Spectra®, E = 97 GPa) to minimize belt elongation (Salzar et al., 2013). The belt ends were clamped using metal plates and bolts (Figure 4), and steel belt cables were attached to each belt end to trasmit the pulling force from the pneumatic piston. The mass of the belt was tabulated to allow computational modeling of the belt since the inertial effect of the belt during the testing was not compensated in the belt pulling force in the Results section. There was belt slack during the PMHS683 tests due to the weights of the clamps and belt cable loadcell. To resolve this issue, another custom belt was built to lighten the weight, and the belt cable loadcell was moved from right next to the clamps to after the first pulley the belt cable went through.

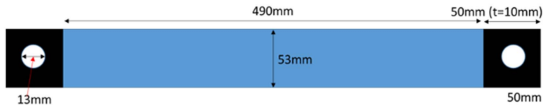

(a) Belt used for PMHS683

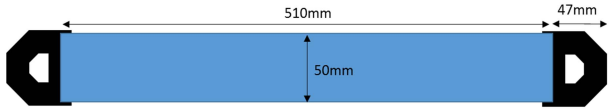

(b) Belt used for PMHS700 and Dummy
Figure 4. Belt geometry

Table 3.
Mass of belt and belt loadcell

Part	**Mass [g]**	
	PMHS683	PMHS700 and Dummy
belt	55	38
clamps	335	33
bolts on clamps	48	6
pins for the hole at belt ends	13	13
belt total (exc. loadcell)	451	90
belt loadcells	83	83

Instrumentation

<u>Sensor data</u> The force and moments from loadcells were filtered using CFC180 filter, and the belt displacement and belt 3-dimensional kinematics data was not filtered (Table 4). The belt pulling forces and displacements were not scaled for PMHS responses. Instead, the flesh thickness around the pelvic region was provided (see Flesh Thickness).

Table 4.
List of measurement for belt pull test

Measurement	Description	Filter
Belt force	belt cable loadcell (not inertially compensated for the mass of the belt, belt cable, and belt cable loadcells)	CFC180
Belt displacement	laser displacement sensor and video analysis	None
Reaction force and moment	6-axis spine mount loadcell	CFC180

Belt kinematics and skin deformation The Aramis optical displacement and strain mapping system (Aramis v6.2, GOM) was used to determine detailed kinematics of the belt, thorax, and abdomen of the subject during test. Note that the belt kinematics in the Results section was measured at the midline of the belt on the sagittal plane at the ASIS while the initial belt position in the Test matrix section was measured at the upper edge of the belt to follow Reed et al.'s method (2013). Lastly, a high speed x-ray system was used to record relative motion between belt and pelvis in sagittal plane during the lap belt test.

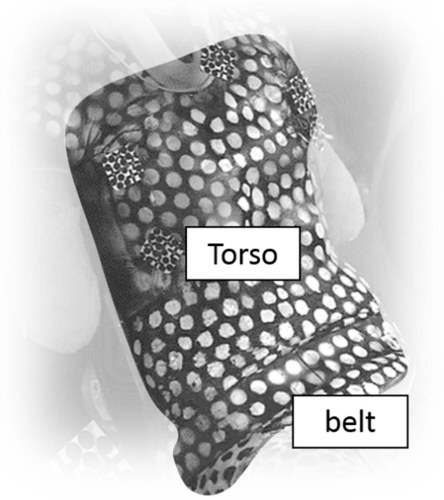

Figure 5 Pattern on the skin and belt for tracking

Test Condition

Coordinate Systems The SAE coordinate system was used to process the test data, and the upper right front corner of the seat was chosen as the origin for the global coordinate system (Figure 6). To obtain the desired belt position and angle, the seat was moved in X-direction and the D-ring and anchors were moved in Z-direction. Note that the positions of the D-ring and the anchors can be adjusted separately. Although the seat was moved during the positioning, the origin was attached to the front right corner of the top surface of the seat during data processing. In this way, only the positions of the anchors and the D-ring needed to be adjusted for the modeling.

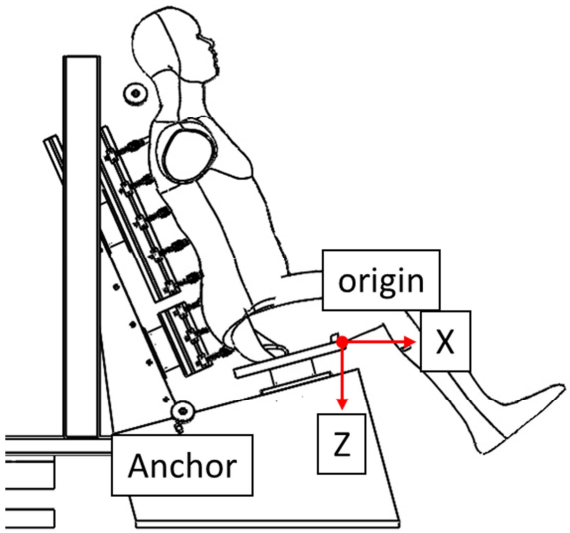

Figure 6 Global coordinate system and d-ring and anchor locations (origin: right front corner of the top surface of the seat)

PMHS and dummy positioning It was targetted to obtain 44 degrees of pelvic angle from vertical axis and C7 re ASIS X, which is a function of stature and BMI, was targeted to be around 265 mm. It was difficult to obtain the desired ASIS to C7 distance due to the range of adjustability of the spine mount system.

Table 5.
PMHS and dummy position

Measurement		PMHS683	PMHS700	Dummy
Pelvic angle [deg]	aft of vertical	44	37	55
	roll angle	-3	-5	0
ASIS to C7 (fore-aft) [mm]		304	347	285 (Upper and rearmost upper spine)

Definition of lap belt position The belt location was measured following the method used by Reed et al. (2013). The location of the upper edge of the belt was calculated by taking an average of the location of the upper edge at left and right sides of ASIS (anterior superior iliac spine) in the sagittal plane (Figure 7). Note that while Belt Z was within a range of Reed et al.'s volunteer belt fit tests during the belt pull test, Belt X was located more rearward due to the more reclined torso angle during the spine mounting.

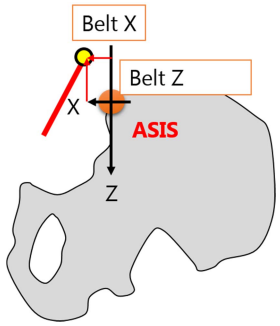

Figure 7 Belt position measurement

Test matrix Both the PMHS and the Hybrid III dummy were tested using a lap belt only condition by pulling both ends at the same time (Table 6). Although the belt was positioned to a target position based on the location of

ASIS from palpating on the skin during the tests, the calculated belt position, which was obtained by combining CT scan data of pelvis and spine mounts and belt position data from Aramis, were provided in Table 6. The lap belt angle was measured in the sagittal plane (XZ plane) using an inclinometer. Belt position, belt angle, belt force, and initial stroke rate were varied to see the effects of those on the responses of the abdominal area of the PMHS and the dummy. Note that the angles of belt and belt cable were different during PMHS683 tests due to relatively heavy weight of the belt clamps (Table 3) and the position of the belt cable loadcells.

Table 6
Test Matrix for PMHS683 (angle: X to -Z)

Test Name	Belt Upper Edge Position w.r.t ASIS (X, Z), Belt and Belt Cable Angles	Load limit (initial loading rate)	run#
PMHS683	(-8, -25) mm, belt cable: 52 deg, belt: 61 deg	1 kN (0 m/s)	3
	(-17, -31) mm, belt cable: 35 deg, belt: 55 deg	1 kN (0 m/s)	5
	(-16, -26) mm, belt cable: 44 deg, belt: 59 deg	3 kN (2 m/s)	7
PMHS700	(-12, -53) mm, 45 deg	1 kN (3 m/s)	3
	(-16, -55) mm, 45 deg	3 kN (4 m/s)	4
	(-46, -66) mm, 45 deg	1 kN (3 m/s)	5
	(-35, -69) mm, 45 deg	3 kN (4 m/s)	6
HybridIII	(22, -9) mm, 65 deg	3 kN (4 m/s)	6
	(22, -7) mm, 65 deg	1 kN (3 m/s)	7
	(15, -25) mm, 32 deg	1 kN (3 m/s)	8
	(7, -43) mm, 35 deg	1 kN (3 m/s)	9
	(7, -43) mm, 35 deg	3 kN (4 m/s)	10

RESULTS

Flesh Thickness

The flesh thickness of the the two PMHS and the dummy was measured on the sagittal plane at ASIS and mid-sagittal plane (Figure 8). The flesh thickness of PMHS683 was 15 mm and 38 mm on the sagittal plane at ASIS and the mid-point of ASIS of the subject, respectively. The flesh thickness of PMHS700 was 40 mm and 70 mm on the sagittal plane at ASIS and the mid-point of ASIS of the subject, respectively. The flesh thickness of the dummy was 25 mm and 63 mm on the sagittal planes at ASIS and at the mid-point of ASIS, respectively. Note that the geometry of the pelvis of the Hybrid III dummy is different from that of the PMHS. It does not have a protruded area at the tip of iliac wings like the PMHS.

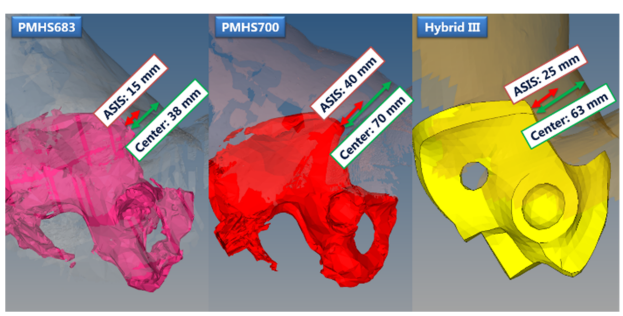

Figure 8 Flesh thickness around ASIS

Belt Kinematics and Belt Force

PMHS700 The time histories of belt pulling force and displacement and kinematics of the belt midline at ASIS were shown in Figure 9. The belt moved toward the pelvis at the beginning due to the initial belt angle and moved mostly horizontally afterwards. Although a honeycomb was used to limit the belt force, the belt pulling force exceeded the load limit in the beginning of the events as the belt loaded the pelvis through the flesh. Note that all

the honeycombs that were used in the testing were pre-crushed to ensure its limiting load. In the PMHS700-3 test, the belt slid over the iliac crest on the left side but caught near the ASIS on the right side. As the load limit increased and/or initial belt position heightened (Figure 9b-d), the belt completely slid over the pelvis in the end. Interestingly, once the belt completely slid over the iliac crest, the belt intrusion amounts into the abdomen were similar between low and high load limit cases (Figure 9c-d). The belt pulling force subsided after the belt slid over the iliac crest, and the belt stopped due to the limit of the range of motion of the pneumatic cylinder. The lower spine reaction force, which was the resultant force of F_x and F_z, showed similar peak forces for the lower load limit cases and lower peak forces for the higher load limit cases with time delays compared to the belt pulling forces.

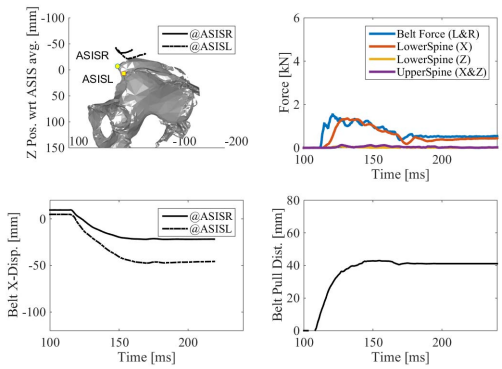

(a) PMHS700-3 (load limit, 1kN)

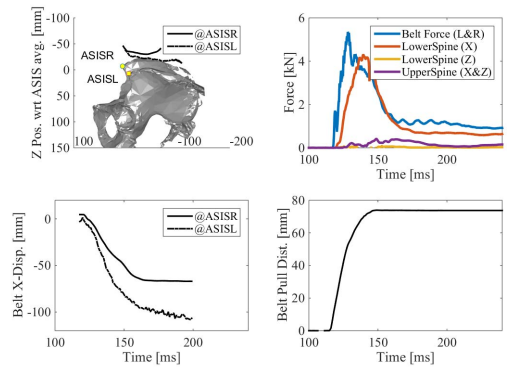

(b) PMHS700-4 (load limit, 3kN)

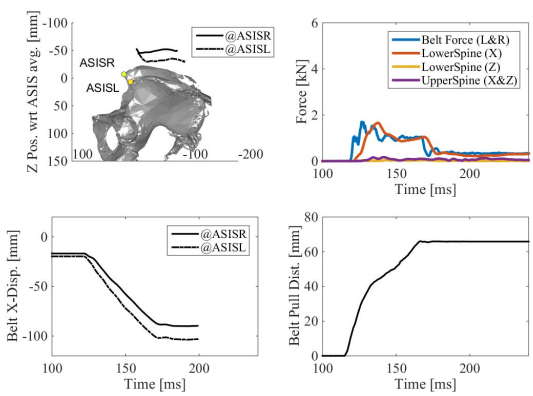

(c) PMHS700-5 (load limit, 1kN)

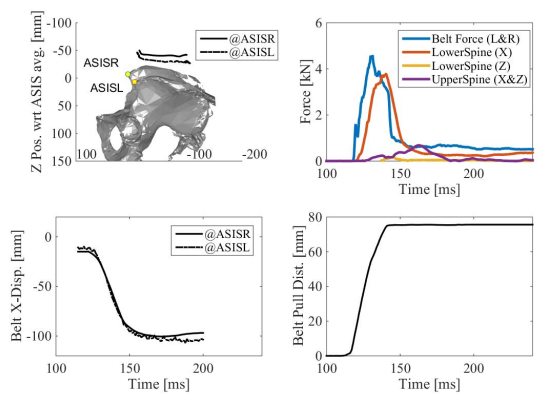

(d) PMHS700-6 (load limit, 3kN)

Figure 9. Belt pulling displacement and force time histories (PMHS700)

<u>PMHS683</u> Although the slack of the belt made the responses of the PMHS683 less desirable to use for model validation, the PMHS683 test provided belt kinematics both sliding over the pelvis (Figure 10a-b) and staying at the ASIS (Figure 10c). The belt showed downward motion when the belt stayed in front of the ASIS, and the maximum belt pulling distance was similar for the lower load limit (Figure 10a) and the higher load limit cases (Figure 10b). During the PMHS683-5 test, the belt moved toward the pelvis initially and slid over the pelvis in the end showing large amount of belt intrusion toward the abdomen (Figure 10c). The belt pulling force subsided to almost zero after the pneumatic piston reached its limit of range of motion. The belt was completely over the ASIS during the PMHS683-1 test (Figure 10d). The belt initially penetrated the abdomen due to 10 N of preload. With 1 kN of load limit, the belt intruded toward the abdomen more than 50 mm.

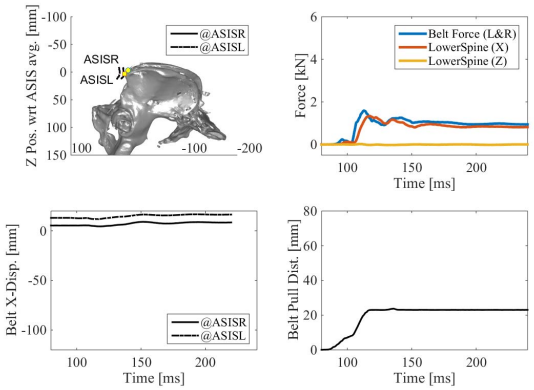

(a) PMHS683-3 (load limit, 1kN)

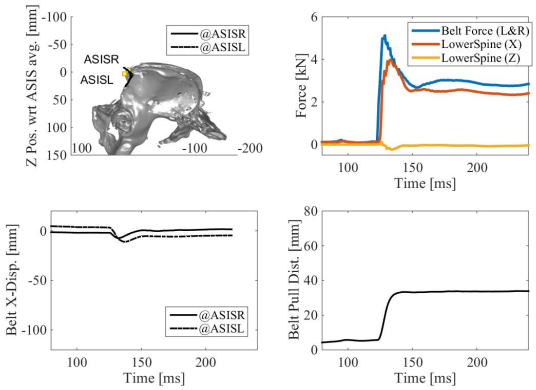

(b) PMHS683-7 (load limit, 3kN)

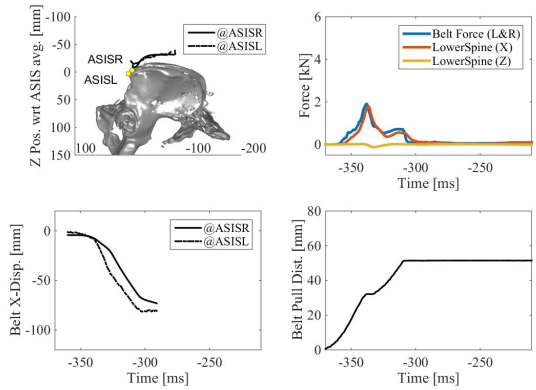

(c)PMHS683-5 (load limit, 1kN)

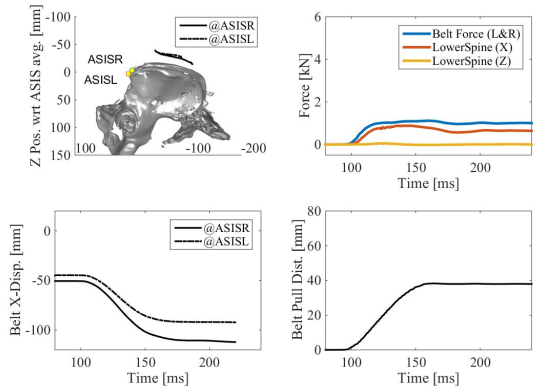

(d) PMHS683-1 (load limit, 1kN)

Figure 10. Belt pulling displacement and force time histories (PMHS683)

<u>High speed X-ray</u> The high speed x-ray was used during the PMHS683 tests (Figure 11). The x-ray images confirmed that the belt stayed in front of the pelvis during the PMHS683-3 and PMHS683-7 tests and it slid over the pelvis during PMHS683-5 tests. It was difficult to see the ASIS due to the over exposure around ASIS from the high speed x-ray images.

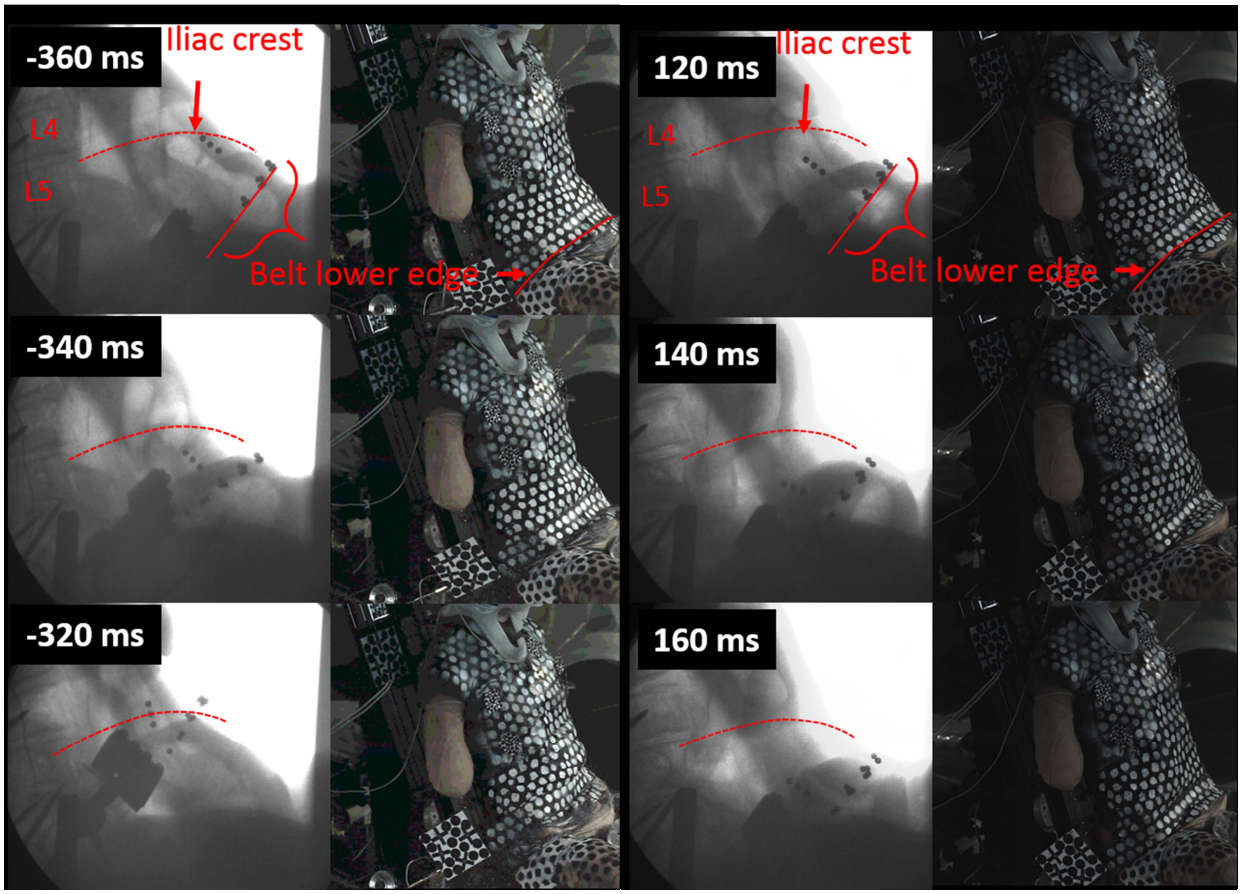

(a) PMHS683-5 *(b) PMHS683-7*

Figure 11 Snapshot of high speed x-ray

Hybrid III The belt did not completely slide over the pelvis during either HybridIII-9 (Figure 12a) or HybridIII-10 (Figure 12b) tests but the belt did show slight upward motion during the HybridIII-10 test. The dummy showed less belt intrusion (Figure 12b) toward the abdomen compared to both PMHS700-4 (Figure 9b) and PMHS683-5 (Figure 10c). Note that PMHS683-5 was tested with the 1kN of load limit while HybridIII-10 was tested with the 3 kN of load limit. The HybridIII-8 test (Figure 12c) showed lower peak belt pulling displacement than that of PMHS683-3 but this difference may come from the initial belt slack during the PMHS683-3 test. The HybridIII-6 test (Figure 12d) showed similar peak belt pulling displacement as that of PMHS683-7 (Figure 10b).

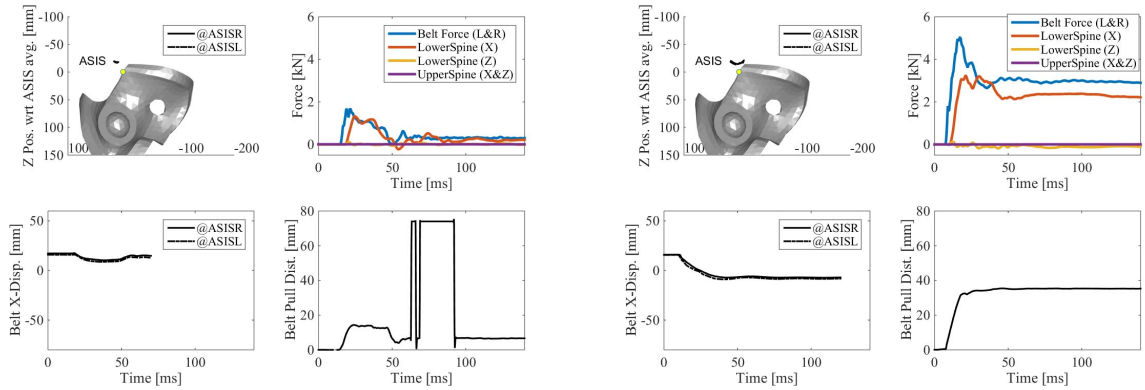

(a) HybridIII-9 (load limit, 1kN) (b) HybridIII-10 (load limit, 3kN)

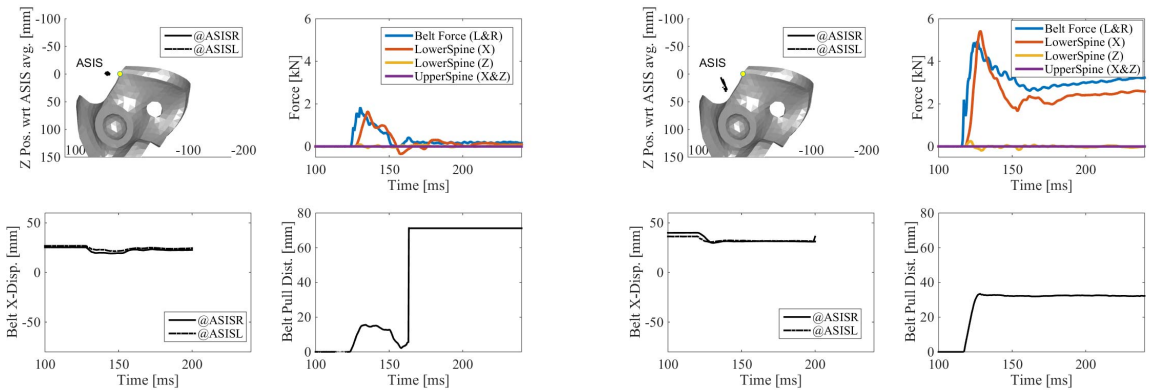

(a) HybridIII-8 (load limit, 1kN) (b) HybridIII-6 (load limit, 3kN)
Figure 12. Belt pulling displacement and force time histories (Hybrid III)

Injury Summary
Neither PMHS showed any signs of abdominal injury. PMHS683 showed a right iliac wing fracture and initially had a healed right iliac wing fracture. It seems that the right iliac wing of PMHS683 was not completely healed prior to death.

DISCUSSION

A new test rig to investigate subject to lap belt interaction was developed in the current study. To measure the belt kinematics, 3-dimensional motion tracking was used and provided useful information for understanding belt kinematics when the belt slid over the pelvis and for future computational model validation. Through the testing, the weight of the custom belt was reduced and the location of the belt cable loadcell was changed to resolve the belt initial slack issue. There was no initial slack issue with the older design of the custom belt on the table-top configuration, which was tested on subjects in a supine posture, but there was a problem in a seated posture.

An obese (PMHS700) and a normal weight (PMHS683) PMHS were tested in a seated posture under lap belt loading conditions to chracterize abdominal region. The belt was positioned near the ASIS and either slid over the pelvis or stayed in front of ASIS. With the aid of 3-dimensional motion tracking, the belt kinematics was well documented for validation of a computational human body model. Due to the belt slack issue in the PMHS683 tests, it was decided to use PMHS700 test results for human body model validation. Although there was a belt slack problem during the PMHS683 tests, the high speed x-ray images taken during the test confirmed that the belt kinematics measured using the Aramis system was reasonable.

For the cases that the belt slid over the pelvis, the belt force peaked in the beginning of the events while the belt was compressing the pelvis, and subsided while the belt slid over the pelvis. The reaction force from the spine mount

loadcells showed time delay, which indicates the inertial forces from the soft tissue and/or pelvis (Figure 10 and Figure 12). The PMHS700 showed larger time delays in lower spine reaction forces compared to the belt pulling forces than those of the PMHS683, and it may have stemmed from the heavier soft tissue of the PMHS700 (obese) than that of the PMHS683 (normal weight) (Table 1). It should be noted that the spine mounts that were holding the lumbar spine and pelvis showed the downward motion about 10 mm during the PMHS700-4 test (Figure 9b) from 132 ms to 145 ms, but it was after the lower spine reaction force reached 3.5 kN.

For the cases that the belt stayed on the pelvis, the belt showed little motion in X direction while showing about 20 mm of downward motion for 1 kN of load limit (Figure 10a and 30 mm of downward motion for 3 kN of load limit (Figure 10b). Although the high speed x-ray images provided qualitative information about the belt kinematics, it showed that the belt was at almost the same locations with respect to ASIS to that of the initial location at the end of the event. Therefore, the downward motion observed from the Aramis system was due to the pelvic rotation in Y direction rather than the belt sliding downward relative to ASIS (Figure 10a and b).

PMHS683-5 had 9 mm more rearward and 6 mm higher initial belt position than that of PMHS683-3 (Table 6). The 11 mm of difference in initial belt position drastically changed the test outcome (Figure 10a and c).

For model validaiton, the belt displacement time histories can be used as an input condition, and belt pulling force, spine reaction force, and the kinematics of the midline of the belt can be used as an target response. It will be important for a computation model to show the sudden increase of the belt pulling force in the beginning and the decrease of the belt pulling force afterwards with similar belt intrusion toward the abdomen prior to investigation of the submarining phenomenon. In addition, the model should be able to capture the transition between the belt sliding over the pelvis and the belt staying in front of the pelvis, for use in submarining investigation.

Althougth the current study limited due to small number of the PMHS and issues in the test fixture during the PMHS683 tests, it provided detailed information on the belt kinematics during the lap belt to the subject interaction in simulated real world driving conditions. It should be noted that the torso of the PMHS was more reclined (C7 was located about 50 to 65 mm rearward than that of the normal driving posture).

ACKNOWLEDGEMENTS
The author would like to acknowledge and thank the Hyundai Motor Group for funding this research and providing valuable participation, review and feedback throughout the process. The opinions, findings, and conclusions expressed in this manuscript are those of the authors and do not necessarily reflect the views of the Hyundai Motor Group. Additionally, the author would like to acknowledge Rob Salzar, Dennis Roethlisberger and Sara Heltzel for helping the test, Joey White for manufacturing the test rig, and Tim Gillispie for the proofread.

REFERENCES

ADOMEIT, D. & HEGAR, A. 1975. Motion Sequence Criteria and Design Proposals for Restraint Devices in Order to Avoid Unfavorable Biomechanic Conditions and Submarining. *SAE Technical Paper 751146.* SAE International.

FOSTER, C. D., HARDY, W. N., YANG, K. H., KING, A. I. & HASHIMOTO, S. 2006. High-speed seatbelt pretensioner loading of the abdomen. *Stapp car crash journal,* 50**,** 27-51.

LAMIELLE, S., CUNY, S., FORET-BRUNO, J., PETIT, P., VEZIN, P., VERRIEST, J. & GUILLEMOT, H. 2006. Abdominal injury patterns in real frontal crashes: influence of crash conditions, occupant seat and restraint systems. *Annual proceedings / Association for the Advancement of Automotive Medicine. Association for the Advancement of Automotive Medicine,* 50**,** 109-24.

LAMIELLE, S., VEZIN, P., VERRIEST, J.-P., PETIT, P., TROSSEILLE, X. & VALLANCIEN, G. 2008. 3D deformation and dynamics of the human cadaver abdomen under seatbelt loading. *Stapp car crash journal,* 52**,** 267-94.

LUET, C., TROSSEILLE, X., DRAZETIC, P., POTIER, P. & VALLANCIEN, G. 2012. Kinematics and dynamics of the pelvis in the process of submarining using PMHS sled tests. *Stapp car crash journal,* 56**,** 411-42.

POPLIN, G. S., MCMURRY, T. L., FORMAN, J. L., HARTKA, T., PARK, G., SHAW, G., SHIN, J., KIM, H. J. & CRANDALL, J. 2015. Nature and etiology of hollow-organ abdominal injuries in frontal crahses. *Accident Analysis & Prevention,* (in press).

REED, M. P., EBERT, S. M. & HALLMAN, J. J. 2013. Effects of driver characteristics on seat belt fit. *Stapp car crash journal,* 57**,** 43-57.

SALZAR, R., LAU, S., LESSLEY, D., SOCHOR, M., SHAW, C., KENT, R. & CRANDALL, J. 2013. Thoracic response to shoulder belt loading: comparison of tabletop and frontal sled tests with PMHS. *Traffic Inj Prev. ,* 14**,** 159-67.

URIOT, J., BAUDRIT, P., POTIER, P., TROSSEILLE, X., PETIT, P., GUILLEMOT, H., GUERIN, L. & VALLANCIEN, G. 2006. Investigations on the belt-to-pelvis interaction in case of submarining. *Stapp car crash journal,* 50**,** 53-73.